Dissertation

submitted to the
Combined Faculties of the Natural Sciences and Mathematics
of the Ruperto-Carola-University of Heidelberg, Germany
for the degree of
Doctor of Natural Sciences

Put forward by

Viviana Niro

Born in Venaria Reale, Italy

Oral examination: June 7th 2010

Indirect detection of Dark Matter with neutrinos

Referees: Prof. Dr. Manfred Lindner
Prof. Dr. Tilman Plehn

Zusammenfassung

In dieser Doktorarbeit wird die indirekte Detektion von Dunkler Materie mittels Neutrinos untersucht. Wir führen eine detaillierte Berechnung der Neutrino-Spektren durch, die von Annihilationen Dunkler Materie innerhalb der Sonne und der Erde herrühren, wobei wir alle Prozesse mit einbeziehen, die während der Propagation auftreten können: Oszillationen und Wechselwirkung mit Materie. Wir analysieren systematisch alle Möglichkeiten der direkten Vernichtung von Dunkler Materie in Neutrinos für die beiden Fälle von skalarer und fermionischer Dunkler Materie. Außerdem berechnen wir die Vernichtungs-Querschnitte für Diagramme verschiedener Topologien. Hierbei identifizieren wir die vielversprechendsten Szenarien, für welche auch das Verhalten des Wirkungsquerschnittes angegeben wird. Danach beschreiben wir die Phänomenologie der leptophilen Dunklen Materie und zeigen auf, wie die experimentellen Limits an den von Annihilationsprozessen in der Sonne herrührenden Neutrinofluss dieses Modell als Erklärung der Ergebnisse des DAMA-Experiments in Bedrängnis bringen. Schließlich wird eine detaillierte Analyse des erwarteten Neutrino-Flusses stammend von Neutralino-Annihilationsprozessen innerhalb der Sonne und der Erde präsentiert. Hierbei berücksichtigen wir sowohl teilchenphysikalische als auch astrophysikalische Unsicherheiten und unterteilen den Fluss in durchgehende und stoppende Myonen.

Abstract

In this doctoral thesis, we discuss indirect Dark Matter detection with neutrinos. We perform a detailed calculation of the neutrino spectra coming from Dark Matter annihilations inside the Sun and the Earth, taking into account all the possible processes that could occur during propagation: oscillation and interaction with matter. We examine in a systematic way the possibilities of Dark Matter annihilation directly into neutrinos, considering the case of scalar and fermionic Dark Matter. We explicitly calculate the annihilation cross section for different typologies of diagrams. We identify the most favourable scenarios, for which the behaviour of the cross section is given. We then describe the phenomenology of the leptophilic Dark Matter and show how experimental bounds on the neutrino flux coming from annihilations inside the Sun disfavour this model as explanation of the DAMA results. Finally, a carefull analysis of the neutrino flux expected from neutralino annihilations inside the Sun and the Earth is presented. We consider uncertainties coming from both particle physics and astrophysics and we divide the fluxes in through-going and stopping muons.

Contents

1 Introduction

The roots of our current knowledge and understanding of the Universe can be traced back to the 1929, when the Hubble's law was presented for the first time [1]. Edwin Hubble and Milton Humason proposed a linear proportionality between the redshifted light emitted from galaxies and their distances. If the redshift is interpreted as Doppler effect, related to the recession velocity of galaxies, the conclusion that the Universe is expanding will be reached. After this discovery, the idea of a static Universe has gradually been abandoned and the cosmological models of Big Bang began to take over. Nowadays, after the recent data from type-Ia supernovae [2], we know that the expansion of the Universe is accelerating.

Results from many different observations, carried out in the past decades, have provided a precise understanding of the composition of our Universe, bringing cosmology to face its "golden age". In particular, a lot of different experimental evidences point towards the existence of a form of non-luminous matter, baptized with the name "Dark Matter", which should account for almost 23% of the total mass-energy of the Universe and for almost 84% of its mass. Thus, by far most of the Universe is made of a kind of matter different from ordinary one.

One of the most exciting and difficult challenges of particle physics is to understand the real nature of Dark Matter (DM). A rich zoo of candidates for DM is present in the literature. All these particles arise in theories beyond the Standard Model (SM) of particle physics. However, depending on the model, the characteristics of the DM particle can be rather different and the values of the mass and the scattering cross section can vary within several orders of magnitude.

This ignorance might be partially attenuated by the investigation of physics at the electroweak (EW) scale, that will be provided by the Large Hadron Collider (LHC) at CERN. Since the end of November 2009, the LHC is operating again and its forthcoming results will hopefully be fundamental to test the physics beyond the SM. At the same time, it will be able to restrict the viable DM candidates among those with masses around

the EW scale.

Despite that, even with the detection of a new particle that could successfully act as DM, the accelerator experiments cannot directly prove that the same particle is present in the galactic halo. For this reason, direct detection experiments that search for scattering of DM particles off atomic nuclei inside a detector are fundamental. There are several experiments now running and taking data, which use different materials and detection techniques. Among them, only the DAMA experiment has searched for a model-independent DM signature: an annual modulation in the count rate due to the Earth's motion with respect to the Sun. In April 2008, the DAMA collaboration has released new data [3], where a modulated signal is detected at $8.2\,\sigma$ confidence level. These new results have received particular attention from the theoretical particle physics community, in the attempt of reconciling them with the negative results from the other direct detection experiments. So far, the DAMA experiment is the only one that has claimed a detection of DM.

Another possibility to detect DM is to search for its annihilation products (such as γ-rays, antimatter and neutrinos) in the Milky Way galactic center and in the galactic halo, in dwarf spheroidal galaxies and in celestial bodies, like the Earth or the Sun. Recently, there arose an increased interest in this field, in particular due to the cosmic ray anomaly revealed at the end of October 2008 by the satellite experiment PAMELA [4]. An excess in the positron flux has been detected, while no excess has been found for antiprotons. This anomaly could be caused by DM annihilation in the galactic halo or by astrophysical objects such as pulsars.

The annihilation of DM particles can produce also high-energy neutrinos, which can be detected through water Cherenkov detectors, like Super-Kamiokande [5], or through neutrino telescopes, like IceCube [6], ANTARES [7] and its future extension KM3Net [8]. Being neutral, neutrinos are not deflected by magnetic fields and have only weak interactions, so they can travel unperturbed through the interstellar medium.

The role of neutrinos in physics is often compared to the one of X-rays in diagnostic radiography, since with their detection we are able to get an "image" of regions of space or of celestial bodies that are accessible only partially with other methods, if at all. A remarkable example is given by the measurements of the solar neutrino flux, through which the Standard Solar Model has been confirmed and important information on neutrinos has been derived, i.e., the resonant oscillation in matter. Now that we gained a good knowledge of the neutrino physics and of the neutrino oscillation parameters, it is possible to make precise predictions regarding the neutrino flux coming from DM annihilation.

It has been shown in several papers, see e.g. Refs. [9, 10, 11, 12], that this method represents a promising tool to detect DM, since neutrinos conserve directionality and are the only particle that can escape from celestial bodies with energies high enough to be detected. The common hope is that the solar neutrino example could be repeated and that now, through the analysis of the high-energy neutrino flux, we could obtain important information on DM properties, like branching ratios and the mass. No excess in the neutrino flux has been detected so far, with respect to the expected background.

However, the Super-Kamiokande limits, derived from analyses of the data collected from May 1996 to July 2001 [13], are able to put stringent bounds on the DM scattering and annihilation cross section. New future data will be able to restrict the allowed DM configurations even more or, maybe, to detect an important signal.

In this thesis, the indirect DM detection through the neutrino portal is considered. In Chapter 2, a brief review on the physics of DM is given. We report the main evidences and observations for DM and their main astrophysical uncertainty: the density profile of the DM in the halo. We also discuss the DM velocity distribution and the different detection methods. Finally, a summary of the most common candidates present in the literature will be given.

Chapter 3 focuses on the indirect search for DM using neutrinos. We explain how to calculate the neutrino flux from the Sun and the Earth, considering in particular the capture rate and the neutrino propagation aspects. Also the case of the galactic center is analyzed. We finally discuss the neutrino-muon conversion and the main present and future detectors.

In Chapter 4, a model-independent detailed analysis of the DM annihilation directly into neutrinos is given. We initially review the theory of massive neutrinos and the most common neutrino mass models. For each of these scenarios, we analyze the implications on the annihilation cross section, considering separately a scalar or a fermionic DM particle. We then identify the generically unsuppressed cases. For the most promising ones, we explicitly show the behaviour of the annihilation cross sections and the bounds coming from various experiments.

In Chapter 5, the indirect detection with neutrinos is compared with the results from direct detection experiments. In the first part, we present the phenomenology of the leptophilic DM and we reanalyze in this context the Super-Kamiokande bounds on the muon flux coming from the Sun. The obtained constraints are then confronted with the DAMA annual modulation region and with the limits from other direct detection experiments. In the second part, we consider the light neutralino as DM candidate, in the framework of an effective MSSM model. We derive the flux of stopping and through-going muons expected from all the allowed supersymmetric configurations and from those compatible with the DAMA results.

Finally, Chapter 6 contains a summary and the conclusions of our work.

The work presented in this thesis has been partially already published in Refs. [14, 15]. During my Ph.D., I have been involved also in other projects, on topics different from the ones contained in this thesis, see Refs. [16, 17, 18] for more details.

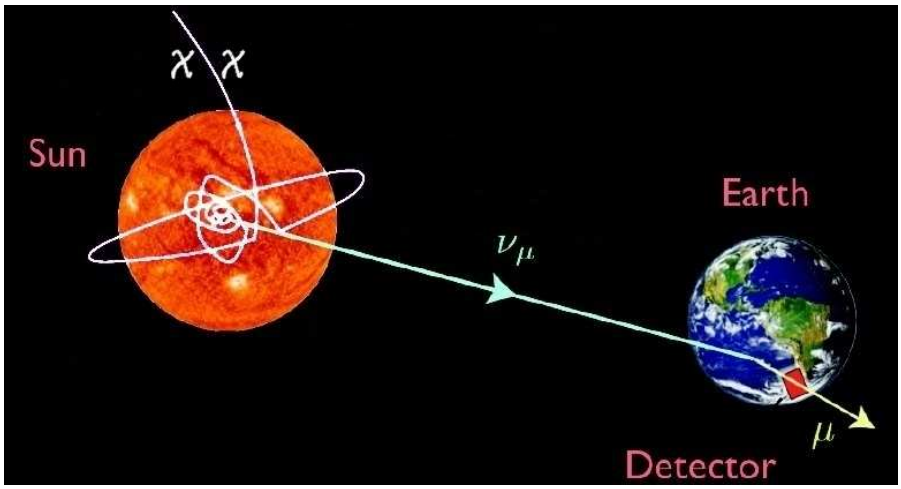

Figure 1.1: Schematic mechanism for indirect Dark Matter detection with neutrinos, in the case of annihilation inside the Sun.

2
The Dark Matter

In this Chapter, we review the physics of DM. In Sec. 2.1 we report the main cosmological evidences that point towards the DM postulation and in Sec. 2.2 we discuss the DM density profile in the galactic halo and its velocity distribution. The experimental methods to detect DM are presented in Sec. 2.3, while Sec. 2.4 contains a summary of the most important DM candidates. Exhaustive reviews on the DM topic are given in Refs. [19, 20, 21, 22].

2.1 Evidence and observations

To find the first origin of the DM idea, we have to go back to the 1933. Studying the Coma cluster, F. Zwicky found a discrepancy of two orders of magnitude between the mass inferred by dispersion velocity measurements of the galaxies in the cluster and the one expected by the analysis of the luminous components [23]. In 1936, S. Smith also arrived at a similar conclusion with an analysis of the Virgo cluster [24]. The subsequent evidences for DM arrived only after more than thirty years. V. Rubin and K. Ford measured in 1970 the velocity rotation curve of the Andromeda Nebula [25] and found a flat behaviour at large radii. Three years later, M. Roberts and A. Rots extended the analysis to different galaxy types [26]. A systematic study of the velocity dispersions in spiral galaxies was presented in 1980 by V. Rubin, K. Ford and N. Thonnard [27]. These last results blew away skepticisms and conviced the astronomy community that the presence of DM would be necessary to explain the rotation curves, if Newtonian dynamics was valid at the scale of galaxies and galaxy clusters. Indeed, applying the Newton's law of gravity, the rotational velocity as a function of the distance r is given by

$$v_{\rm rot}(r) = \sqrt{\frac{G\,M(r)}{r}}\,, \tag{2.1}$$

with G being Newton's gravitational constant and $M(r)$ the mass contained within a distance r from the center. The observation of flat rotation curves implies that the mass increases linearly with the distance from the center, in contrast to the distribution of luminous matter. Thus, we can picture galaxies and clusters as surrounded by a DM halo that is spherically distributed.

The analysis of rotation curves has been extended more recently to a large number of spiral galaxies, see for instance Ref. [28]. These observations represent one of the strongest hints for DM at the level of galaxies.

At the scale of clusters, compelling evidences for DM arise from gravitational lensing techniques. Einstein's theory of general relativity predicts that a massive object deforms the space-time curvature. Since the light rays follow geodesics, they are deflected by strong gravitational fields. The deviation from a straight-line path is proportional to the mass of the object, that acts like an optical lens. Usually, quasars are used as sources, since they are distant and very bright.

Two different types of gravitational lensing are manly used in DM searches: strong and weak lensing. In the first case, the bend in the light path is clearly detected by the presence of multiple images of the same object, arcs and Einstein rings. Studying these effects, it is possible to infer that DM is needed also at the scale of galaxy clusters [29]. In the case of weak lensing, instead, the deformations are much smaller and cannot be identified using only one source, since multiple images are not present. Therefore, a large number of galaxies is usually considered and a statistical analysis is done to reveal possible correlated distortions and elongations. From the shapes and orientations of the galaxies, the mass of the lens can be reconstruct. It has been shown in Ref. [30] that weak lensing represents a powerful tool to measure the presence of DM.

Two recent outstanding applications of the gravitational lensing methods are given by the so-called "Bullet Cluster" [31] and "Baby Bullet" [32] observations. They represent examples of collisions between two clusters of galaxies. During this process, the stars of the galaxies and the DM halos behave as collisionless components, since they interact only through gravity. Electromagnetic interactions, instead, affect strongly the intergalactic gas distributions that, as result, become separated from the galaxies. This can be seen by comparing the "image" of the colliding clusters in visible light, obtained by the Hubble telescope, and the one in X-rays, observed by Chandra. The DM distribution is then gathered from gravitational lensing methods and it is found to follow the luminous one. Since the hot gas represents most of the baryonic matter presents in the clusters, the result from gravitational lensing can be interpreted as a clear evidence for the presence of DM. Moreover, these observations are not only a success of the DM model, but also a robust disproval of MOND (Modified Newtonian dynamics) theories at the scale of galaxy clusters. Indeed, if a modification of Newton's law of gravity would be the explanation of the flat rotational curves, the lensing would follow the distribution of the hot interstellar medium, this being the major source of baryonic matter.

At cosmological scales, the most convincing evidence of dark matter arises from the analysis of the Cosmic Microwave Background (CMB). This electromagnetic radiation was first predicted by G. Gamow in 1946 [33] and later on discovered by A. Penzias

and R. Wilson in 1965 [34]. The CMB consists of relic photons that decoupled from the matter in the early Universe. The detection of this radiation is the most convincing confirmation of the Big Bang Model. For a review of the CMB physics, see Ref. [35].

The COBE satellite revealed that the CMB radiation follows a thermal black body spectrum with temperature $T = 2.728 \pm 0.004$ K (95% C.L.) [36]. It also detected for the first time some small fluctuations in the CMB temperature [37]. The anisotropies $\delta T/T$ were measured with precision by the WMAP satellites to be at the 10^{-5} level [38].

The measurements performed by WMAP have been fundamental to determine the geometry and composition of the Universe. They are considered as milestone for the actual model of cosmology. After WMAP, our Universe appears as flat and dominated by an unknown form of energy, called "Dark Energy", which is usually denoted by the Greek letter "Λ". The CMB observations are also a key ingredient to obtain with good accuracy the actual amount of DM, which amounts to about 23% of the total mass-energy of the Universe.

To define the content of the Universe, the density parameter $\Omega_i = \rho_i/\rho_c$ is usually introduced. The critical density ρ_c is the density at which the Universe has a vanishing spatial curvature:

$$\rho_c = \frac{3H_0^2}{8\pi G} \simeq 1.9 \times 10^{-29}\, h^2 \ \mathrm{g\,cm^{-3}}\,, \tag{2.2}$$

where H_0 is the Hubble constant at the present time, which is commonly rewritten as $H_0 = 100\, h$ km Mpc^{-1} s^{-1}. From the five-years WMAP data, the following parameters at 1σ confidence level are found [39]:

$$\Omega_\Lambda = 0.742 \pm 0.030\,, \tag{2.3}$$

$$h = 0.719^{+0.026}_{-0.027}\,, \tag{2.4}$$

$$\Omega_{DM} h^2 = 0.1099 \pm 0.0062\,, \tag{2.5}$$

$$\Omega_b h^2 = 0.02273 \pm 0.00062\,, \tag{2.6}$$

where with Ω_b we have denoted the density fraction of baryons present in the Universe. It is remarkable that the value of $\Omega_b h^2$ obtained with WMAP is in good agreement with the one obtained through Big Bang Nucleosynthesis [40]. The current dominance of Dark Energy (DE) has also been confirmed by observations of type-Ia supernovae [2]. The data from galaxy clusters, CMB and supernovae are combined all together to derive with high precision the matter and energy contents of the Universe. The complementarity of these observations is clearly visible in the left panel of Fig. 2.1.

The presence of DM is fundamental to explain the formation processes of stars, galaxies and clusters. After recombination, the baryons collapse in structure, because they fall in the gravitational potential wells created by the DM. Depending on the type of DM, different structure formation scenarios are present. The DM is divided in two main categories: Hot Dark Matter (HDM), if the particles are relativistic when they decouple from the primordial plasma, and Cold Dark Matter (CDM), if they are non-relativistic. The first case will lead to a "top-down" structure formation, in which only clusters and superclusters of galaxies can initially form. All the structures at small scales are indeed

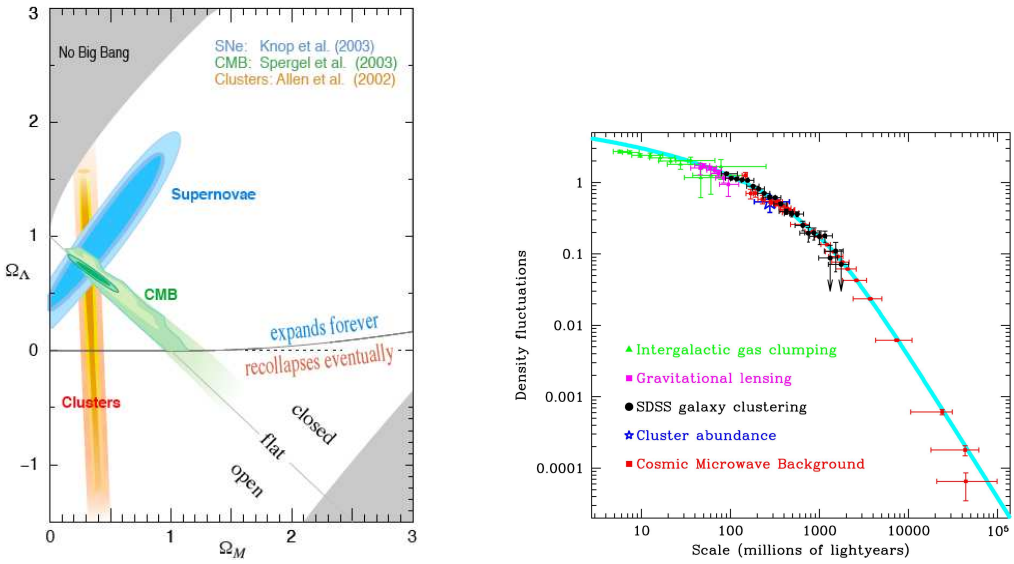

Figure 2.1: Concordance model of the Universe (left panel) and evidences for DM at different astrophysical scales (right panel).

washed out by the pressure of Hot Dark Matter. In the second case, instead, a "bottom-up" formation can be realized. Small structures collapse first and then merge together to form larger objects.

The Sloan Digital Sky Survey (SDSS) [41] and the 2dF Galaxy Redshift Survey (2dF-GRS) [42] are two galaxy surveys that are mapping portions of the sky. They have detected, respectively, over 800 000 and over 200 000 galaxies at different redshift. This information has allowed to study the large-scale structure of the Universe, revealing the presence of voids, filaments and walls.

The N-body computer simulations show that the hierarchical model of structure formation, driven by CDM, can reproduce the observed structure present in the Universe. These results are robust evidences that most of the DM should be present in the form of CDM.

We wish to recall that the bottom-up formation model is also supported by observations of the so-called Lyman-α Forest. This is a collection of Lyman-α absorption lines, caused by the presence of intergalactic gas, in high redshift ($z \simeq 2-4$) spectra of quasars. This set of data provides information on the distribution of neutral hydrogen, which is then compared to numerical simulations. The outcome is that the presence of CDM is essential to correctly reproduce the observed distributions, see e.g. Ref. [43].

All the observations described have been crucial to test the DM hypothesis at different astrophysical scales. A summary of all these evidences is given in the right panel of Fig. 2.1. The concordance between the different measurements has led to consider as the Standard Model of Big Bang Cosmology the one in which the Universe is constituted by

manly DE and CDM. This is commonly referred as "ΛCDM model".

2.2 Density and velocity distributions

The presence of DM at different astrophysical scales is confirmed by many observations, which we have summarized in the previous Section. On the other hand, the actual DM density distribution in the galaxies is still not known precisely. From the measurements of rotational curves, we know that the DM profile should decrease as $\rho_\chi \propto r^{-2}$, at large radii from the galactic center, but information on the innermost part is difficult to obtain from the data. For this reason, the N-body simulations represent the common tool used to derive DM profiles. This numerical method suffers, however, from numerous complications. Most notably, the fact that baryons are not included in the simulations makes it difficult to explore the very central region ($r \lesssim 1$ kpc) of the galaxies.

Moreover, the presence of a Supermassive Black Hole (SBH) in the inner part of a galaxy could change the DM distribution at very small scales. The models of adiabatic growth of a SBH predict the presence of a spike around the SBH [44]. In this case, the DM mass distribution would follow a power-law and the annihilation signals from the galactic center would be significantly increased.

However, it was pointed out in Ref. [45] that the merger history of the galaxy and the SBH can also influence the presence of the spike and that core scouring effects of merging black holes can actually reduced the DM density in the central region of the galaxies, see also Ref. [46].

Using N-body simulations results, the DM density profile $\rho(r)$ is usually parameterized as follows:

$$\rho(r) = \rho_0 \left(\frac{r_0}{r}\right)^\gamma \left(\frac{1+(r_0/r_s)^\alpha}{1+(r/r_s)^\alpha}\right)^{(\beta-\gamma)/\alpha} , \tag{2.7}$$

where the "scale radius" r_s is the distance at which $\rho \propto r^{-2}$, $r_0 = 8.5$ kpc is the distance of the Solar System from the galactic center and ρ_0 is the local DM density. The values of the parameters α, β, γ, r_s for the Isothermal [47], Navarro-Frenk-White [48] and Moore [49] profiles are reported in Tab. 2.1. Recent numerical simulations prefer the Einasto profile [50]:

$$\rho(r) = \rho_s \exp\left[-\frac{2}{\alpha}\left(\left(\frac{r}{r_s}\right)^\alpha - 1\right)\right] , \tag{2.8}$$

with α, ρ_s and r_s fixed to the values in Tab. 2.1. In Fig. 2.2 the different behaviours of the density profiles in the central region is clearly visible. We explicitly show also the extrapolation to the very small scale $r \lesssim 1$ kpc.

Beyond the density profiles described before, other scenarios are possible. In Ref. [51] these possibilities have been analyzed extensively. The DM density distributions were classified into the following categories: spherically symmetric matter density ρ with isotropic velocity dispersion, spherically symmetric matter density with non-isotropic velocity dispersion, axisymmetric models and triaxial models. For each model, the allowed ranges for the local DM density ρ_0 are derived. Assuming maximal or minimal non-halo

Halo model	α	β	γ	r_s[kpc]
Isothermal	2	2	0	5
NFW	1	3	1	20
Moore	1.5	3	1.5	28
Halo model	α	ρ_s[GeV/cm^3]	-	r_s[kpc]
Einasto	0.17	0.06	-	20

Table 2.1: Parameters for the Isothermal, NFW, Moore and Einasto Dark Matter density profiles.

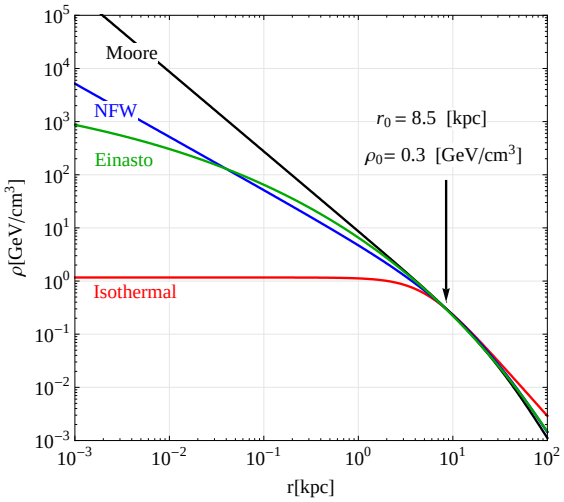

Figure 2.2: The different DM density profiles, as predicted by N-body simulations. The local DM density ρ_0 has been fixed to the default value of 0.3 GeV cm^{-3}.

components in the Galaxy, the intervals are determined using constraints on the local rotational velocity v_0 from the galactic rotational curve: 170 km s^{-1} $\leq v_0 \leq$ 270 km s^{-1} [52] at 90 % C.L.. A standard value of ρ_0, commonly used in the literature, is 0.3 GeV cm^{-3}.

If the density profile is an essential quantity for the estimation of the DM annihilation signal, the velocity distribution function $f_{\rm gal}(\mathbf{v})$ of DM particles at the Earth's location enters the calculation of even rates in direct detection experiments.

Once the density distribution ρ and the gravitational potential Φ are fixed, the six-dimensional phase-space distribution function $F_{\rm gal}(\mathbf{r}, \mathbf{v})$ can be determined using the method of Eddington. The velocity distribution function $f_{\rm gal}(\mathbf{v})$ is then given by $F_{\rm gal}(\mathbf{r}_0, \mathbf{v})$, where $\mathbf{r}_0 = (r_0, 0, 0)$ is the Earth's location in the Galaxy, with $r_0 \simeq 8.5$ kpc.

For spherically symmetric models with isotropic velocity dispersion, the local velocity distribution can be approximated by a Maxwell-Boltzmann distribution, which is usually truncated at a maximal escape velocity $v_{\rm esc}$, since DM particles with high kinetic energy

can escape the gravitational field of the Galaxy:

$$f_{\rm gal}(\mathbf{v}) = N\left(e^{-\mathbf{v}^2/v_0^2} - e^{-v_{\rm esc}^2/v_0^2}\right), \quad \text{for } v < v_{\rm esc}\,, \tag{2.9}$$

with N being a normalization factor. The common default values, compatible with rotational data, are $v_0 = 220$ km s^{-1} [52] and $v_{\rm esc} = 650$ km s^{-1} [51]. The root mean square velocity of the DM is thus given by $\bar{v} = \sqrt{3/2}\,v_0 \simeq 270$ km s^{-1}.

The DM velocity distribution in the Earth's reference frame $f(\mathbf{v})$ is obtained from the halo distribution function $f_{\rm gal}$ through a Galilean velocity transformation:

$$f(\mathbf{v}) = f_{\rm gal}(\mathbf{v} + \mathbf{w}_\oplus(t))\,, \tag{2.10}$$

where $\mathbf{w}_\oplus(t)$ is the velocity of the Earth in the galactic reference frame, whose modulus is given by

$$w_\oplus(t) = v_\odot + v_\oplus \cos\gamma \cos\left[\omega(t - t_0)\right]\,, \tag{2.11}$$

where $v_\odot \simeq (220 + 12)$ km s^{-1} is the Sun's velocity with respect to the galactic frame, including the local Keplerian velocity as well as the Sun's peculiar velocity, and $v_\oplus \simeq 30$ km s^{-1} is the velocity of the Earth relative to the Sun. The angle $\gamma \simeq \pi/3$ is the inclination of the ecliptic with respect to the galactic plane, $\omega = 2\pi/T$ with $T = 1$ year and $t_0 \simeq 2^{\rm nd}$ of June is the time of the year when the Earth's and Sun's velocities are aligned in the same direction. As we will discuss in Sect. 2.3.1, the motion of the Earth with respect to the Sun gives rise to a modulated even rate with a phase of 1 year, which can be revealed by direct detection experiments.

2.3 Dark Matter searches

In this Section we discuss the different DM searches. Sect. 2.3.1 is devoted to direct detection techniques, while in Sect. 2.3.2 the indirect detection methods are summarized. Finally, in Sect. 2.3.3, we present the actual limits provided by collider experiments. A review on DM searches is given in Ref. [53].

2.3.1 Direct detection

The presence of DM particles in the galactic halo could be incontrovertibly proved by the observation of their scatterings with the nuclei of a target material. To reveal the rare DM interactions, detectors must have high target mass, a precise control of the background and a low energy threshold. The nuclear recoil due to DM scattering off a nucleus can induce different signals inside a detector: heat deposition, ionization and scintillation. Most of the existing experiments are hybrid detectors that profit from the simultaneous measurement of two signals. We report in Tab. 2.2 the most important ones, divided according to their detection techniques.

Techniques	Experiments
Scintillation	DAMA, KIMS, ANAIS
Scintillation & Heat	CRESST
Scintillation & Ionization	ZEPLIN, XENON, WARP, ArDM
Ionization & Heat	CDMS, EDELWEISS
Bubble chamber	COUPP, PICASSO

Table 2.2: Direct detection experiments divided with respect to their detection techniques.

The differential event rate dR/dE_R for DM scattering, in units of counts per energy per kg detector mass per day, is given by the following expression:

$$\frac{dR}{dE_R} = \frac{\eta}{\rho_{\rm det}} \frac{\rho_\chi}{m_\chi} \int_{v \geq v_{\rm min}} d^3\mathbf{v} f(\mathbf{v})\, v\, \frac{d\sigma_N}{dE_R}(\mathbf{v}, E_R)\,, \tag{2.12}$$

where $E_R = E_\chi - E'_\chi$ is the recoil energy, i.e. the energy deposited in the detector, η is the number density of target particles, $\rho_{\rm det}$ is the mass density of the detector, ρ_χ is the local density of the DM particle χ and m_χ is its mass. The astrophysical uncertainties are contained in the local DM velocity distribution in the rest frame of the detector $f(\mathbf{v})$. We have denoted by $v_{\rm min}$ the minimal DM velocity that can lead to a recoil energy E_R (note that $v = |\mathbf{v}|$). For example, in the case of elastic scattering $\chi N \to \chi N$, $v_{\rm min} = [m_N E_R/(2\mu_N^2)]^{1/2}$, with $\mu_N = m_\chi m_N/(m_\chi + m_N)$ being the DM-nucleus reduced mass. Note that, if the target contains different elements (like in the case of NaI crystals), the sum over the corresponding counting rates is implied.

The differential cross section $d\sigma_N/dE_R$ encodes all particle and nuclear physics factors and is given by the sum of the spin-independent (SI) and the spin-dependent (SD) cross sections. Using the assumption of isotropy, the differential cross section can be rewritten at low energy as [54]

$$\frac{d\sigma_N}{dE_R}(\mathbf{v}, E_R) = \frac{1}{E_R^{\rm max}} \left(\sigma_N^{SI}\, F^2(E_R) + \sigma_N^{SD}\, \frac{S(E_R)}{S(0)} \right)\,, \tag{2.13}$$

where $\sigma_N^{SI,SD}$ is the zero momentum DM-nucleus effective cross-section and $E_R^{\rm max}$ is the maximum recoil energy that, for elastic scattering, is equal to $2\mu_N^2 v^2/m_N$. The functions $F(E_R)$ and $S(E_R)$ are, respectively, the SI and SD nuclear form factors. Different parameterizations for the SI form factor are used in the literature. The simplest one is given by an exponential function,

$$F(E_R) = \exp(-E_R/(2\, q_0))\,, \tag{2.14}$$

with $q_0 = 3\hbar^2/(2m_\chi R_0^2)$ and R_0 being the nuclear radius

$$R_0 = [0.91\,(m_N/\text{GeV})^{1/3} + 0.3] \times 10^{-15}\,\text{m}\,. \tag{2.15}$$

Another common parameterization is represented by the Helm form factor, defined as

$$F(E_R) = 3\, e^{-\kappa^2 s^2/2}\, \frac{\sin(\kappa r) - \kappa r \cos(\kappa r)}{(\kappa r)^3}\,, \tag{2.16}$$

with $\kappa = \sqrt{2\, m_N\, E_R}$, $s = 1$ fm, $r = \sqrt{R^2 - 5s^2}$ and $R = 1.2$ fm $A^{1/3}$.

The SD form factor is instead cast in the form:

$$S(E_R) = (a_p + a_n)^2 S_{00}(E_R) + (a_p - a_n)^2 S_{11}(E_R) + (a_p + a_n)(a_p - a_n) S_{01}(E_R)\,, \tag{2.17}$$

with a_p and a_n being the DM couplings to protons and neutrons. The functions S_{00} and S_{11} are, respectively, the isoscalar and isovector spin-dependent form factors and S_{01} is the interference term.

The cross section on protons and neutrons, $\sigma_{p,n}^{SI,SD}$, are then related to the ones on nuclei, $\sigma_N^{SI,SD}$, by the simple relations

$$\sigma_N^{SI} = \frac{[Z f_p + (A - Z) f_n]^2}{f_{p,n}^2} \frac{\mu_N^2}{\mu_p^2} \sigma_{p,n}^{SI}\,, \tag{2.18}$$

$$\sigma_N^{SD} = \frac{4}{3}\, \lambda_{p,n}^2 J(J+1) \frac{\mu_N^2}{\mu_p^2} \sigma_{p,n}^{SD}\,, \tag{2.19}$$

where μ_p is the reduced DM-proton mass, A is the atomic mass number, Z is the atomic number and $f_{p,n}$ are the couplings of the DM to protons and neutrons. We have denoted by J the total angular momentum of the nucleus and

$$\lambda_{p,n} = \frac{a_p \langle S_p \rangle + a_n \langle S_n \rangle}{a_{p,n}\, J}\,, \tag{2.20}$$

with $\langle S_p \rangle$ and $\langle S_n \rangle$ being the averaged spin expectaction values of the proton and the neutron inside the nucleus.

Note that, from the experimental measurements of the even rates dR/dE_R, it is possible to derive information on the quantity $\rho_\chi \sigma^{SI,SD}$ only, for a fixed velocity distribution function $f(\mathbf{v})$. Indeed, in general, the DM could consist of different components, with densities much smaller than the standard value 0.3 GeV cm^{-3}.

Since the velocity distribution function $f(\mathbf{v})$ is a function of time, as discussed in Sect. 2.2, also the DM rate is expected to vary during the year, due to the motion of the Earth around the Sun. Therefore, in each energy bin k, the number of signal events is given by

$$S_k = \int_{E_k} dE_R\, \frac{dR}{dE_R} \simeq S_{0,k} + S_{m,k} \cos\left[\omega (t - t_0)\right]\,, \tag{2.21}$$

where $S_{0,k}$ is the average signal, $S_{m,k}$ is the modulation amplitude, $\omega = 2\pi/T$ with $T = 1$ year, and $t_0 = 152.5$ days (corresponding to the 2^{nd} of June). The function $S_{m,k}$ can be approximated as

$$S_{m,k} \simeq \frac{1}{2} \left(\int_{E_k} dE_R\, \frac{dR}{dE_R}(\text{June 2}) - \int_{E_k} dE_R\, \frac{dR}{dE_R}(\text{December 2}) \right)\,. \tag{2.22}$$

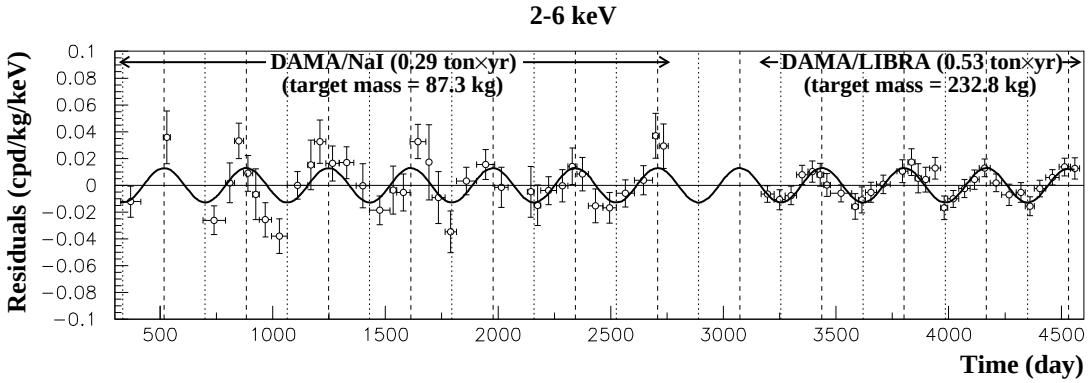

Figure 2.3: The time-dependent residual rate in the DAMA/NaI and in the DAMA/LIBRA annual modulation experiments. Figure taken from Ref. [3].

A seasonal effect in the count rate is identified as being due to the DM scatterings, in case the following requirements are fullfilled: it is modulated as a cosine function with a period of one year, a peak around the 2$^{\text{nd}}$ of June is present and a modulation amplitude $\leq 7\%$ is observed. Moreover, since the modulation is due to DM induced recoils, it must be present only in the low energy bins and only in the single hit events. It is really difficult that systematic effects can fulfil all these requirements.

The investigation of the annual modulation signature has been carried out by the DAMA collaboration, with the use of scintillation light from NaI(Tl) crystals as detection technique. They have collected data with the DAMA/NaI detector [53], over 7 annual cycles, and with the DAMA/LIBRA detector [3], over 4 annual cycles, corresponding to a total exposure of 0.82 tons yr. The combined results show a modulation signal with $8.2\,\sigma$ significance, as can be clearly seen in Fig. 2.3.

The interpretation of this seasonal variation as caused by DM elastic scatterings on nuclei is tightly constrained by bounds coming from other direct detection experiments. In particular, in the case of the spin-independent cross section, only a light DM particle with mass of the order $m_\chi \lesssim 10$ GeV might be marginally compatible with the limits from CDMS [55] and XENON10 [56], see Refs. [57, 58, 59, 60, 61, 62, 63, 64] for recent works. In the case of the spin-dependent cross section, instead, the DAMA annual modulation region is not in conflict with CDMS and XENON10 limits, but strong constraints from the COUPP [65], KIMS [66] and PICASSO [67] experiments apply [63]. Note that here and in the following we use the acronym "DAMA" to denote the combined DAMA/NaI and DAMA/LIBRA data.

An important and still not completely clarified aspect of the direct detection search is represented by the channeling effect [68]. The scattered nucleus loses its energy by electromagnetic and nuclear interactions, but only the first kind of interaction leads to a scintillation signal in the detector. Therefore, in general, just a fraction q of the total nuclear recoil energy E_R is measured. The event energy is measured in equivalent electron

energy (in keVee), defined by $q \times E_R$ for the total nuclear recoil energy E_R in keV. The parameter q si called "quenching factor" and for the nuclei in the DAMA detector, one has that $q_{Na} \simeq 0.3$ and $q_I \simeq 0.085$. In Refs. [68, 69] it has been pointed out that particles travelling along crystal planes lose all their energy electronically and thus $q \sim 1$. These are called "channeled events". So far this effect has not been confirmed experimentally in the relevant energy range [70]. However, if present, the channeling effect could play an important role in the analysis of the DAMA data, since it could sizably shift the annual modulation region [68].

If more complicated scenarios than elastic scattering are considered, the formulae for the event rates might change and the partial discrepancy between the DAMA result and other experiments might be attenuated. For example, this is the case for inelastic DM scattering off nuclei, see Sect. 2.4.2 for more details. In this scenario, the expression for $v_{\rm min}$ is modified and the DAMA allowed region, derived for a spin-dependent interaction, would be in agreement with all the experimental data [71]. A lot of other models have been proposed to reconcile all the results of direct detection experiments. These include mirror world DM [72], DM with electric or magnetic dipole moments [73] and leptophilic DM [14].

The CDMS collaboration has recently released new results [74], in which two events survive after background reduction. These could be due to DM interactions inside the detector at 90% confidence level.

Finally, we want to remember that the velocity distribution function of DM particles can influence the DM event rate in direct detection experiments. This effect has been recently analyzed in Ref. [75].

2.3.2 Indirect detection

In this Section we summarize the main indirect DM searches. A detailed review on this topic is given in Ref. [76].

Monochromatic photons with energy $E_\gamma \simeq m_\chi$ would represent a clear DM signature. Unfortunately, they can only be produced at one-loop level, since the DM particle is electrically neutral. Thus, the branching ratio for this channel is usually suppressed. There are, however, four other processes through which γ-rays can be produced by DM annihilation: i) bremsstrahlung emission by charged particles; ii) decays of hadrons, like π^0, coming from quark hadronization; iii) annihilation into three-body final states, one of which is a photon; iv) synchrotron radiation due to $e^\pm$ propagation in the galactic magnetic field. Searches for γ-rays from DM annihilation in the galactic center, in the galactic ridge and in dwarf spheroidal satellite galaxies are carried out by the HESS telescope [77] and by the Fermi space satellite [78].

The PAMELA (Payload for Anti-Matter Exploration and Light-nuclei) satellite [4] and the balloon experiments ATIC [79] and PPB-BETS [80] have recently obtained important results on positron and antiproton searches.

The PAMELA satellite revealed an excess in the positron fraction, starting from energies of 10 GeV, while no excess with respect to the background estimation was reported

in the antiproton flux, see the upper panel of Fig. 2.4. In Ref. [81], the authors have systematically studied the possibilities to fit these experimental data under the hypothesis that the PAMELA anomaly in the cosmic ray flux is due to DM annihilations. They identified two different scenarios in which a satisfactory fit could be obtained: i) the DM particle annihilates predominantly into leptons and has a mass above a few hundred GeV; ii) the DM particle annihilates into W, Z or Higgses and has a mass greater than 10 TeV. These characteristics are rather exotic, since most of the theoretical models predicts a DM particle with a mass lower than $\mathcal{O}$(TeV) and with a negligible branching ratio into leptons. A possibility to explain the PAMELA data with DM is represented by a leptophilic DM, that we will briefly discuss in Sect. 2.4.3.

The DM framework is not the only possibility to explain the PAMELA anomaly. Indeed, an astrophysical nearby electron source, like a pulsar or a supernova remnant, could account for the excess in the positron fraction [82]. Moreover, the claim of DM evidence from these data is, to some extend, model-dependent, since the estimation of the astrophysical background flux suffers from big uncertainties [83].

A rise in the total flux of positrons and electrons has been measured for the first time by the PPB-BETS experiment. More recently, the ATIC balloon has detected the presence of an abrupt peak at energies of about 400-500 GeV. This last result has catalyzed a lot of attention, since for its particular spectral feature it could be interpreted as a DM annihilation signal. However, the HESS [84] and Fermi [85] data do not confirm the presence of this peak. They, instead, report a more smooth behaviour, but an excess is still present respect to the conventional expected background. These experimental results are reported in the lower panel of Fig. 2.4.

Severe constraints on the DM interpretation of the PAMELA/Fermi anomaly arise from the analysis of the photon flux produced by charged particles. While propagating in the Galaxy, the $e^{\pm}$ can undergo inverse Compton scattering with the photons of the starlight, of the infrared light or of the CMB. The production of γ-rays through this mechanism should not exceed the existing limits provided by HESS and FERMI. Moreover, the synchrotron radiation bounds coming from radio observations represent another strong constraint on the DM annihilation scenario. Both γ-rays and synchrotron emission prefer a cored isothermal DM density profile. Indeed, a steep DM density profiles, like NFW, Moore and Einasto, would easily violate the experimental bounds, see e.g. Ref. [86].

The DM particles could also be indirectly detected by two other annihilation products: antideuterons and neutrinos. The GAPS [87] and AMS-02 [88] experiments search for antideuterons $\bar{D}$ from DM annihilations in the galactic center and in the galactic halo. The indirect detection technique through neutrinos, will be presented in detail in Chapter 3.

2.3.3 Collider experiments

The bound from the Z-boson decay width is one of the strongest constraints imposed by collider experiments on a light DM particle χ. From the analysis of the data from the

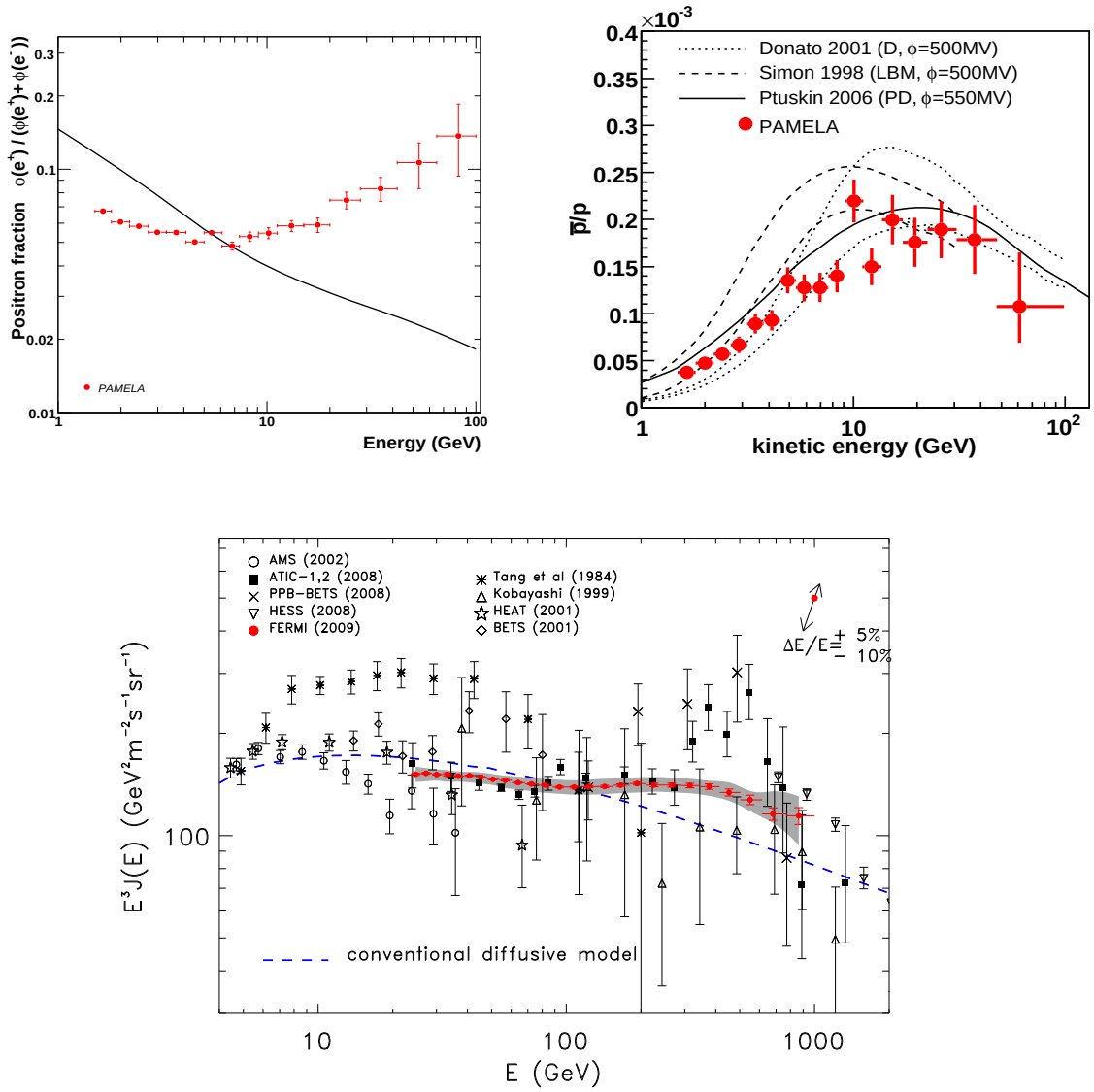

Figure 2.4: Data from the PAMELA satellite on the positron fraction and on the antiproton flux (upper panel), figures taken from Ref. [4]. The spectrum of electron plus positron, provided by the Fermi satellite (lower panel), figure taken from Ref. [85].

e^+e^- collider experiment LEP2, the decay width $\Gamma_{Z\to\chi\chi}$ is required to be less than 4.2 MeV [89].

Existing limits on the mass of DM candidates are, unfortunately, strictly dependent on the specific model considered. Indeed, experimental bounds have usually been placed on new electrically charged particles. From LEP2 data, their masses are now forced to be greater than 100 GeV. Once a particular model is fixed, these limits can be translated to limits on the DM mass. The most common example is represented by supersymmetric models with gaugino mass unification at the GUT scale (we refer to Sect. 2.4.1 for more details on Supersymmetry and its DM candidates). In this specific framework, the mass of the lightest neutralino is set to be equal to half the mass of the charginos. Thus, in this case, the allowed range on the chargino mass, $m_{\tilde{\chi}_1^\pm} \gtrsim 103$ GeV, implies a lower limit of about 50 GeV on the lightest neutralino. However, we want to stress that no bound on the lightest neutralino mass is predicted by collider experiments, in the case that no gaugino mass unification is assumed.

Important constraints on new particles and on new physics models are provided by electroweak precision measurements, carried on by the LEP2 and Tevatron experiments. The precision data are commonly expressed using the Peskin-Takeuchi parameters: S, T and U. The best-fit value on the S parameter disfavours new chiral fermions beyond the SM ones, while the T parameter sets a limit on the vacuum expectaction value of new non-singlet scalars [89]. The U parameter, instead, is defined as $(S_W - S_Z)$, with $S_W\,(S_Z)$ given by the difference between the W-boson (Z-boson) self-energy at $Q^2 = M_W^2\,(M_Z^2)$ and $Q^2 = 0$. Other robust limits can be inferred from the following experimental searches: measurements of the $b \to s + \gamma$ decay process, with an actual limit of $2.89 \leq B(b \to s + \gamma) \times 10^{-4} \leq 4.21$ [90]; measurements of the muon anomalous magnetic moment $a_\mu \equiv (g_\mu - 2)/2$, whose deviation Δa_μ from the theoretical evaluation within the SM is equal to $(-98 \leq \Delta a_\mu \times 10^{11} \leq 565)$ [91]; the upper bound on the branching ratio $BR(B_s^0 \to \mu^- + \mu^+)$, that is set to $BR(B_s^0 \to \mu^- + \mu^+) < 1.2 \times 10^{-7}$ [92]. All these constraints have to be taken into account when a specific DM candidate is considered. For an exhaustive explanation of the different experimental searches at colliders, regarding Supersymmetry and New Physics in general, we refer to Ref. [89].

Through the future LHC proton-proton collisions at 14 TeV center-of-mass energy, new important results on physics beyond the SM can be achieved. These will provide further strong hints for a specific DM candidate. However, in most of the models present in the literature, the DM particle can, in general, be produced at colliders only after a long decay chain, which makes the extrapolation of its properties rather involved. For instance, in the case of supersymmetric models, we could have $\tilde{q} \to \tilde{\chi}_2^0 q \to \tilde{l} l q \to \tilde{\chi}_1^0 l l q$, where we have denoted the lightest neutralino by $\tilde{\chi}_1^0$. The precise value of its mass could be extracted by an analysis of the mass distribution endpoints or "edges". For a dedicated description of this method, we refer to Ref. [93]. Moreover, to disentangle different models with DM candidates, for example Supersymmetry and Extra Dimensions, it is fundamentally important to measure the spin of the lightest neutral particle produced in the decay chain. This possibility has been vastly analyzed in Ref. [94].

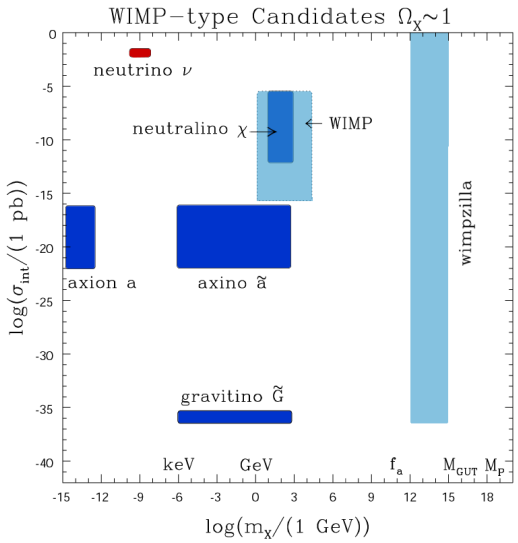

Figure 2.5: Summary of the most common Dark Matter particles as a function of their masses and cross sections, taken from Ref. [97].

2.4 Dark Matter candidates

Astrophysics provides us with compelling evidences of DM. Unfortunately, on the particle physics side, several models predict candidates with rather different characteristics: the DM mass can range from about 10^{-15} GeV to 10^{15} GeV and the scattering cross section can span several order of magnitude, from around 10^{-35} pb to 1 pb. The various possibilities for DM candidates fulfill, however, some common properties: the DM particle is stable or at least very long-lived and neutral under electric charge and colour charge.

In Sect. 2.4.1, we focus on Weakly Interacting Massive Particles (WIMPs) as DM candidates, while in Sect. 2.4.2, we summarize the more common non-WIMP candidates. The different characteristics for each model can be seen in Fig. 2.5. In Sect. 2.4.3, we also report examples of DM particles with more exotic interactions. For recent reviews on DM candidates we refer to Refs. [95, 96].

2.4.1 WIMP candidates

The WIMPs are the more common DM candidates considered in the literature. These are particles created thermally in the Early Universe, with a weak cross section and with a mass around the EW scale. The main motivation for the WIMP hypothesis is that its characteristics are sufficient to obtain a relic density in agreement with the WMAP data, reported in Eq. (2.5). This prediction is the so-called "WIMP miracle".

The complete relic abundance calculation for a thermal relic χ is reported in Ref. [98], to which we refer for more details. Here, we just report the final expression that can be

cast as

$$\Omega_\chi h^2 = \frac{x_f}{g_{*s}^{1/2}(T_f)} \frac{3.3 \times 10^{-38}\,\mathrm{cm}^2}{\langle \sigma_{\mathrm{ann}} v \rangle_{\mathrm{int}}} \,. \tag{2.23}$$

In the previous formula, we have defined the variable x as m_χ/T, with m_χ being the mass of the thermal relic and T the temperature of the Universe. Its value at the freeze-out temperature T_f is denoted with x_f. The function g_{*s} encodes the number of relativistic degrees of freedom:

$$g_{*s} = \sum_{i=\mathrm{bosons}} g_i \left(\frac{T_i}{T}\right)^3 + \frac{7}{8} \sum_{i=\mathrm{fermions}} g_i \left(\frac{T_i}{T}\right)^3 \,, \tag{2.24}$$

where the factor 7/8 for fermions arises from Fermi-Dirac statistics, on the contrary to the Bose-Einstein one. Finally, $\langle \sigma_{\mathrm{ann}} v \rangle_{\mathrm{int}}$ is the thermally-averaged annihilation cross section, integrated with weight $1/x^2$ from the freeze-out till today:

$$\langle \sigma_{\mathrm{ann}} v \rangle_{\mathrm{int}} = \int_{x_f}^{\infty} dx \, \frac{1}{x^2} \, \langle \sigma_{\mathrm{ann}} v \rangle_x \simeq a + \frac{b}{2x_f} \,, \tag{2.25}$$

where we have used the low velocity expansion $\langle \sigma_{\mathrm{ann}} v \rangle_x \simeq a + b/x$, for the DM being a non-relativistic particle.

The approximate freeze-out temperature can be found using the following equation [98]:

$$x_f + \frac{1}{2} \ln\left(x_f \, g_*(T_f)\right) = \ln\left(9 \times 10^{10} \, g \, \frac{m_\chi}{100\,\mathrm{GeV}} \, \frac{\langle \sigma_{\mathrm{ann}} v \rangle_{x_f}}{5 \times 10^{-37}\,\mathrm{cm}^2}\right) \,, \tag{2.26}$$

where g is the number of degrees of freedom of the DM particle and

$$g_* = \sum_{i=\mathrm{bosons}} g_i \left(\frac{T_i}{T}\right)^4 + \frac{7}{8} \sum_{i=\mathrm{fermions}} g_i \left(\frac{T_i}{T}\right)^4 \,. \tag{2.27}$$

Considering $m_\chi \simeq 100$ GeV, $g = 2$ and $\langle \sigma_{\mathrm{ann}} v \rangle_{x_f} \simeq 5 \times 10^{-37}\,\mathrm{cm}^2$, Eq. (2.26) leads to $x_f \simeq 20$ and, correspondingly, $g_*(T_f) \simeq 80$. Using these values with Eq. (2.23), we find $\Omega_\chi h^2 \simeq 0.15$, in agreement with the 1σ range allowed by WMAP data.

The main WIMP candidates arise from New Physics models at the EW scale. These proposed high-energy theories attempt to solve some of the problems of the SM, in particular the one-loop quadratically divergent quantum corrections to scalar masses, also called the "hierarchy problem" [99].

In the following, we briefly discuss the WIMP candidates present in three extensions of the SM: Supersymmetry, Extra Dimensions and Little Higgs theories. In each of these different models, the WIMP candidate is stable, because it is protected by a conserved quantum number: R-parity, K-parity and T-parity, respectively.

Supersymmetric particles

Supersymmetric theories are based on a symmetry between fermions and bosons [99, 100].

Minimal Supersymmetric Standard Model		
Interaction eigenstates		Mass Eigenstates
$\tilde{q}_L, \tilde{q}_R$	squark	$\tilde{q}_1, \tilde{q}_2$
$\tilde{l}_L, \tilde{l}_R$	slepton	$\tilde{l}_1, \tilde{l}_2$
$\tilde{\nu}_L$	sneutrino	$\tilde{\nu}_L$
$\tilde{g}$	gluino	$\tilde{g}$
$\tilde{W}^{\pm}$	wino	$\tilde{\chi}^{\pm}_{1,2}$
$\tilde{H}^{\pm}$	higgsino	charginos
$\tilde{B}$	bino	
$\tilde{W}^3$	wino	$\tilde{\chi}^0_{1,2,3,4}$
$\tilde{H}^0_u$	higgsino	neutralinos
$\tilde{H}^0_d$	higgsino	

Table 2.3: Particle content of the MSSM. We report explicitly the interaction and mass eigenstates.

The Minimal Supersymmetric Standard Model (MSSM) is the minimally supersymmetric version of the SM, in which to each fermion of the SM there is an associated spin-0 particle and to each Higgs or gauge boson there is a spin-1/2 particle. We wish to recall that two Higgs doublets are necessary in the MSSM to avoid gauge anomalies. In Table 2.3 we list all the particles present in the MSSM and their corresponding names.

No experimental observations have been found so far for the existence of superpartners. These particles, if they exist, are thus forced to be heavier than their SM companions and Supersymmetry (SUSY) is expected to be a broken symmetry. The simplest way to break SUSY is through the introduction of "soft terms" in the MSSM Lagrangian [99]. These are terms that explicitly break SUSY, without introducing ultraviolet divergences.

If we wrote in the superpotential W all the possible gauge invariant and renormalizable terms, we would obtain a theory that violates both baryon number B and lepton number L. This would lead to extremely fast proton decay, in contrast to the experimental data that set the proton lifetime to be $\mathcal{O}(> 10^{33})$ years. This problem is easily overcome with the postulation of a Z_2 symmetry called "R-parity", defined as

$$P_R = (-1)^{3(B-L)+2s}\,, \tag{2.28}$$

where s is the spin of the particle. For all the SM particles $R = 1$, while for the superpartners $R = -1$. If R-parity is conserved, the interaction terms that lead to proton decay are forbidden. Moreover, the lightest supersymmetric particle (LSP) represents a well motivated DM candidate, in case it is neutral. Indeed, the LSP has to be stable, since it cannot decay to SM particles without violating R-parity. A review on SUSY DM

is given in Ref. [101] and its collider, direct and indirect detection has been analyzed in Ref. [102].

In most of the SUSY models, the LSP is the lightest one of the neutralinos $\tilde{\chi}_1^0$. Neutralinos are four mass eigenstates, given by linear combinations of the bino $\tilde{B}$, the neutral wino $\tilde{W}^3$ and of the two Higgsino states $\tilde{H}_d^0$, $\tilde{H}_u^0$:

$$\tilde{\chi}_i^0 \equiv a_1^{(i)}\tilde{B} + a_2^{(i)}\tilde{W}^3 + a_3^{(i)}\tilde{H}_d^0 + a_4^{(i)}\tilde{H}_u^0 \qquad (i = 1, 2, 3, 4)\,. \tag{2.29}$$

These states are eigenstates of the following mass matrix:

$$M_{\tilde{\chi}^0} = \begin{pmatrix} M_1 & 0 & -m_Z\, c_\beta\, s_{\theta_W} & m_Z\, s_\beta\, s_{\theta_W} \\ 0 & M_2 & m_Z\, c_\beta\, c_{\theta_W} & -m_Z\, s_\beta\, c_{\theta_W} \\ -m_Z\, c_\beta\, s_{\theta_W} & m_Z\, c_\beta\, c_{\theta_W} & 0 & -\mu \\ m_Z\, s_\beta\, s_{\theta_W} & -m_Z\, s_\beta\, c_{\theta_W} & -\mu & 0 \end{pmatrix}, \tag{2.30}$$

where we have used the notation $c_\alpha \equiv \cos\alpha$ and $s_\alpha \equiv \sin\alpha$. The angle β is related to the ratio of the Higgs vacuum expectaction values $v_u = \langle H_u^0 \rangle$ and $v_d = \langle H_d^0 \rangle$:

$$\tan\beta = v_u/v_d\,, \tag{2.31}$$

with $v_u^2 + v_d^2 \sim (174\text{GeV})^2$. The angle θ_W is the Weinberg angle, whose value at the Z-boson mass scale is $\sin^2\theta_W \simeq 0.23120$.

The μ parameter in the neutralino mass matrix comes from the Higgs mixing mass term present in the superpotential of the MSSM:

$$W_{\text{MSSM}} \supset \mu(H_u)_\alpha(H_d)_\beta\epsilon^{\alpha\beta} = \mu(H_u^+ H_d^- - H_u^0 H_d^0)\,, \tag{2.32}$$

where we have denoted by $H_u = (H_u^+, H_u^0)$ and $H_d = (H_d^0, H_d^-)$ the chiral superfields and with $\alpha, \beta = 1, 2$ the weak isospin indices. The parameters M_1 and M_2 come from the bino $\tilde{B}$ and winos $\tilde{W}^i$ mass terms present in the soft SUSY breaking Lagrangian:

$$\mathcal{L}_{\text{MSSM}}^{\text{soft}} \supset -\frac{1}{2}(M_1\tilde{B}\tilde{B} + M_2\tilde{W}^i\tilde{W}^i + M_3\tilde{g}\tilde{g} + c.c.)\,, \tag{2.33}$$

where, for completeness, we have also reported the gluino $\tilde{g}$ soft breaking mass term.

The gaugino mass parameters M_i $(i = 1, 2, 3)$ are in principle free parameters, but they are usually assumed to unify to a common value called $m_{1/2}$ at the Grand Unified (GUT) scale $M_{\text{GUT}} \sim 2 \times 10^{16}$ GeV, where the gauge couplings of the MSSM unify [99]. Using the renormalization group equations, it is possible to derive the following relation between M_1 and M_2:

$$M_1 = \frac{5}{3}\tan^2\theta_W M_2\,, \tag{2.34}$$

valid at each energy scale. In particular, at the EW scale, the following relation holds:

$$M_1 \simeq 0.5\, M_2\,. \tag{2.35}$$

If the gaugino soft breaking parameters, M_1 and M_2, and the Higgs mixing parameter μ are much greater than the electroweak scale, i.e. $M_1, M_2, \mu \gg m_Z$, the neutralino eigenstates assume the following approximate compositions:

$$\tilde{\chi}_i^0 \simeq \{\tilde{B}, \tilde{W}^3, \frac{1}{\sqrt{2}}(\tilde{H}_d^0 - \tilde{H}_u^0), \frac{1}{\sqrt{2}}(\tilde{H}_d^0 + \tilde{H}_u^0)\}\,, \tag{2.36}$$

with mass values given by

$$m_{\tilde{\chi}_i^0} \simeq \{M_1, M_2, |\mu|, |\mu|\}\,. \tag{2.37}$$

From the previous expressions, we can trace the two asymptotic behaviours of the lightest neutralino. For large values of the soft breaking parameters M_1 and M_2, $\tilde{\chi}_1^0$ is "higgsino-like", with a mass determined mainly by the μ value: $m_{\tilde{\chi}_1^0} \simeq \mu$; on the contrary, for large values of μ, the lightest neutralino is "bino-like", with $m_{\tilde{\chi}_1^0} \simeq M_1 \simeq 0.5\, M_2$.

The LEP2 experiment has searched for charginos through the channel $e^+e^- \to \tilde{\chi}_1^+\tilde{\chi}_1^-$, where $\tilde{\chi}_1^\pm$ denotes the lightest chargino. The experimental lower bound of $m_{\tilde{\chi}_1^\pm} \gtrsim 103$ GeV can be considered as a lower bound also on the M_2 and μ parameters ($M_2, \mu \gtrsim 103$ GeV), since the chargino mass matrix in the basis $(\tilde{W}^+, \tilde{H}_u^+, \tilde{W}^-, \tilde{H}_d^-)$ assumes the form

$$M_{\tilde{\chi}^\pm} = \begin{pmatrix} 0 & X^T \\ X & 0 \end{pmatrix}\,, \tag{2.38}$$

with

$$X = \begin{pmatrix} M_2 & \sqrt{2}\, m_Z\, s_\beta\, c_{\theta_W} \\ \sqrt{2}\, m_Z\, c_\beta\, c_{\theta_W} & \mu \end{pmatrix}\,. \tag{2.39}$$

Therefore, the bound on the gaugino mass parameter M_2 implies a bound on the lightest neutralino of about 50 GeV. We want, however, to stress that $m_{\tilde{\chi}_1^0}$ might be smaller than this value, in an effective MSSM model in which the gaugino mass unification of Eq. (2.35) does not hold [58, 103]. In this case, the lowest possible values of the lightest neutralino mass are determined by the M_1 parameter and $\tilde{\chi}_1^0 \simeq \tilde{B}$. A theoretical model with $M_1 = R\, M_2$ and $0.01 \leq R \leq 0.5$ will be employed in Chapter 5 to analyze the muon fluxes expected by the neutralino configurations compatible with the DAMA annual modulation region.

The neutralino couplings to the Z-boson are proportional to $(a_3^2 - a_4^2)$, with a_3 and a_4 the two higgsino fractions. Remember, indeed, that trilinear couplings between the Z-boson and two W^3-bosons or two B-bosons do not exist in the SM. Therefore, the couplings between the Z-boson and two winos $\tilde{W}^3$ or binos $\tilde{B}$ are absent in the MSSM. Very light neutralinos, with $m_{\tilde{\chi}_1^0} < m_Z/2$, are almost in a pure bino configuration ($a_1 \simeq 1$). Therefore, most of the light neutralino configurations will survived to the constraints imposed by Z-boson decay width. The $\tilde{\chi}_1^0$ can have a sizable mixing with $\tilde{H}_d^0$ only for small μ values.

Besides the neutralino, also the sneutrino $\tilde{\nu}$, the supersymmetric partner of the SM neutrino, can be a viable LSP. In the framework of the simple MSSM, in which only the

left-handed neutrinos exists, the sneutrino has been tightly constrainted by direct DM detection experiments [104], since its large coupling to the Z-boson induces a scattering cross section off nucleons higher than the experimental limits. Because of the same coupling, also the annihilation cross section results really large, implying a very small sneutrino relic density [105].

Sneutrinos have been reanalyzed in extended model in which right-handed neutrinos are added to the MSSM and lepton-number violating terms are included [106]. They have also been studied in the framework of the Next-to-Minimal Supersymmetric Model in which, beyond the right-handed neutrinos, also a singlet scalar is added [107]. In these non-minimal models the sneutrino turns out to still be a viable DM candidate.

Another SUSY DM candidate is represented by the gravitino, the superpartners of the graviton. This particle does, however, not belong to the WIMP category, having a cross section that is much lower than the standard weak interaction one, as can be seen from Fig. 2.5. The gravitino may or may not be thermally produced and it is usually assumed to decay, as otherwise its relic density would be much higher than the one derived from the WMAP data. Strong constraints on this type of DM come from Big Bang Nucleosynthesis, since the gravitino decay products could alter the primordial abundances of light elements. This is also known as "cosmological gravitino problem". A working scenario in which the gravitino represents a viable DM candidate, in agreement with cosmological data, is represented by a SUSY model with small R-parity violating terms [108]. Unfortunately, it is extremely difficult to detect the gravitinos, since they have only gravitational interactions.

Kaluza-Klein particles

Kaluza-Klein particles are a kind of excitations of the SM fields. They appear in Extra Dimensional models, in which space-time is considered to have more dimensions than the standard four. To reconcile these theories with the observed four-dimensional Universe, the Extra Dimensions are compactified. It is possible that standing waves are present in the extra compactified dimensions. Their existence would predict an infinite number of states, the so-called "Kaluza-Klein tower", with energy values given by $E = n\,h\,c/R$, where R is the radius of the extra dimension, n is an integer, h is the Planck's constant and c is the speed of light. This prediction is a peculiar characteristic of this type of models.

In models of Universal Extra Dimensions [109], a discrete symmetry arises from momentum conservation in the Extra Dimension. This is called "K-parity" and, in analogy to R-parity, it ensures that the lightest Kaluza-Klein particle (LKP) is stable and thus a good DM candidate [110]. In many Extra Dimensions models, the LKP results to be the first Kaluza-Klein excitation of the photon. The DM particle in this case is a boson, in contrast to the SUSY neutralino.

Little Higgs particles

Little Higgs models have been proposed as a solution of the hierarchy problem, alterna-

tively to Supersymmetry and Extra Dimensions. In these models, the Higgs boson is a pseudo-Nambu-Goldstone boson arising from a global symmetry, broken spontaneously at the TeV scale. As a consequence, the Higgs mass is stable, with respect to one-loop corrections up to an energy of about 10 TeV. More details on Little Higgs models and on their phenomenology can be found in Ref. [111].

The Little Higgs models can provide a good DM candidate if a discrete symmetry, called "T-parity", is implemented. The SM particles are even under this symmetry, while all the heavy particles predicted by the model are odd. The lightest T-odd particle (LTP) is stable and in most of the models it is the heavy photon [112].

2.4.2 Non-WIMP candidates

In this Section we summarize some of the most common non-WIMP DM candidates: neutrinos, axions and axinos, and wimpzilla particles.

Neutrinos

The SM neutrinos have been considered in the past as possible DM candidates. The Big Bang model, indeed, predicts the existence of a cosmic neutrino background, with a relic density given by

$$\Omega_\nu\, h^2 = \frac{\sum_i m_i}{94\,\mathrm{eV}}\,, \tag{2.40}$$

where we have denoted by m_i the i-th neutrino mass. Considering the limit on the electron neutrino mass from the tritium β-decay experiments [89], the sum of the neutrino masses can be at most equal to 6 eV, implying that $\Omega_\nu\, h^2 \leq 0.06$. Therefore, SM neutrinos can only be a subdominant DM component.

More stringent constraints on the contribution of SM neutrinos to the DM come from the analysis of the WMAP data on CMB anisotropies, combined with supernovae and large scale structure observations [113]. We wish to recall that neutrinos would act as HDM and would induce a top-down scenario in structure formation, which is not supported by data from the SDSS and the 2dFGRS. The limit at 95% C.L. on the sum of the neutrino masses is about 0.67 eV, which translates into $\Omega_\nu\, h^2 \leq 0.007$.

Hypothetical neutrinos without SM interactions, besides mixing with SM neutrinos, could also behave as DM particles. They are called "sterile neutrinos" and they usually act as Warm Dark Matter, i.e. a type of DM with intermediate characteristics between CDM and HDM. Their mass range is tightly constrained by X-ray bounds and constraints on the DM relic abundance. The actual allowed region depends on the sterile neutrino production mechanism: for non-resonant production, a lower bound of 1.8 keV and an upper bound of 4 keV is set, while for resonant production the corresponding bounds are weaker, with a lower bound of 1 keV and an upper bound of 50 keV, see Ref. [114] for a review.

In principle, other $SU(2)_L$ doublets, containing heavy neutrinos, could be added to the SM. Currently, the mass of heavy neutrinos is constrained to be heavier than 45 GeV,

from data on the invisible Z-boson decay width. An upper bound on the mass is set to 300 GeV, a value above which the heavy neutrinos would overclose the Universe. The allowed mass window for heavy neutrinos could be reduced even more, in case an asymmetry between neutrinos and anti-neutrinos is present, see e.g. Ref. [115].

Axions and axinos

The Peccei-Quinn theory [116], which aims to solve the strong-CP problem of QCD, predicts the existence of a neutral particle, called "axion", that could form the DM. Direct searches and astrophysical constraints, from globular clusters and from the supernova 1987A, restrict the axion to have an extremely small mass, between 10^{-6} eV and 10^{-3} eV, and a very low cross section with the SM particles.

The CERN Axion Solar Telescope (CAST) is a strong magnet pointing towards the Sun, searching for axions. If these particles exist, they could be produced in the Sun by photon scatterings with protons and electrons, in the presence of strong electric fields. The CAST experiment, using an intense magnetic field, would then convert the axions back to X-ray photons. By now, no experiment has detected axions. The only evidence was reported by the PVLAS collaboration in 2005 [117], but this result has been ruled out by new data, obtained after an upgrade of the experiment [118].

In SUSY models, also the fermionic partner of the axion, the axino, could be a good DM candidate [119].

Wimpzilla particles

Superheavy DM particles with a mass $m_\chi > 10^{10}$ GeV are usually called "wimpzillas". These particles are no thermal relics of the early Universe, but arise from non-thermal processes like, for example, gravitational production at the end of inflation [120]. They can play an important role also in astrophysics, since they could explain the observed cosmic rays, at energies above the GZK cutoff, as due to annihilations or decays of wimpzilla particles [121].

2.4.3 Non-standard Dark Matter interactions

In Sect. 2.3.1, we presented the physics of DM direct detection, assuming that the DM particle scatters elastically off nuclei inside a detector. However, different models beyond this common scenario have been proposed as well. In this Section we briefly discuss two models in which the DM has "non-standard interactions": inelastic DM and leptophilic DM.

Inelastic Dark Matter

The inelastic Dark Matter (iDM) scenario has first been proposed in Ref. [122] to explain the results obtained by the DAMA/NaI experiment. Recently, this model has been reconsidered in several papers, see for instance Ref. [123], in the light of the DAMA/LIBRA an-

nual modulation data. The two main hypotheses of iDM are: i) the existence of an excited state χ^* of the DM particle χ with a small mass splitting $\delta = m^*_\chi - m_\chi \simeq 100$ keV, ii) a suppressed elastic scattering $\chi N \to \chi N$, with respect to the inelastic process $\chi N \to \chi^* N$.

In this framework, the minimal DM velocity necessary to deposit an energy E_R in the detector is

$$v_{\min} = \frac{1}{\sqrt{2 m_N E_R}} \left(\frac{m_N E_R}{\mu_N} + \delta \right) . \tag{2.41}$$

The different kinematics of iDM leads to several consequences: scattering on heavy nuclei is favoured over that on light ones, as can be deduced from the expression of $v_{\min}$, the annual modulation signal is enhanced and the low-energy events are suppressed [124].

The analyses reported in Ref. [123] have shown that iDM with spin-independent cross section is a viable DM candidate, consistent at the same time with the DAMA data and with the limits from the CDMS [55], XENON10 [56], KIMS [66], ZEPLIN [125] and CRESST [126] experiments. The iDM with dominantly spin-dependent cross section has been studied in Ref. [71]. This scenario is able to explain the DAMA results and to fulfill the strong constraints on spin-dependent cross sections coming from the COUPP [65], KIMS [66] and PICASSO [67] experiments. Theoretical models for iDM have been presented, for example, in Refs. [124, 127].

Leptophilic Dark Matter

In leptophilic models, the DM particle couples mainly to leptons rather than to quarks. They have been introduced for two main reasons. First, they could explain the excess in cosmic rays, detected by PAMELA and ATIC (see Sect. 2.3.2), in terms of a DM scenario. Second, they could reconcile the DAMA results with the other direct detection experiments. Indeed, electronic events can contribute to the scintillation light signal in the DAMA detector, but are rejected by most of the other DM experiments, like CDMS and XENON10.

A simple model of leptophilic DM has been presented in Ref. [128]. In this constext, a Dark Sector (DS) is added to the SM and the DM χ is a Dirac fermion charged under a new Abelian gauge symmetry $U(1)_{DS}$. All the SM particles are odd under a discrete DS-parity, while the DM is even.

The Lagrangian of the DS is given by

$$\mathcal{L}_{DS} = -\frac{1}{4} F'^2_{\mu\nu} + \bar{\chi} \gamma^\mu D_\mu \chi + |D_\mu \phi|^2 - M_\chi \bar{\chi} \chi - V_{DS}(\phi) \, , \tag{2.42}$$

where ϕ is a scalar Higgs field that breaks the gauge group $U(1)_{DS}$ and F' is the field strength of the new gauge boson U. The latter is supposed to be leptophilic and to mediate the coupling between the SM and the DS (at least some of the SM leptons must be charged under the new gauge group). Tight constraints from measurements of lepton magnetic dipole moments and from different low-energy leptonic cross sections force the U boson to have a small coupling to the electron and the muon [128]. The correct annihilation cross section to explain the PAMELA/ATIC data is provided by

the Sommerfeld enhancement [129] for a DM mass of $\mathcal{O}(800$ GeV) and for a U boson of mass 1-10 GeV. Moreover, within this model, the authors identify a region of the allowed parameter space, where the DAMA results are consistent with the lack of detection by the other experiments.

In Chapter 5 we will analysis the lepthophilic DM scenario using a model independent formalism and, in particular, we will show how constraints coming from indirect detection with neutrinos can provide strong bounds.

3

Indirect detection with neutrinos

In this Chapter, the method of indirect DM detection with neutrinos is presented in detail. The basic ingredients for the calculation of the neutrino flux coming from celestial bodies, like the Sun and the Earth, are given in Sect. 3.1. In Sect. 3.2, instead, the neutrino flux from the galactic center is considered. The calculation of the muon flux is presented in Sect. 3.3.

3.1 Neutrino flux from the Sun and the Earth

In Sect. 3.1.1, we summarize the main formulae which we employed to evaluate the capture rates of DM particles by celestial bodies. The process of neutrino production is discussed in Sect. 3.1.2, while the neutrino propagation aspects are treated in Sect. 3.1.3.

3.1.1 Capture and annihilation rates

If DM particles exist in the galactic halo, they have a finite probability to scatter with the nuclei present in the Sun or the Earth. Through subsequent scatterings, they lose energy and once their velocity is less than the escape velocity of the body, they become gravitationally bound. Being captured, the DM particles will continue to cross the celestial body and scatter with its nuclei. In this way, their velocities will gradually decrease and they will sink into the central part of the body, where they accumulate. In Ref. [130], the authors found that this process always occurs for the standard WIMP cross section.

The calculation of the DM capture by the Sun and the Earth has been firstly carried on by Gould, in Ref. [131]. Considering a spherically symmetric shell of material, the DM capture rate per unit shell volume may be written as

$$\frac{dC}{dV} = \int_0^\infty dv \frac{\bar{f}(v)}{v} \, u \, \Omega(u) \,, \tag{3.1}$$

where v is the velocity of the DM at infinity (far from the gravitational potential of the body), while $u = \sqrt{v^2 + u_{\rm esc}^2}$ is the one at the DM-nucleus interaction point and $u_{\rm esc}$ is the escape velocity at that particular point of the celestial body. The velocity distribution $\bar{f}(v)$ is defined as

$$\bar{f}(v) = v^2 2\pi \int_{-1}^{1} d\cos\theta \, f(\mathbf{v}) \,, \tag{3.2}$$

where $f(\mathbf{v})$ is the Maxwell-Boltzmann distribution of the DM particles, as seen by an observer that moves with a velocity $v_\odot$ relative to the DM halo,

$$f(\mathbf{v}) = \frac{n_\chi}{(\pi v_0^2)^{3/2}} \exp\left(-\frac{(\mathbf{v}+\mathbf{v}_\odot)^2}{v_0^2}\right) , \tag{3.3}$$

with $n_\chi = \rho_\chi / m_\chi$ being the local Dark Matter number density that we fixed to the standard value of 0.3 GeV cm^{-3}. For the calculation of the capture rate, we assume $v_\odot = v_0 = 220$ km s^{-1}.

The function $\Omega(u)$ denotes the rate of DM scatterings from a velocity v to a velocity less that $u_{\rm esc}$. If the DM elastic scattering cross section σ_N is isotropic and velocity independent, and if the temperature of the shell can be neglected, the following simple relation holds [131]:

$$\Omega(u) = \sigma_N \, n_N \, u \, \mathcal{P} \,, \tag{3.4}$$

where n_N is the number density of nuclei with mass m_N in the celestial body and $\mathcal{P}$ is the probability that the DM scatters at a velocity less than $u_{\rm esc}$,

$$\mathcal{P} = \frac{1}{v^2 + u_{\rm esc}^2} \left(u_{\rm esc}^2 - \frac{v^2}{\beta_-}\right) \; \theta\left(\sqrt{\beta_-}\, u_{\rm esc} - v\right) , \tag{3.5}$$

with $\beta_- = 4 m_\chi m_N / (m_\chi - m_N)^2$.

If the DM particles scatter on elements heavier than hydrogen, the differential cross section should also contain a form factor, see Eq. (2.13). Using the exponential parameterization given in Eq. (2.14), the expression of the scattering probability $\mathcal{P}$ is modified to

$$\mathcal{P} = \int_{m_\chi v^2/2}^{E_R^{\rm max}} dE_R \, \frac{1}{E_R^{\rm max}} \exp\left(-\frac{E_R}{q_0}\right) \; \theta\left(\sqrt{\beta_-}\, u_{\rm esc} - v\right) , \tag{3.6}$$

where $E_R = m_\chi \Delta u^2/2$, with $\Delta u^2 = u^2 - u_f^2$, u_f being the DM velocity after the scattering. The quantity $E_R^{\rm max}$ is equal to $2\mu_N^2 \, u^2 / m_N$.

The total capture rate C is then obtained by integrating Eq. (3.1) over the radius of the body and by summing over the different elements i present in the body. The final expression can be cast in the form [131, 132]

$$C = \sum_i \left(\frac{8}{3\pi}\right)^{1/2} \left[\sigma_{N,i} \frac{\rho_\chi}{m_\chi} \bar{v}\right] \left[\frac{M_i}{m_{N,i}}\right] \left[\frac{3\tilde{u}_{\rm esc}^2}{2\bar{v}^2} \langle\phi\rangle_i\right] \xi(\infty) S_i \,, \tag{3.7}$$

where $\tilde{u}^2_{\rm esc}$ is the escape velocity at the surface of the body ($\tilde{u}^2_{\rm esc} \simeq 618$ km s^{-1} for the Sun and $\tilde{u}^2_{\rm esc} \simeq 11.2$ km s^{-1} for the Earth), M_i is the total mass of the element i in the body and $\langle\phi\rangle_i$ is the reduced gravitational potential, $\phi(r) = u^2_{\rm esc}(r)/\tilde{u}^2_{\rm esc}$, averaged over the mass distribution of the element i. The factor $\xi(\infty) \simeq 0.75$ is a suppression factor due to the motion of the solar system with respect to the halo. The function S_i takes into account the kinematical properties occurring in the DM-nucleus interactions. Its analytic expression can be found in Ref. [131].

In Fig. 3.1, we present the capture rate for some of the most abundant elements present in the Sun. The solar composition is taken from the solar model BS2005-AGS,OP [133] for light elements, up to ^{16}O, and from Ref. [134] for the heavier elements. We neglect the effect of DM evaporation [135], that can be important only for DM masses lower than 10 GeV, and the gravitational effects from planets like Jupiter, recently studied in Refs. [130, 136]. In the left panel of Fig. 3.2, instead, the capture rate of the Earth is displayed. The different peakes are due to resonant capture of DM on oxygen, magnesium, silicon and iron.

The DM particles could be capture by celestial bodies also through inelastic scatterings on nuclei and through elastic scatterings on electrons. For the analysis of the former case, we refer to Ref. [137], while we describe in the following the scenario of DM capture by the Sun, due to interactions with electrons. This possibility will then be applied to the study of leptophilic DM, carried out in Chapter 5.

In the calculation of the capture rate that we have described above, the DM particles are assumed to interact with material at zero temperature, neglecting the solar temperature of about 1.5×10^7 K in the center and 8.1×10^4 K at the surface. Although this is a reasonable assumption for DM candidates interacting with hydrogen and the other nuclei, it fails for the case of DM scattering on the free electrons in the Sun. Indeed, the effect of a non-zero temperature on the capture rate depends on the ratio of the thermal velocity of the target to the DM velocity. The thermal kinetic energy $k_B T$ is independent of the mass, but the thermal velocity is larger by a factor $\sqrt{m_p/m_e} \simeq 45$ for electrons compared to hydrogen.

We calculate the rate for DM capture by a body at finite temperature following Ref. [131] and considering the temperature distribution for the electrons inside the Sun as predicted by the solar model BS2005-AGS,OP [133]. In the right panel of Fig. 3.2, we show the effect of the non-zero temperature on the capture rate for electrons, hydrogen and all other nuclei in the Sun. We find that the capture rate on electrons is enhanced by about one order of magnitude, while the effect is hardly visible at the scale of the plot for hydrogen. The temperature effect can be neglected for scattering off heavier nuclei.

The annihilation rate Γ is expressed in terms of the capture rate by the formula [138]

$$\Gamma = \frac{C}{2} \tanh^2 \left(\frac{t}{\tau_A} \right) , \tag{3.8}$$

where t is the age of the macroscopic body ($t = 4.5$ Gyr for Sun and Earth), $\tau_A = (C C_A)^{-1/2}$, and C_A depends on the DM annihilation cross section and on the effective

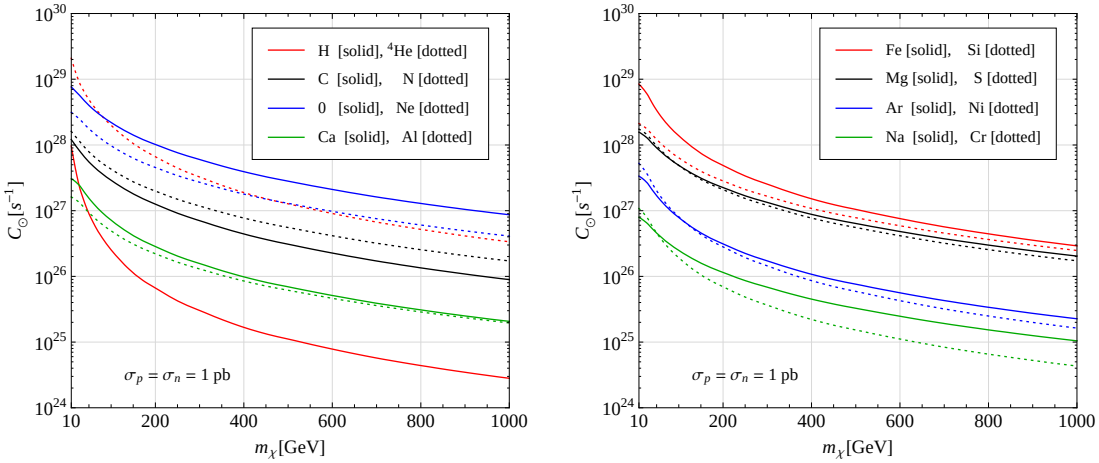

Figure 3.1: Capture rate $C_\odot$ in the Sun as a function of the Dark Matter mass, assuming scattering off the different nuclei inside the Sun, with a scattering cross section of $10^{-36}\,\mathrm{cm}^2$.

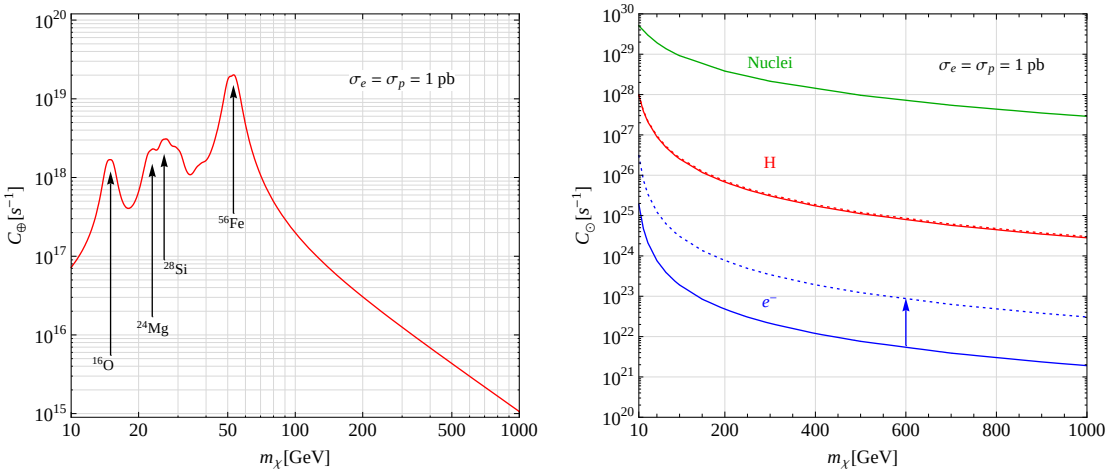

Figure 3.2: Left panel: capture rate $C_\oplus$ in the Earth as a function of the Dark Matter mass, assuming a scattering cross section of $10^{-36}\,\mathrm{cm}^2$. Right panel: capture rate $C_\odot$ in the Sun as a function of the Dark Matter mass, assuming scattering off electrons, hydrogen, and all other nuclei in the Sun, with a scattering cross section of $10^{-36}\,\mathrm{cm}^2$. The solid curves correspond to scattering off particles at zero temperature, whereas the dotted curves show the effect of the actual temperature distribution inside the Sun for electrons and hydrogen.

volume V_0 of the confining region in which the DM particles are trapped:

$$C_A = \frac{\langle \sigma_{\rm ann} v \rangle}{V_0} \left(\frac{m_\chi}{20 \text{ GeV}} \right)^{3/2} . \tag{3.9}$$

We denote by $\langle \sigma_{\rm ann} v \rangle$ the thermally averaged total annihilation cross section times the relative velocity, at the present time. The volume of the confining region is explicitly given by

$$V_0 = \left(\frac{3 m_{Pl}^2 T}{2\rho \times (10 \text{ GeV})} \right)^{3/2} , \tag{3.10}$$

where T and ρ are the central temperature and the central density of the celestial body. For the Earth $V_0 = 2.3 \times 10^{25}$ cm^3 ($T = 6000$ K, $\rho = 13$ g cm^{-3}) and for the Sun $V_0 = 6.6 \times 10^{28}$ cm^3 ($T = 1.4 \times 10^7$ K, $\rho = 150$ g cm^{-3}).

We recall that, according to Eq. (3.8), in a given macroscopic body the equilibrium between capture and annihilation (i.e. $\Gamma \simeq C/2$) will be established only if $t \gtrsim \tau_A$.

The expression for the annihilation rate given above refers to a macroscopic body as a whole. This is certainly enough for the Sun which appears to us as a point source. On the contrary, in the case of the Earth, one also has to define an annihilation rate referred to a unit volume at point $\mathbf{r}$ from the Earth center:

$$\Gamma(r) = \frac{1}{2} \langle \sigma_{\rm ann} v \rangle n^2(r) , \tag{3.11}$$

where $n(r)$ is the DM spatial density, which may be written as [138]

$$n(r) = n_0 \, \mathrm{e}^{-\tilde{\alpha} \, m_\chi \, r^2} . \tag{3.12}$$

Here, $\tilde{\alpha} = 2\pi G\rho/(3T)$ and n_0 is a normalization such that

$$\Gamma = \frac{1}{2} \langle \sigma_{\rm ann} v \rangle \int d^3 r \, n^2(r) . \tag{3.13}$$

Concerning the annihilation into neutrinos, more exotic scenarios has been studied as well, in which for example high energy electrons resulting from DM annihilations in the Sun could escape the Sun in case the DM annihilates into long-lived states [139]. For our study we will neglect this situation.

3.1.2 Neutrino production

Once the DM particles are accumulated in the center of the Sun or the Earth, they can annihilate, producing directly neutrinos with energies $E_\nu \simeq m_\chi$, where m_χ is the DM mass. In the framework of the SUSY neutralino, the branching ratio for this annihilation channel is proportional to the neutrino mass, and thus negligible. However, depending on the nature of the DM particle and on the particular channel through which the annihilation occurs, there might be cases where the direct neutrino production is unsuppressed.

In Chapter 4 we will systematically classify all the different possibilities, reporting for each of them the associate annihilation cross sections.

The DM particles can annihilate also into charged leptons, quarks, gauge and Higgs bosons, which can then decay or hadronize producing neutrinos. In Ref. [140], the authors have used a PYTHIA Monte Carlo simulation to calculate the spectra of neutrinos, coming from DM annihilation in the Sun and in the Earth, for the following channels: $b\bar{b}$, $\tau\bar{\tau}$, $c\bar{c}$, $q\bar{q}$, gg (with $q = u, d, s$ quarks). Three main differences and improvements have been implemented in Ref. [140] with respect to previous calculations. The first one is the prediction of the neutrino spectra for the different neutrino flavours: ν_e, ν_μ and ν_τ (not only ν_μ, like in previous works). The second main improvement consists of an appropriate implementation of the energy loss that hadrons and leptons can experience before decaying. Finally, the third difference is represented by the calculation of the neutrino spectra for light quarks u, d, s, that were usually neglected in previous calculations.

We will use the initial neutrino spectra of Ref. [140] for the analyses of the leptophilic and the light neutralino DM, reported in Chapter 5.

3.1.3 Neutrino propagation

For a precise estimate of the neutrino flux at the detector site, it is important to take into account the main processes that can occur during the neutrino propagation: the oscillation and the incoherent interaction with matter. These effects have been vastly analyzed in Refs. [140, 141], and have then been applied to specific model-dependent studies, see e.g. Refs. [142, 143].

The equations that describe the evolution of the neutrino spectra can be formally written using the density matrix formalism:

$$\frac{d\rho}{dr} = -i\,[H,\rho] + \left.\frac{d\rho}{dr}\right|_{NC} + \left.\frac{d\rho}{dr}\right|_{CC} . \tag{3.14}$$

The first term describes the oscillations of neutrinos in matter, with the total Hamiltonian given by the sum of the vacuum one and of the Wolfenstein potential:

$$H_{\rm w} = \frac{M_{\rm w}}{2E} \pm \sqrt{2}\,G_F\,N_e\,\mathrm{diag}(1,0,0)\,, \tag{3.15}$$

where $G_F = 1.66 \times 10^{-5}$ GeV^{-2} is the Fermi constant and N_e is the matter electron density. The minus (plus) sign holds for (anti-)neutrinos and $M_{\rm w} = U\mathrm{diag}(m_1^2, m_2^2, m_3^2)U^\dagger$ is the mass matrix in the weak basis $(\nu_e, \nu_\mu, \nu_\tau)$. The matrix U is the Pontecorvo-Maki-Nakagawa-Sakata (PMNS) matrix, often parameterized as

$$U = \mathrm{diag}(1,\, e^{i\alpha},\, e^{i\beta}) \cdot \begin{pmatrix} c_{12}c_{13} & s_{12}c_{13} & s_{13}\,e^{i\delta_{\rm CP}} \\ -s_{12}c_{23} - c_{12}s_{13}s_{23}\,e^{i\delta_{\rm CP}} & c_{12}c_{23} - s_{12}s_{13}s_{23}\,e^{i\delta_{\rm CP}} & c_{13}s_{23} \\ s_{12}s_{23} - c_{12}s_{13}c_{23}\,e^{i\delta_{\rm CP}} & -c_{12}s_{23} - s_{12}s_{13}c_{23}\,e^{i\delta_{\rm CP}} & c_{13}c_{23} \end{pmatrix} , \tag{3.16}$$

where $c_{ij} \equiv \cos\theta_{ij}$ and $s_{ij} \equiv \sin\theta_{ij}$. The parameter δ is the Dirac CP-violating phase, while α and β are the two Majorana phases, absent in the case of Dirac neutrinos. The Majorana phases do not appear in the oscillation probability formulae for neutrinos and, therefore, oscillation experiments do not provide any information on their values. The possibility of distinguishing Dirac from Majorana neutrinos is given by other kinds of experiments, like neutrinoless-double-β decay.

In Ref. [144], the authors made a three flavours global fit for the neutrino oscillation parameters, using data from solar, atmospheric, reactor (KamLAND and CHOOZ) and accelerator (K2K and MINOS) experiments. They found the following best-fit values, with 1σ errors, for the mixing angle parameters:

$$\begin{aligned} \sin^2\theta_{12} &= 0.304^{+0.022}_{-0.016}\,, \\ \sin^2\theta_{23} &= 0.50^{+0.07}_{-0.06}\,, \\ \sin^2\theta_{13} &= 0.01^{+0.016}_{-0.011}\,, \end{aligned} \tag{3.17}$$

and for the mass squared differences

$$\begin{aligned} \Delta m^2_{21} &= 7.65^{+0.23}_{-0.20} \times 10^{-5}\,\mathrm{eV}^2\,, \\ |\Delta m^2_{31}| &= 2.40^{+0.12}_{-0.11} \times 10^{-3}\,\mathrm{eV}^2\,. \end{aligned} \tag{3.18}$$

The sign of Δm^2_{31} is still unknown. It can be positive for normal mass ordering ($m_1 < m_2 < m_3$) or negative for inverted mass ordering ($m_3 < m_1 < m_2$). No experimental information on the value of δ_{CP} is present at the moment.

In our study, the neutrino mixing angles θ_{12} and θ_{23} and the squared mass differences are fixed to their best-fit values reported in Eqs. (3.17)-(3.18). We consider the case of normal mass ordering and we set the oscillation parameter θ_{13} to zero. A different choice of θ_{13} would marginally affect the prediction on the neutrino flux, as reported in Refs. [140, 141].

The second term in Eq. (3.14) takes into account the neutrino energy loss and their reinjection due to neutral current interactions. The last term, instead, represents the neutrino absorption and the ν_τ regeneration through charged current interactions. The explicit expressions of these terms are reported in Appendix A.

For DM annihilation inside the Sun, the integro-differential equation (3.14) for the density matrix has been solved numerically by a `Fortran` program. In Fig. 3.3 and Fig. 3.4 we report our results for the propagated neutrino spectra at one astronomical unit, in the case of the $\nu\bar{\nu}$ and of the $\tau\bar{\tau}$ annihilation channel. These spectra will be used in Chapter 5 in the context of a leptophilic DM candidate. Our results of Fig. 3.3 and Fig. 3.4 match very well with the ones given in Refs. [140, 141]. Notice how the effects of incoherent neutrino interactions are clearly visible from the propagated spectra of the $\nu\bar{\nu}$ annihilation channel.

In the case of annihilations inside the Earth's core, the calculation of the neutrino spectra can be further simplified. Indeed, the interactions with matter can be neglected, since the mean free paths of neutrinos, in the core and in the mantle, are much bigger

than the Earth's radius $R_\oplus$ for $E_\nu \lesssim 10$ TeV (for anti-neutrinos, the mean free paths are almost a factor two greater, due to the difference in the cross-sections):

$$\lambda^{\rm core} = \frac{1}{\sigma_\nu N_e^{\rm core}} \simeq 3.6 \times 10^4 \frac{R_\oplus}{(E_\nu/{\rm GeV})}\,, \qquad \lambda^{\rm mantle} = \frac{1}{\sigma_\nu N_e^{\rm mantle}} \simeq 9.2 \times 10^4 \frac{R_\oplus}{(E_\nu/{\rm GeV})}\,. \tag{3.19}$$

Therefore, for the propagation inside the Earth, only the oscillation effects can be taken into account. Moreover, for $E_\nu \gtrsim 1$ GeV, the dependence on the "solar" parameters Δm^2_{21} and θ_{12} is extremely weak and can be neglected. Since in our analyses we are considering vanishing θ_{13}, Earth's matter effects are negligible and neutrino oscillations are driven by the "atmospheric" parameters Δm^2_{31} and θ_{23}. In this case, the main oscillation channel is $\nu_\mu \leftrightarrow \nu_\tau$ and the value of the oscillation and the survival probability $P_{\alpha\beta}$ is simply given by the vacuum two-flavors formula:

$$P_{\alpha\beta}(r, E_\nu) = \delta_{\alpha\beta} - \epsilon_{\alpha\beta} \sin^2(2\theta) \sin^2\left(1.27\, \frac{(\Delta m^2_{31}/{\rm eV}^2)(r/{\rm km})}{(E_\nu/{\rm GeV})}\right)\,, \tag{3.20}$$

where the parameter $\epsilon_{\alpha\beta}$ is equal to 1 (-1) for $\alpha = \beta$ $(\alpha \neq \beta)$.

In the case of the Earth, the differential muon-neutrino flux at the detector, from the annihilation channel f and as a function of the zenith angle θ_z, can be written as:

$$\frac{d\phi_{\nu_\mu}}{dE_\nu\, d\cos\theta_z} = \frac{\Gamma_\oplus}{4\pi R^2_\oplus}\, BR_f \left(G_{\mu\mu}(\theta_z, E_\nu)\, \frac{dN^f_{\nu_\mu}}{dE_\nu} + G_{\mu\tau}(\theta_z, E_\nu)\, \frac{dN^f_{\nu_\tau}}{dE_\nu}\right)\,, \tag{3.21}$$

where the function $G_{\alpha\beta}(\theta_z, E_\nu)$ encodes the dependence on the oscillation probability and on the DM distribution inside the Earth. Using Eq. (3.12), we find the following expression:

$$G_{\alpha\beta}(\theta_z, E_\nu) = \frac{2\,(2\, m_\chi\, \tilde\beta)^{3/2}}{\pi^{1/2}\, R_\oplus} \int_0^y dr\, \exp\left[-2\, m_\chi\, \tilde\alpha\, \left(r^2 + R^2_\oplus - r y\right)\right]\, P_{\alpha\beta}(r, E_\nu)\,, \tag{3.22}$$

with $y \equiv 2\, R_\oplus \cos\theta_n$, $\theta_n \equiv \pi - \theta_z$ and $\tilde\beta = \tilde\alpha\, R^2_\oplus$. The differential muon anti-neutrino flux at the detector can be obtained by a formula analogous to Eq. (3.21). In Fig. 3.5 we report our results for the neutrino spectra at the detector site, in the case of the $b\bar b$ and of the $\tau\bar\tau$ annihilation channel. We will use these spectra in Chapter 5, considering the light neutralino as DM particle. The spectra of Fig. 3.5 have been compared with the ones of Refs. [140, 141], finding a very good agreement. Note the oscillatory behaviour of the spectra due to the neutrino propagation along the radius of the Earth.

The neutrino flux at the detector, from the annihilation channel f with branching ratio BR_f, is given by

$$\frac{d\phi^f_\nu}{dE_\nu} = BR_f \frac{\Gamma}{4\pi d^2} \frac{dN^f_\nu}{dE_\nu}\,, \tag{3.23}$$

with dN^f_ν/dE_ν being the neutrino spectrum after propagation and d being the distance between the source and the detector (the Sun-Earth distance or the Earth's radius).

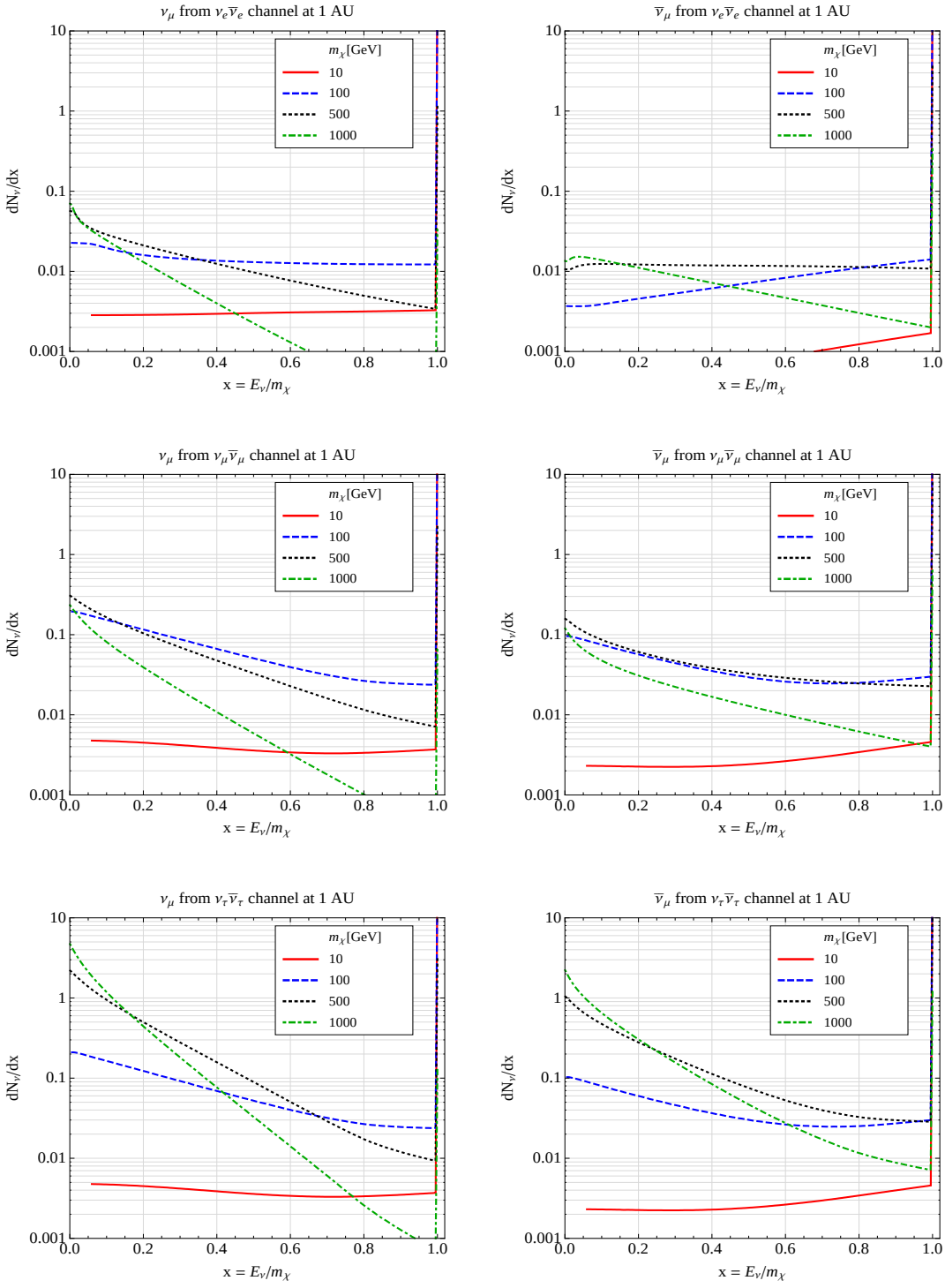

Figure 3.3: Spectra of muon (anti-)neutrinos at 1 AU, for DM pair-annihilation inside the Sun into $\nu_e\,\bar{\nu}_e$, $\nu_\mu\,\bar{\nu}_\mu$ and $\nu_\tau\,\bar{\nu}_\tau$. The spectra at the production are given by a δ function centered at $E_\nu = m_\chi$.

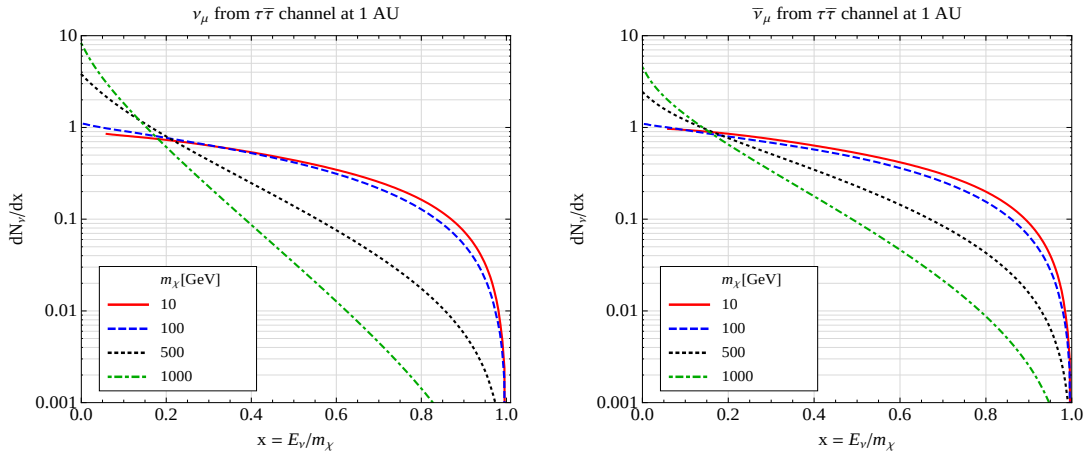

Figure 3.4: Spectra of muon (anti-)neutrinos at 1 AU, for DM pair-annihilation inside the Sun into $\tau\bar{\tau}$.

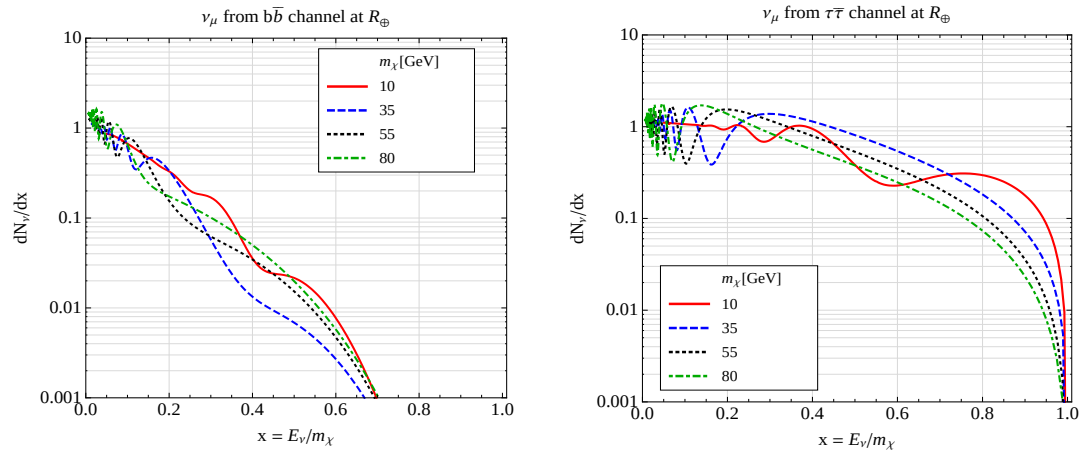

Figure 3.5: Spectra of muon neutrinos at $R_\oplus$, for DM pair-annihilation inside the Earth into $b\bar{b}$ (left panel) and $\tau\bar{\tau}$ (right panel). The spectra of anti-neutrinos are equivalent.

3.2 Neutrino flux from the galactic center

The galactic center (GC) region represents another site to look for neutrino signal coming from DM annihilations. The great advantage of the GC signal, with respect to signals in neutrinos coming from celestial bodies (like the Earth and the Sun), is represented by its direct proportionality to the DM annihilation cross section. Indeed, no dependence on the scattering cross section is present.

Suppose that a pair of DM particles with mass m_χ annihilates near the center of the Milky Way into $\nu_\alpha \bar{\nu}_\beta$, with α and β flavour indices. The flux of muon neutrinos, arriving at the Earth from a solid angle $\Delta\Omega$ will be then given by (see e.g. Ref. [145])

$$\frac{d\phi_{\nu_\mu}}{dE_\nu} = \frac{J\Delta\Omega}{4\pi} \frac{r_0 \rho_0^2}{2\, m_\chi^2} (\sigma_{\rm ann} v)_{\alpha\beta} \frac{dN_{\nu_\alpha}}{dE_\nu} \mathcal{P}(\nu_\alpha \to \nu_\mu)\,, \tag{3.24}$$

where $\sigma_{\rm ann} v$ is the annihilation cross section times the relative velocity between the two DM particles, r_0 is the distance of the Earth from the center of the Galaxy and ρ_0 is the local DM density. The oscillation probability $\mathcal{P}(\nu_\alpha \to \nu_\mu)$ is given by $\sum_i |U_{\alpha i}|^2 |U_{\mu i}|^2$, with U being the neutrino mixing matrix of Eq. (3.16). The function J is defined as [146]

$$J = \frac{1}{\Delta\Omega} \int_{\Delta\Omega} d\Omega \int_{\rm l.o.s} \frac{ds}{r_0} \frac{\rho^2(r)}{\rho_0^2} = \frac{1}{\Delta\Omega} \int_0^{2\pi} d\varphi \int_0^{\psi} \sin\psi \, d\psi \int_0^{s_{\rm max}} \frac{ds}{r_0} \frac{\rho^2(r)}{\rho_0^2}\,, \tag{3.25}$$

with $\rho(r)$ being the DM density profile and $r = \sqrt{s^2 + r_0^2 - 2 r_0 s \cos\psi}$. The upper limit of the integration is given by $s_{\rm max} = \sqrt{(r_{\rm halo}^2 - \sin^2\psi\, r_0^2)} + r_0 \cos\psi$, where $r_{\rm halo} \gtrsim$ tens of kpc is the size of the DM halo. An equation analogous to Eq. (3.24) can be written for the antineutrino flux.

It has been shown in Refs. [147, 148, 149, 150] that the neutrino signal coming from the GC can be used to set a limit on the total DM annihilation cross section. However, as we have discussed in Sect. 2.2, the DM density profile is not well known close to the center of the Milky Way, since the presence of the baryons, that constitute the dominant matter component in the central region of the Galaxy, is not included in the numerical N-body simulations. For this reason, the neutrino flux coming from a small angular region around the GC can suffer from large astrophysical uncertainties, which can be partially reduced if a large angular region is considered, for definiteness a cone-half angle of about 30° around the GC. In any case, to be conservative, it is always preferable to calculate the neutrino flux from the GC considering the DM density profile that provides the smallest signal, i.e. the isothermal profile, for which we report the values of $J\Delta\Omega$ in Table 3.1. For comparison, also the values in the case of a NFW profile are given.

We also want to add that the presence of a Supermassive Black Hole, in the center of the Milky Way, could influence the central part of the DM density profile and alter the slope of the extrapolated profiles of Fig. 2.2. In particular, a spike or a trough toward the GC could be present, depending on the merging history of the Galaxy.

It has been recently shown in Refs. [151, 152] that the neutrino flux from the GC can be clearly observable at neutrino telescopes if the DM particles annihilate mainly into

$J\Delta\Omega$	5°	10°	20°	30°
Isothermal	0.3	1.2	4.1	7.3
NFW	5.9	10.5	17.2	21.9

Table 3.1: Values of the angular factor $J\Delta\Omega$ in the case of an isothermal and a NFW DM density profile.

neutrinos and if the annihilation cross section is roughly two orders of magnitude greater that the one expected from a standard WIMP: $\sigma_{\rm ann}v \simeq 6 \times 10^{-24}$ cm^3 s^{-1}. For smaller cross sections, instead, the atmospheric neutrino background dominates over the DM signal.

3.3 Muon flux

The neutrinos coming from DM annihilations can undergo charge current interactions with the nucleons present in the rock or in the ice below the detector. Among the charged leptons produced, muons can be easily detected by their Cherenkov light emission. In Sect. 3.3.1, the neutrino-muon conversion process is summarized. The background to the DM annihilation signal in neutrinos is discussed in Sect. 3.3.2, while in Sect. 3.3.3 the main muon detectors are described.

3.3.1 Neutrino-Muon conversion

For the calculation of upward-going muons, i.e. muons coming from below the detector, we follow the formalism described in Refs. [153, 154], which we briefly summarize in this Section. The double energy differential muon flux is defined as:

$$\frac{d^2\phi_\mu}{d\cos\theta_z dE_\mu dE_\nu} = N_A \int_0^\infty dX \int_{E_\mu}^{E_\nu} dE'_\mu \; g(E_\mu, E'_\mu; X) \; S(E_\nu, E'_\mu)\,, \tag{3.26}$$

where N_A is Avogadro's number and

$$S(E_\nu, E'_\mu) = \frac{d\phi_\nu}{d\cos\theta_z dE_\nu} \left[\mathcal{N}_p \frac{d\sigma_\nu^p}{dE'_\mu}(E_\nu, E'_\mu) + \mathcal{N}_n \frac{d\sigma_\nu^n}{dE'_\mu}(E_\nu, E'_\mu)\right] \tag{3.27}$$

is the product of the differential neutrino flux and the differential Charged Current (CC) cross section, which is mainly due to Deep Inelastic Scattering (DIS) for the energy $E_\nu > 1$ GeV. The expressions for the differential cross sections $d\sigma_\nu^{p,n}/dE_\mu$ are given in Appendix B. The parameters $\mathcal{N}_p$ and $\mathcal{N}_n$ are the fractional numbers of protons and neutrons at the point of muon production. If the interaction can be assumed to occur in standard rock, like for the Super-Kamiokande detector, we have $\mathcal{N}_p \simeq \mathcal{N}_n \simeq 0.5$, since the number of protons is almost equal to the number of neutrons ($Z \simeq 11, A \simeq 22$); if the interaction occurs inside the ice, like for IceCube, we have $\mathcal{N}_p \simeq 5/9$ and $\mathcal{N}_n \simeq 4/9$.

The function $g(E_\mu, E'_\mu; X)$ represents the probability that a muon with energy E'_μ will have an energy E_μ after a distance X, due to energy-loss processes. The average rate of muon energy loss can be written as [155]:

$$-\frac{dE}{dx} = a(E) + b(E)\ E\,, \tag{3.28}$$

where $a(E)$ represents the energy loss due to ionization and $b(E)$ the one due to radiative effects. For muon energies in the GeV-TeV range, the dependence of the parameters a and b on the energy can be neglected and the function $g(E_\mu, E'_\mu; X)$ can be approximated by the following analytic expression [153]:

$$g(E_\mu, E'_\mu; X) = \frac{\delta(X - X_0)}{a + bE_\mu}\,, \tag{3.29}$$

where X_0 is the mean muon range in matter,

$$X_0(E'_\mu, E_\mu) = \frac{1}{b} \ln \frac{a + bE'_\mu}{a + bE_\mu}\,, \tag{3.30}$$

with E'_μ and E_μ being, respectively, the initial and the final energy of the muon. Standard values for the quantities a and b in rock are

$$a \simeq 2.2 \times 10^{-3}\,\mathrm{GeV}/\left(\mathrm{g\,cm^{-2}}\right)\,, \tag{3.31}$$

$$b \simeq 4.4 \times 10^{-6}\,/\left(\mathrm{g\,cm^{-2}}\right)\,. \tag{3.32}$$

Substituting the expression for $g(E_\mu, E'_\mu; X)$, the differential muon flux acquires the form

$$\frac{d\phi_\mu}{d\cos\theta_z dE_\mu} = N_A\ \frac{1}{a + bE_\mu} \int_{E_\mu}^{m_\chi} dE_\nu \int_{E_\mu}^{E_\nu} dE'_\mu\ S(E_\nu, E'_\mu)\,, \tag{3.33}$$

with m_χ being the DM mass.

The total muon flux can then be divided in through-going muons (muons that pass through the detector) and stopping muons (muons that stop inside the detector) by using the formula

$$\Phi_\mu^{S,T}(\cos\theta_z) = \frac{1}{A(L_{\min}, \theta_z)} \int_{E_\mu^{th}}^{\infty} dE_\mu\ \frac{d\phi_\mu}{d\cos\theta_z dE_\mu}\ A^{S,T}(L(E_\mu), \theta_z)\,, \tag{3.34}$$

where E_μ^{th} is the energy threshold of the detector for upward-going muons, L the mean muon stopping range in water $L(E_\mu) \equiv X_0(E_\mu, m_\mu)$ and $L_{\min} \equiv L(E_\mu^{th})$. The functions $A^{S,T}(L, \theta_z)$ represent the detector effective areas for stopping and through-going muons, while $A(L_{\min}, \theta_z)$ is the total effective area of the detector, i.e. the projected area that corresponds to internal path-lengths longer than $L_{\min}$, for a fixed value of the zenith angle θ_z.

The classification of upward-going muons into the two subcategories reported above is strictly detector-dependent, since it depends on the shape and the size of the detector. For a detector with cylindrical geometry (with radius R and height H), it has been shown in Ref. [156] that the function $A(L, \theta_z)$ acquires the form:

$$A(L,\theta_z) = 2RH \sin\theta_z \sqrt{1-x^2} \; + \; 2R^2 |\cos\theta_z| \left[\cos^{-1} x - 3x\sqrt{1-x^2}\right] \Theta(L_{\max}(\theta_z) - L)\,, \tag{3.35}$$

with $x = L\sin\theta_z/2R$ and $L_{\max}(\theta_z) = \min\left[2R/\sin\theta_z, H/|\cos\theta_z|\right]$. The effective area for stopping muons $A^S(L,\theta_z)$ is given by Eq. (3.35) and the one for through-going muons is $A^T(L,\theta_z) \equiv [A(L_{\min},\theta_z) - A(L,\theta_z)]$.

In the case of contained events (the neutrino-muon conversion takes place inside the detector volume), the energy differential muon flux is given by [151, 152]

$$\frac{d\Phi_\mu}{dE_\mu} = \int_0^D dz \int_{E_\mu}^{m_\chi} dE_\nu \frac{dP_{\rm cont}}{dz dE_\mu} \frac{d\phi_\mu}{dE_\nu}\,, \tag{3.36}$$

where D is the size of the detector and

$$\frac{dP_{\rm cont}}{dz dE_\mu} = n_p \frac{d\sigma_\nu^p}{dE_\mu}(E_\nu, E_\mu) + n_n \frac{d\sigma_\nu^n}{dE_\mu}(E_\nu, E_\mu)\,, \tag{3.37}$$

where n_p and n_n are the number densities of protons and neutrons in the detector: $n_{p,n} = N_A \mathcal{N}_{p,n} \rho$, with ρ being the density of the detector material.

3.3.2 Atmospheric background

For the indirect DM search with neutrinos, the background to a possible signal is represented by atmospheric neutrinos with GeV-TeV energies. Solar neutrinos, instead, do not contribute to the background, since they have MeV energies.

The interactions of primary cosmic rays with the nuclei in the Earth's atmosphere produce π and K mesons, which then generate atmospheric muons and neutrinos through the decay chains

$$\begin{aligned} \pi^\pm, K^\pm \to \quad & \mu^\pm + \nu_\mu(\bar\nu_\mu) \\ & \hookrightarrow e^\pm + \bar\nu_e(\nu_e) + \bar\nu_\mu(\nu_\mu)\,. \end{aligned}$$

Atmospheric muons coming from above the detector reach the Earth's surface before the decay processes $\mu^\pm \to e^\pm + \bar\nu_e(\nu_e) + \bar\nu_\mu(\nu_\mu)$ can occur. To avoid the big background of atmospheric muons, the DM search is done looking only for upward-going muons. In this way, only atmospheric neutrinos will contribute to the background.

In our studies, we will use the atmospheric neutrino fluxes as calculated by Honda et al. [157]. In the literature, two other commonly used results are the FLUKA fluxes by Battistoni et al. [158] and the Bartol fluxes by Barr et al. [159]. These different predictions lead to an uncertainty of order 10% in the flux estimations.

3.3.3 Muon detection

As mentioned before, the muons are detected using the Cherenkov radiation emitted when a charged particle moves faster than the speed of light in water. This radiation has a typical form of a ring and can be recorded using photomultipliers. From the brightness of the ring, the energy of the charged particle can be inferred and, from measurements of its shape, it is possible to distinguish muons from electrons. Electrons produce fuzzy rings, since they generate electromagnetic showers inside the detector. Muons, instead, do not suffer from multiple scatterings and are more easy to detect and identify, since they produce rings with sharp edges.

In the following, we discuss the main characteristics of the Super-Kamiokande underground detector and we also briefly present other existing and planned neutrino telescopes, present in the Northern (ANTARES, NEMO, NESTOR, KM3Net) and in the Southern hemisphere (IceCube).

Super-Kamiokande

The Super-Kamiokande (SK) detector is an underground water Cherenkov detector, located in Japan in the city of Hida, that now includes the old Kamioka town. It is a cylindrical stainless steel tank, with a diameter of 39.3 m and an height of 41.4 m, filled with 50 000 tons of ultra-pure water. An internal stainless steel structure divide the detector volume into an outer and inner detector. The latter has a radius of $R = 16.9$ m and an height of $H = 36.2$ m.

This neutrino observatory has been in operation since 1996 and it is expected to run for another ten years. By measuring the solar neutrino flux, it has provided the first detection of neutrino oscillations in 1998 [160]. In the same year, it also detected fundamental evidences for the discovery of atmospheric neutrino oscillations [161]. The SK detector has also been used to search for proton decay, for supernovae neutrinos and for neutrinos from DM annihilation.

The SK collaboration classifies the data into three main categories: fully-contained events (FC), partially contained events (PC) and upward-going muon events. The last ones are then divided in two subcategories: upward stopping muon events and upward through-going muon events [13]. Usually, only through-going muons are used for the analysis of neutrinos coming from DM annihilations, since for $m_\chi \gtrsim 18$ GeV almost 90% of the muons produced fall in this category [5]. However, for a smaller DM mass, a great part of the upward-going muon signal would be in stopping muons, rather than through-going. For this reason, we will consider both subcategories of upward going-muons in the study of the light neutralino signal, reported in Chapter 5.

The SK detector has an energy threshold $E_\mu^{th} = 1.6$ GeV, that corresponds to a path-length cut $L_{\min} = 7$ m applied on upward-going muons, see the left panel of Fig. 3.6. In the right panel of Fig. 3.6 we report the effective area for the SK detector, obtained using Eq. (3.35) and the size of the inner detector.

The upward-going muons can be divided into through-going and stopping muons, applying Eq. (3.34). Using the tabulated values of Ref. [163] for the muon energy loss in

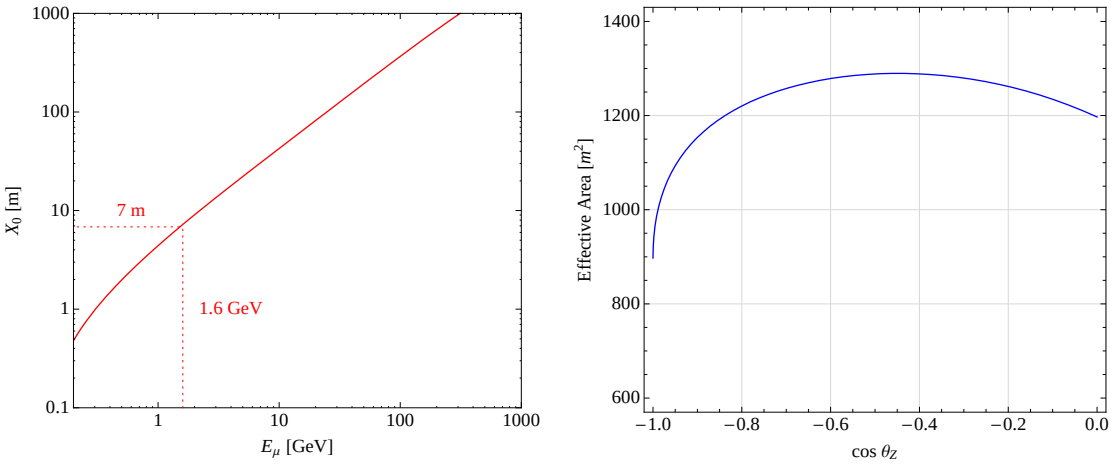

Figure 3.6: Left panel: muon range in water. Right panel: zenith angle dependence of the effective area for the Super-Kamiokande detector, obtained using the analytic expression reported in Eq. (3.35). The agreement with the Monte Carlo simulation of Ref. [162] is excellent.

rock and in water, we calculate the expected muons background coming from atmospheric neutrinos. Our results, shown in Fig. 3.7, reproduce with great accuracy the zenith angle distributions as predicted by the SK collaboration.

The limits on the muon fluxes coming from DM annihilations in the Sun and in the Earth can be defined as [5]

$$\Phi_\mu(\theta_z;\, 90\%\ \text{C.L.}) = \frac{N_{90}}{A(L_{\rm min}, \theta_z) \times T}\,, \tag{3.38}$$

where N_{90} is the upper Poissonian limit at 90% C.L., given the measured events and the muon background from atmospheric neutrinos, and T is the detector lifetime. We do not consider the detector efficiency, since it is almost equal to 100% for upward-going muons. Using Eq. (3.38) and the SK data collected from May 1996 to July 2001 [13], we find the following limits on through-going (Φ_μ^T) and stopping (Φ_μ^S) muons at 90% confidence level:

$$\Phi^T_{\mu,\rm Sun} \lesssim 1.2 \times 10^{-14}\ \text{cm}^{-2}\,\text{s}^{-1}\,, \tag{3.39}$$

$$\Phi^S_{\mu,\rm Sun} \lesssim 0.5 \times 10^{-14}\ \text{cm}^{-2}\,\text{s}^{-1}\,, \tag{3.40}$$

$$\Phi^T_{\mu,\rm Earth} \lesssim 0.8 \times 10^{-14}\ \text{cm}^{-2}\,\text{s}^{-1}\,, \tag{3.41}$$

$$\Phi^S_{\mu,\rm Earth} \lesssim 0.5 \times 10^{-14}\ \text{cm}^{-2}\,\text{s}^{-1}\,. \tag{3.42}$$

The limits for the Earth are obtained considering a cone half-angle $\theta \simeq 25^\circ$ around the Earth's center, while the values reported for the Sun are valid for a cone half-angle $\theta \simeq 20^\circ$

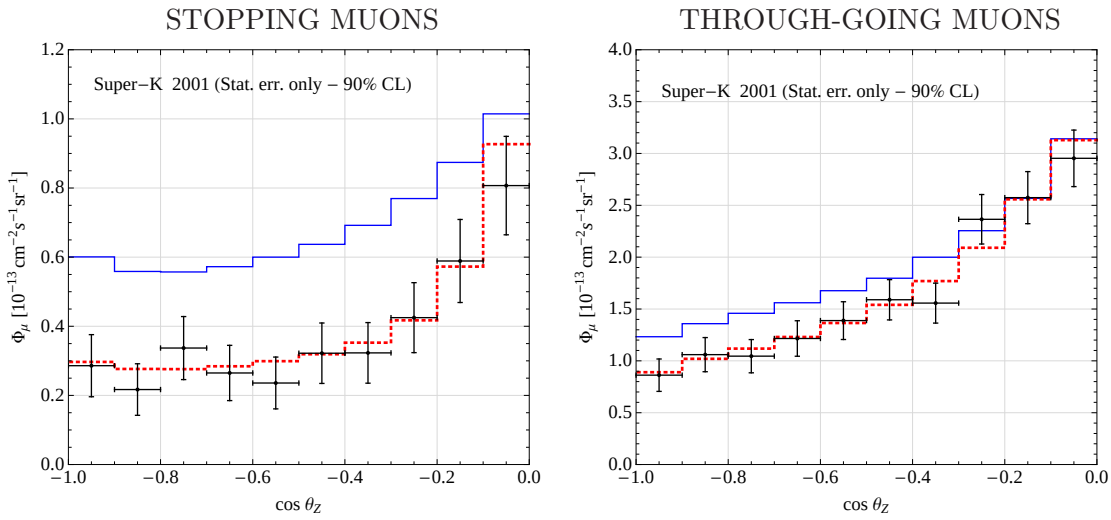

Figure 3.7: Upward stopping and through-going atmospheric muons at the Super-Kamiokande detector. The solid blue (dashed red) lines represent the expected muon fluxes without (with) oscillations. The data points are taken from [13]. We report only the statistical error at 90% confidence level. The agreement with the Monte Carlo simulations of Ref. [162] is extremely good.

around the direction of the Sun. The values for through-going muons are consistent with the ones provided by the SK collaboration [5].

Note that in the calculation of the muon flux, we have neglected the kinematical angle between the neutrino and muon direction, which can be relatively large for muons close to threshold. In any case, the average deflection angle is at most of the same order of the angular bin over which we integrate our signal, for the stopping and for the through-going muons. Considering also the detector resolution, neglecting the kinematical angle does not affect our results in a relevant way. This is confirmed by the quite good agreement we obtain in our calculation of the atmospheric neutrino events with the SK evaluation [162].

The values reported in Eqs. (3.39)÷(3.42) can be compared with the muon flux induced by DM annihilations and can be used to set limits on the DM scattering cross section. We will apply these limits in the study of the muon flux for leptophilic and the light neutralino DM, see Chapter 5.

In Fig. 3.8, we display the ratios between the muon fluxes at the Super-Kamiokande detector, arising from DM pair annihilations into $b\bar{b}$ and $\tau\bar{\tau}$, and the DM annihilation rates, in the case of the Sun and the Earth. The muons have been divided into stopping and through-going events. Since the light neutralinos annihilates manly into $b\bar{b}$ for $m_\chi \lesssim 30$ GeV, it is clear from the plots that the category of stopping muons will provide the dominant signal for low values of the neutralino mass.

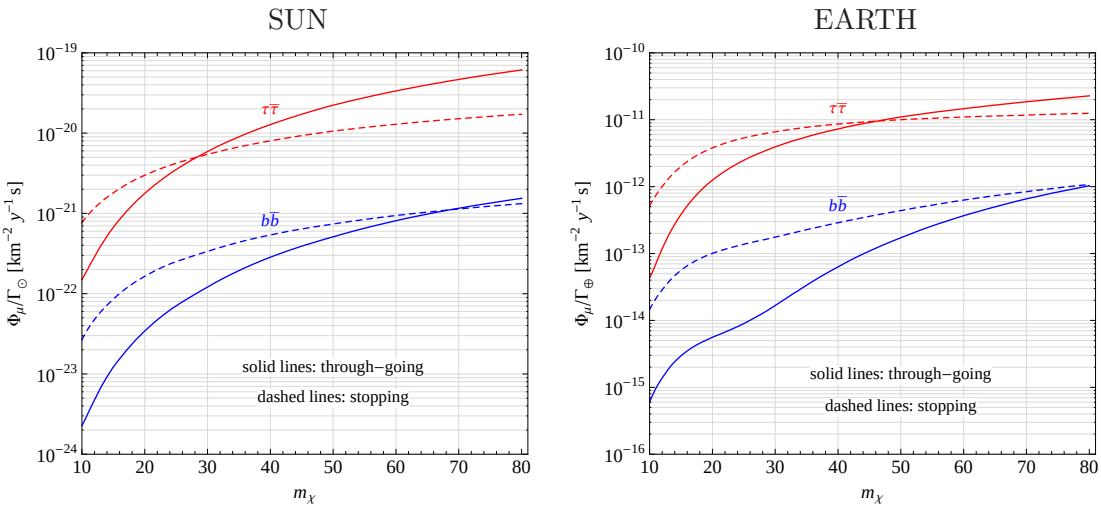

Figure 3.8: Ratio between the muon flux Φ_μ and the annihilation rate Γ, for DM pair-annihilation inside the Sun and the Earth, as a function of the DM mass m_χ. We consider the $\tau\bar{\tau}$ and the $b\bar{b}$ annihilation channels and we divide between upward stopping (dashed lines) and through-going muons (solid lines), considering the geometry of the Super-Kamiokande detector.

Northern hemisphere

The ANTARES detector is a water Cherenkov detector in the deep Mediterranean Sea, offshore from Toulon in France [7]. It consists of 12 strings, covering an area of 0.1 km^2, with a height of 350 m and is by now the largest neutrino telescope on the Northern hemisphere.

The construction of two other small neutrino telescopes in the Mediterranean Sea is ongoing: NEMO in the Sicilian Sea [164] and NESTOR [165] near Pylos, in Greece. ANTARES, NEMO and NESTOR are three pilot projects for the future construction of a cubic kilometer telescopes in the Northern hemisphere: the KM3Net project [8]. This future neutrino telescope, with a planned energy threshold of about 50-100 GeV, will be complementary to Ice-Cube, which is located at the South Pole. It will be particularly important for DM searches, as it will be able to look at the galactic center that is hardly visible with a neutrino telescope at the South Pole. In Fig. 3.9, we report the bounds on the DM annihilation cross section $\sigma_{\rm ann}v$ that could be set using contained muon events in a KM3Net-like detector. We have considered a cone half-angle of 30° around the galactic center and we have fixed the muon energy threshold to $E_\mu = 100$ GeV. The exposure is set to one year. The curves are derived assuming that the DM particles annihilate 100% into neutrinos with a flavour-blind branching ratio. We show the limits for the isothermal and the NFW density profiles. The Halo Angular bound has been derived in Ref. [150] comparing the energy spectrum produced by DM pair-annihilation into neutrinos with the atmospheric neutrino background and considering a cone half-angle of about 30°

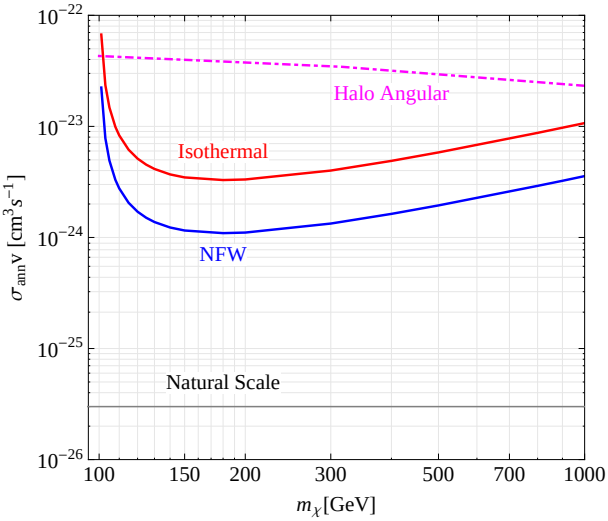

Figure 3.9: Limits (at 3σ level) from contained muon events on the total annihilation cross section $\sigma_{\rm ann}v$, after one year of exposure and for a cone half-angle of 30° around the galactic center. The energy threshold has been fixed to E_μ=100 GeV and we have considered an energy independent effective area equal to $A_{\rm eff}$ =1 km^2 (KM3Net-like detector). We have taken the isothermal and the NFW density profiles. The gray solid line indicates the standard value of $\sigma_{\rm ann}v$ for a thermal relic (natural scale). The Halo Angular line represents the bound from neutrino searches, see text for more details.

around the GC with a value of $J \simeq 25$.

Southern hemisphere

The IceCube detector [166] is a neutrino telescope under construction at the South Pole, that replaced the old AMANDA detector [167]. It will be completed in January 2011 and it will consist of 80 strings, covering one km^3 of volume and 6 additional strings concentrated in the central part, which will form the Deep Core sub-detector. Each string carries 60 Digital Optical Modules (DOM) to detect Cherenkov light.

The recent results of IceCube with 22-strings [6, 168] improved the SK bound on the muon flux Φ_μ in the high mass region: $m_\chi \gtrsim 200$ GeV for the hard annihilation channel (W^+W^-) and $m_\chi \gtrsim 500$ GeV for the soft channel ($b\bar{b}$). The IceCube detector, provided with the Deep Core arrays [169], will also constrain the parameter space at lower masses, improving significantly the SK bound for the mass region $m_\chi \gtrsim 40$ GeV [136]. However, it will not be able to put bounds on really light DM particles, for which the SK bounds will still remain to be the strongest ones.

4

Dark Matter annihilation into neutrinos

The most interesting signal to look for at neutrino telescopes is represented by a monochromatic neutrino signal, which can be produced by DM pair-annihilations directly into $\nu\bar{\nu}$ or into $\nu\nu$ ($\bar{\nu}\bar{\nu}$), if we allow for lepton number violating processes (LNV). The neutrino energy spectra produced in these annihilation channels are constituted of a soft part and a line at energy $E_\nu \simeq m_\chi$. The detection of this kind of signal would provide a clear and distinct hint for a DM annihilation origin.

The main scope of this Chapter is to carefully analyze the DM pair-annihilation into neutrino final states. We restrict our study to the two-body direct production, since this is the golden channel for DM discovery at neutrino telescopes. In our analysis, we distinguish between Dirac and Majorana neutrinos and, in the latter case, we consider explicitly different neutrino mass mechanisms, since this can be fundamental to correctly relate the physical neutrino mass to the neutrinos Yukawa couplings with, e.g., a scalar particle. A brief review of the possible neutrino mass terms is presented in Sect. 4.1. We report in Sect. 4.2 the various possibilities for monoenergetic neutrino production, considering explicitly scalar and fermionic DM, as well as the corresponding s, t, and u channels. For simplicity, we do not extend the Standard Model (SM) gauge group, but we contemplate different $SU(2)_L$ representations for the DM and the mediator particles. This kind of systematic analysis was not presented before in the literature. A summary of all the unsuppressed scenarios is given in Sect. 4.3. We explicitly show the behaviour of the annihilation cross sections for a promising s-channel and t-channel diagram, considering both the case of scalar and fermionic DM. Our results are then compared to experimental limits on μ and τ decays and on lepton flavour violating processes. The constraints coming from neutrino searches are also considered. For specific models in which the DM particles annihilate mainly in neutrinos see e.g. Refs. [170, 171].

4.1 The neutrino mass terms

Throughout our work we consider the SM gauge group, $SU(3)_c \times SU(2)_L \times U(1)_Y$. In this framework, the left-handed components of the neutrinos and the charged leptons form a doublet under $SU(2)_L$, while the right-handed components of the neutrinos, if they are present, are total singlets:

$$L_{\alpha\,L} = \begin{pmatrix} \nu_\alpha \\ \alpha \end{pmatrix}_L \sim (\mathbf{1}, \mathbf{2}, -1)\,, \qquad \nu_{\alpha\,R} \sim (\mathbf{1}, \mathbf{1}, 0)\,, \tag{4.1}$$

where α is the generation index ($\alpha = e, \mu, \tau$). Depending on the nature of the neutrinos, different mass terms can be present in the Lagrangian. If the neutrinos are Dirac particles, they will be associated with a Dirac mass term, see Sect. 4.1.1, while, if they are Majorana particles, a Majorana mass term will be allowed, see Sect. 4.1.2. The most satisfactory ways to explain the smallness of the neutrino mass are represented by the type I and type II see-saw mechanisms, which we briefly review in Sect. 4.1.3. For more details on the physics of massive neutrinos, we refer to Refs. [115, 172]

4.1.1 Dirac mass term

If the neutrinos are Dirac particles, they will get their mass by the SM Higgs mechanism:

$$\mathcal{L}_{\text{mass}} = -Y_D^{\alpha\beta}\,\overline{L_{\alpha L}}\,\tilde{H}\,\nu_{\beta R} + h.c. \;\rightarrow\; -v_H Y_D^{\alpha\beta}\overline{\nu_{\alpha L}}\nu_{\beta R} + h.c.\,, \tag{4.2}$$

where H is the SM Higgs and $v_H = 174$ GeV is its vev. We have used the notation $\tilde{H} \equiv i\sigma_2 H^*$, with σ_2 being the second Pauli matrix. The neutrino mass matrix in the flavour basis $M_\nu = v_H Y_D$ is then related to the diagonal neutrino mass matrix $D_\nu = \text{diag}(m_1, m_2, m_3)$ by

$$M_\nu = U D_\nu U^\dagger\,, \tag{4.3}$$

where U is the leptonic mixing (PMNS) matrix. Note that, since the neutrino masses are small, the Yukawa couplings must be tiny, of the order of $Y_D \sim 10^{-12}$.

4.1.2 Majorana mass term

In case the neutrinos are Majorana particles, beyond the standard mass term of Eq. (4.2), also terms of the form $\overline{(\nu_L)^C}\nu_L$ or $\overline{(\nu_R)^C}\nu_R$ may be allowed. In the first case, a scalar triplet field T, with

$$T = \begin{pmatrix} T^-/\sqrt{2} & T^0 \\ T^{--} & -T^-/\sqrt{2} \end{pmatrix}\,, \tag{4.4}$$

is needed to obtain a term that is gauge invariant under the SM gauge group:

$$\mathcal{L}_{\text{mass}} = -\frac{1}{2}\,Y_L^{\alpha\beta}\,\overline{(L_{\alpha L})^C}\,(i\sigma_2\,T)\,L_{\beta L} + h.c. \;\rightarrow\; -\frac{1}{2}m_L^{\alpha\beta}\overline{(\nu_{\alpha L})^C}\nu_{\beta L} + h.c.\,, \tag{4.5}$$

where $m_L^{\alpha\beta} = v_T Y_L^{\alpha\beta}$, with v_T being the vev of the neutral component of the scalar triplet.

If right-handed neutrinos are present, a Majorana mass term can be written without extending the SM scalar sector, since

$$\mathcal{L}_{\text{mass}} = -\frac{1}{2} M_R^{\alpha\beta} \overline{(\nu_{\alpha R})^C} \, \nu_{\beta R} + h.c. \,, \tag{4.6}$$

is invariant under the SM gauge group. The Majorana mass term could arise from a high energy theory beyond the SM, whose symmetries might be broken at the grand unification scale. In this case, we would expect M_R to be of the order of $10^{14} - 10^{16}$ GeV. Moreover, since M_R is not related to the vev v_H, there is no a priori reason for it to be at the electroweak scale.

4.1.3 See-saw mechanisms

The combination of the Dirac and Majorana mass terms leads to the so-called see-saw mechanisms, where the smallness of the neutrino mass is a consequence of the heavy right-handed neutrino fields.

In the case of a type I see-saw mechanism we have, additionally to Eq. (4.2), also a pure Majorana mass term for the right-handed neutrinos, which we denote in this Section by N_R. The complete neutrino mass term, after symmetry breaking, is given by

$$\begin{aligned} \mathcal{L}_{\text{mass}} &= -\overline{\nu_L} m_D N_R - \frac{1}{2} \overline{(N_R)^C} M_R N_R + h.c. = \\ &= -\frac{1}{2} (\overline{\nu_L}, \overline{(N_R)^C}) \left(\begin{array}{c|c} 0 & m_D \\ \hline m_D^T & M_R \end{array} \right) \begin{pmatrix} (\nu_L)^C \\ N_R \end{pmatrix} + h.c., \end{aligned} \tag{4.7}$$

where $m_D = v_H Y_D$ is the Dirac mass matrix and M_R is the Majorana mass matrix for the right-handed neutrinos. The former is connected to the electroweak scale v_H, while the latter can have a much larger value, since it is a singlet under the SM gauge group. The above Lagrangian is not yet written in the mass basis. Before a complete diagonalization, it is useful to bring the matrix to a block diagonal form, which will then separate the neutrino states into heavy and light ones. Denoting the rotated states by ν' and N', we can write the Lagrangian as

$$\mathcal{L}_{\text{mass}} \approx -\frac{1}{2} (\overline{\nu'_L}, \overline{(N'_R)^C}) \left(\begin{array}{c|c} -m_D M_R^{-1} m_D^T & 0 \\ \hline 0 & M_R \end{array} \right) \begin{pmatrix} (\nu'_L)^C \\ N'_R \end{pmatrix} + h.c. \,, \tag{4.8}$$

where we have neglected the small corrections to the heavy neutrino masses. The rotation required to bring the matrix into this form is only a very tiny one. In the case of only one generation of fermions, the corresponding mixing angle between heavy and light states is $\theta \approx \frac{m_D}{M_R} \sim 10^{-14} - 10^{-12}$. As a consequence, the interaction eigenstate ν_L is essentially a light mass eigenstate, while N_R has only a small fraction $\frac{m_D}{M_R}$ of the light mass eigenstate. In the flavour basis, the corresponding light neutrino mass matrix is given by

$$M_\nu \equiv -m_D M_R^{-1} m_D^T = U D_\nu U^T \,. \tag{4.9}$$

If beyond the terms of Eq. (4.8) a left-handed Majorana mass term m_L is present, a type II see-saw mechanism will be induced. In this case, we would have

$$\mathcal{L}_{\text{mass}} = -\frac{1}{2}(\overline{\nu_L}, \overline{(N_R)^C}) \left(\begin{array}{c|c} m_L & m_D \\ \hline m_D^T & M_R \end{array}\right) \begin{pmatrix} (\nu_L)^C \\ N_R \end{pmatrix} + h.c.\,, \tag{4.10}$$

with $m_L = v_T Y_L$. After a tiny rotation, the above mass matrix assumes the following block diagonal form:

$$\mathcal{L}_{\text{mass}} \approx -\frac{1}{2}(\overline{\nu'_L}, \overline{(N'_R)^C}) \left(\begin{array}{c|c} m_L - m_D M_R^{-1} m_D^T & 0 \\ \hline 0 & M_R \end{array}\right) \begin{pmatrix} (\nu'_L)^C \\ N'_R \end{pmatrix} + h.c. \tag{4.11}$$

Considering only one generation of fermions, the rotation angle is given by

$$\theta \sim \frac{m_D}{M_R - m_L} \approx \frac{m_D}{M_R}\,, \tag{4.12}$$

where we have used the fact that $m_L \ll M_R$, since the correction to the ρ-parameter forces the vev v_T to be $\lesssim \mathcal{O}(1\text{ GeV})$. In the case of see-saw type II, Eq. (4.9) is thus modified to

$$M_\nu \equiv m_L - m_D M_R^{-1} m_D^T = U D_\nu U^T\,, \tag{4.13}$$

where M_ν is the light neutrino mass matrix in flavour space.

4.2 Production of monoenergetic neutrinos

Depending on the gauge quantum numbers assigned to the DM particle and to the neutrino, specific annihilation processes will be allowed in the s, t, u channels. In our analysis, we consider the DM particle χ and the mediator particle ϕ to be a singlet, doublet or triplet representation of $SU(2)_L$. In general, for a scalar ψ_s and for a fermion ψ_f we use the following definitions:

$$\begin{aligned} \psi_{s;1} &\sim (\mathbf{1}, \mathbf{1}, 0)\,, & \psi_{f;1} &\sim (\mathbf{1}, \mathbf{1}, 0) \\ \psi_{s;2} = \begin{pmatrix} \psi^+ \\ \psi^0 \end{pmatrix} &\sim (\mathbf{1}, \mathbf{2}, 1)\,, & \psi_{f;2} = \begin{pmatrix} \psi^0 \\ \psi^- \end{pmatrix} &\sim (\mathbf{1}, \mathbf{2}, -1)\,, \\ \psi_{s;3} = \begin{pmatrix} \psi^+/\sqrt{2} & \psi^{++} \\ \psi^0 & -\psi^+/\sqrt{2} \end{pmatrix} &\sim (\mathbf{1}, \mathbf{3}, 2)\,, & \psi_{f;3} = \begin{pmatrix} \psi^-/\sqrt{2} & \psi^0 \\ \psi^{--} & -\psi^-/\sqrt{2} \end{pmatrix} &\sim (\mathbf{1}, \mathbf{3}, -2)\,. \end{aligned}$$

We will comment later on the possibility of having an $SU(2)_L$ triplet with a null hypercharge.

We present a model independent analysis of all the possible production channels, extending the work presented in Ref. [173], in which the authors restrict themselves to the case of Dirac DM annihilating through an s channel diagram. In Sect. 4.2.1 and Sect. 4.2.2, we present the results for direct neutrino production in the case of scalar and fermionic DM, respectively. To be exhaustive, we explicitly divide the results for four

different neutrino scenarios: Dirac neutrinos, for which the left-handend and the right-handed neutrinos are both present and independent; Majorana neutrinos, in which case the singlet neutrinos $\nu_{\alpha R}$ are not present and the right-handed neutrinos are simply given by the $(\nu_{\alpha L})^C$; Majorana neutrinos with see-saw type I or type II, if the right-handed neutrinos $\nu_{\alpha R}$ are present and acquire generally a heavy mass.

In our study, we do not consider explicitly the case of vector DM. It is known, indeed, that a spin one DM particle can have a sizable branching ratio into neutrinos, see e.g. Ref. [171]. The main aim of our analysis is, instead, to show that also in the framework of a scalar and a fermionic DM the direct neutrino production can be relevant. However, for completeness, we report in Sect. C.3 the explicit expressions for the annihilation cross sections in the case of a vector DM.

We wish to recall that the neutrino production through DM annihilations into three body final states has also been vastly discussed in the literature. For instance, in Ref. [174] the authors analyzed the electroweak bremsstrahlung processes $\chi\chi \to \nu\bar{\nu}Z$ and $\chi\chi \to \nu e W$. The hadronic decays of the weak bosons can lead to the production of photons, which can then be used to further constraint the annihilation cross section value, see e.g. Ref. [175] for the Z-strahlung process. Moreover, the DM annihilation into neutrinos will induce, at loop level, electromagnetic final states, for which the synchrotron radiation bounds of Ref. [176] can be imposed, see Ref. [177] for an exhaustive discussion on this aspect.

4.2.1 Scalar Dark Matter

This Section summarizes the results that we obtained for the case of scalar DM, considering singlet, doublet and triplet representations of $SU(2)_L$. The basic assumptions are that the scalar DM has a null vev $\langle\chi\rangle = 0$ and that it is stable, because being odd under some Z_2-parity, while all the other SM particles are even.

Scalar mediator, s-channel

In the case of a singlet, doublet or triplet scalar mediator, the following Yukawa interactions with the neutrinos are allowed:

$$\mathcal{L}_{Y_{\nu;1}} = -Y_{\nu;1}^{\alpha\beta}\,\overline{(\nu_{\alpha R})^C}\,\phi_{s;1}\,\nu_{\beta R} + h.c.\,, \tag{4.14}$$

$$\mathcal{L}_{Y_{\nu;2}} = -Y_{\nu;2}^{\alpha\beta}\,\overline{L_{\alpha L}}\,\tilde{\phi}_{s;2}\,\nu_{\beta R} + h.c.\,, \tag{4.15}$$

$$\mathcal{L}_{Y_{\nu;3}} = -Y_{\nu;3}^{\alpha\beta}\,\overline{(L_{\alpha L})^C}\,(i\sigma_2\,\phi_{s;3})\,L_{\beta L} + h.c.\,, \tag{4.16}$$

where α and β are flavour indices. We have defined $\tilde{\phi} \equiv i\sigma_2\phi^*$, with σ_2 being the second Pauli matrix. Note that the entries of the Yukawa coupling matrices are in general complex numbers and that a triplet scalar mediator with zero hypercharge $\phi_{s;3} \sim (\mathbf{1}, \mathbf{3}, 0)$ does not couple to neutrinos in a s channel diagram.

The singlet scalar mediator $\phi_{s;1}$ can couple to a pair of scalar DM particles, which transform under $SU(2)_L$ as a singlet, doublet or triplet. However, it will always produce

a physical right-handed (light) neutrino as well as a left-handed (light) anti-neutrino. Both these particles are sterile and making them interacting would require a coupling to the Higgs field (or, equivalently, a helicity flip), which is proportional to m_ν. This would lead to a negligible muon flux at neutrino telescopes. Notice also that the coupling of the singlet scalar to neutrinos, Eq. (4.14), could, in general, generate a violation of lepton number L and is hence connected to Majorana neutrinos. Indeed, the interaction term $\overline{(\nu_R)^C}\,\phi_{s;1}\,\nu_R$ either directly violates lepton number or it forces the singlet scalar to carry lepton number. In the latter case, the coupling of $\phi_{s;1}$ to the SM Higgs, $H^\dagger H\phi_{s;1}$, will be problematic. However, if such a coupling is forbidden in certain specific models, one might still be able to conserve lepton number.

If the doublet scalar mediator $\phi_{s;2}$ does not get a vev, the entries in the Yukawa coupling matrix $Y_{\nu;2}$ could be large, as they do not contribute to the neutrino mass. However, a fundamental problem arises from the coupling to the scalar DM. Since we consider only the cases for which the scalar DM particle does not get a vev, the corresponding vertex must arise from a fundamental 3-scalar coupling in the Higgs potential. In $SU(2)_L$, such a fundamental 3-scalar coupling is impossible, since we have $\mathbf{2}\otimes\mathbf{1}\otimes\mathbf{1} = \mathbf{2}$, $\mathbf{2}\otimes\mathbf{2}\otimes\mathbf{2} = \mathbf{2}\oplus\mathbf{2}\oplus\mathbf{4}$, $\mathbf{2}\otimes\mathbf{3}\otimes\mathbf{3} = \mathbf{2}\oplus\mathbf{2}\oplus\mathbf{4}\oplus\mathbf{4}\oplus\mathbf{6}$. This problem could be overcome if one allowed for a non-vanishing vev $\langle\phi_{s;2}\rangle \neq 0$. However, in this way the Yukawa coupling $Y_{\nu;2}$ becomes directly proportional to the light neutrino mass for the case of Dirac neutrinos. In the presence of a see-saw situation, the Yukawa coupling could be in principle sizable, since it is not directly related to the neutrino mass. Despite that, since the light mass eigenstate of ν_R must be produced, this possibility is suppressed by the mixing angle θ between the heavy and light neutrinos. This is of $\mathcal{O}\left(m_D M_R^{-1}\right)$ and hence very small, for the standard value of $M_R = \mathcal{O}(10^{16}\text{ GeV})$.

The interaction of the triplet scalar mediator $\phi_{s;3}$ with neutrinos, Eq. (4.16), induces a violation of lepton number (in analogy to the singlet scalar mediator $\phi_{s;1}$) and is thus associated only to Majorana neutrinos and not to Dirac neutrinos. In case the scalar mediator has a null vev, the neutrino coupling $Y_{\nu;3}$ is unsuppressed, since is not constrained by the neutrino mass scale. Furthermore, two active neutrinos are produced, since the triplet scalar couples to $\overline{(\nu_L)^C}\nu_L$. This conclusion does not depend on the particular neutrino mass model considered. Indeed, in the case of see-saw type I, the correction factor, resulting from ν_L being not an exact mass eigenstate, is given by $(1-\theta)^2 \simeq 1$. If the neutrinos acquire a mass through a see-saw type II model, the only difference is the presence of an additional Higgs triplet with vev, in order to have the correct see-saw type II neutrino mass formula.

The DM vertex for the case $\langle\phi_{s;3}\rangle = 0$ can come from a fundamental 3-scalar term in the Higgs potential. This coupling is allowed only if χ is an $SU(2)_L$ doublet. In this case, the important term in the Lagrangian is of the form

$$\mathcal{L}_{\chi\phi}^{(2,3)} \supset \gamma_{\chi\phi}^{(2,3)}\left(\chi_{s;2}^\dagger\phi_{s;3}\tilde{\chi}_{s;2}\right) + h.c. \tag{4.17}$$

If the triplet scalar mediator has a nonzero vev, $\langle\phi_{s;3}\rangle \neq 0$, it will contribute to a Majorana neutrino mass $\overline{(\nu_L)^C}\nu_L$ and it will induce a see-saw type II situation. Thus,

the light neutrino mass matrix would be given by

$$M_\nu = v_T Y_{\nu;3} - v_H^2 Y_{\nu;2} M_R^{-1} Y_{\nu;2}^T \,, \tag{4.18}$$

where v_H is the electroweak vev and v_T is the triplet scalar vev. To yield physically realistic light neutrino masses, the entries in the Yukawa coupling matrix $Y_{\nu;3}$ of the triplet to the neutrinos must be very small, in case the triplet contribution dominates the physical neutrino masses.[1] On the other hand, the combination of the Dirac Yukawa coupling $Y_{\nu;2}$ and the heavy neutrino mass matrix M_R has to be tiny as well, if this part dominates the physical neutrino mass. The only case where we can have larger values for $Y_{\nu;3}$, which, in turn, could lead to larger annihilation rates, is the one where there is a cancellation between $v_T Y_{\nu;3}$ and $v_H^2 Y_{\nu;2} M_R^{-1} Y_{\nu;2}^T$ in Eq. (4.18). For simultaneously having Yukawa couplings of $\mathcal{O}(0.1)$ and sub-eV neutrino masses, this cancellation would, however, need to be at the level of 10^{-8} (for $v_T \approx 1$ GeV), which would require a strong fine-tuning. Nevertheless, this possibility might be motivated in a certain specific model.

The corresponding couplings of the $SU(2)_L$ triplet scalar mediator $\phi_{s;3}$ with non vanishing vev to the DM particles can arise from the following terms in the Lagrangian:

$$\mathcal{L}_{\chi\phi}^{(1,3)} = \lambda_{\chi\phi}^{(1,3)} (\chi_{s;1}^\dagger \chi_{s;1}) \mathrm{Tr}(\phi_{s;3}^\dagger \phi_{s;3}) \,, \tag{4.19}$$

$$\begin{aligned} \mathcal{L}_{\chi\phi}^{(2,3)} &= \lambda_{\chi\phi}^{(2,3)} (\chi_{s;2}^\dagger \chi_{s;2}) \mathrm{Tr}(\phi_{s;3}^\dagger \phi_{s;3}) + \beta_{\chi\phi}^{(2,3)} (\chi_{s;2}^\dagger \phi_{s;3}^\dagger \phi_{s;3} \chi_{s;2}) + \\ &+ \left[\gamma_{\chi\phi}^{(2,3)} (\chi_{s;2}^\dagger \phi_{s;3} \tilde{\chi}_{s;2}) + h.c. \right] , \end{aligned} \tag{4.20}$$

$$\begin{aligned} \mathcal{L}_{\chi\phi}^{(3,3)} &= \lambda_{\chi\phi}^{(3,3)} \mathrm{Tr}(\chi_{s;3}^\dagger \chi_{s;3}) \mathrm{Tr}(\phi_{s;3}^\dagger \phi_{s;3}) + \\ &+ \left[\xi_{\chi\phi}^{(3,3)} \mathrm{Tr}(\chi_{s;3} \chi_{s;3}) \mathrm{Tr}(\phi_{s;3}^\dagger \phi_{s;3}^\dagger) + h.c. \right] . \end{aligned} \tag{4.21}$$

The triplet scalar mediator appears as the most promising case for having a sizable neutrino production. However, depending on the specific model, its coupling to the leptons can be subject to constraints coming from different experiments. We postpone the explicit discussion of these bounds to Sect. 4.3.1.

Z-boson mediator, s-channel

The coupling between the neutrinos and the Z-boson comes from the kinetic term in the Lagrangian. We define the covariant derivative as

$$D_\mu = \partial_\mu + i\frac{g}{2}(\boldsymbol{\sigma} \cdot \mathbf{W}_\mu) + i\frac{g'}{2} Y B_\mu \,, \tag{4.22}$$

with $\boldsymbol{\sigma}$ being the Pauli matrices. The couplings g and g' are, respectively, the gauge couplings of $SU(2)_L$ and $U(1)_Y$. The corresponding gauge fields are denoted by W_μ and

[1] Note that, although the vev is forced by the correction to the ρ-parameter to be $v_T \lesssim \mathcal{O}(1\text{ GeV})$, the Yukawa coupling still needs to be tiny to yield sub-eV neutrino masses.

B_μ. Introducing the physical states

$$W_\mu^\pm = \frac{W_\mu^1 \mp i W_\mu^2}{\sqrt{2}}\,, \tag{4.23}$$

$$A_\mu = B_\mu \cos\theta_W + W_\mu^3 \sin\theta_W\,, \tag{4.24}$$

$$Z_\mu = -B_\mu \sin\theta_W + W_\mu^3 \cos\theta_W\,, \tag{4.25}$$

where θ_W is the Weinberg angle, the interaction term of the neutrinos with the Z-boson is given by

$$\mathcal{L}_L^{\rm kin} = \overline{L_L} i\gamma^\mu D_\mu L_L \to -\frac{g}{2\cos\theta_W}\overline{\nu_L}\gamma^\mu \nu_L Z_\mu\,. \tag{4.26}$$

Only if the DM particle transforms as a doublet or triplet under $SU(2)_L$, it can couple to the Z-boson. The specific couplings arise from the following gauge-kinetic terms:

$$\begin{aligned}\mathcal{L}_{\chi;2}^{\rm kin} &= (D_\mu \chi_{s;2})^\dagger (D^\mu \chi_{s;2}) \\ &\to -\frac{ig}{2\cos\theta_W}(\cos^2\theta_W + Y\sin^2\theta_W)\,\partial_\mu \chi^{0,*}\chi^0 Z^\mu \;+\; h.c.\,, \end{aligned}\tag{4.27}$$

$$\begin{aligned}\mathcal{L}_{\chi;3}^{\rm kin} &= {\rm Tr}\left[(D_\mu \chi_{s;3})^\dagger (D^\mu \chi_{s;3})\right] \\ &\to -\frac{ig}{2\cos\theta_W}(2\cos^2\theta_W + Y\sin^2\theta_W)\,\partial_\mu \chi^{0,*}\chi^0 Z^\mu \;+\; h.c.\,, \end{aligned}\tag{4.28}$$

where the covariant derivative for $\chi_{s;2}$ is defined analogously to Eq.(4.22), while for $\chi_{s;3}$ it is given by

$$D_\mu \chi_{s;3} = \partial_\mu\, \chi_{s;3} + i\frac{g}{2}\left[\boldsymbol{\sigma}\cdot \mathbf{W}_\mu, \chi_{s;3}\right] + i\frac{g'}{2} Y B_\mu \chi_{s;3}\,. \tag{4.29}$$

Fermionic mediator, t&u-channels

For the t and u-channel diagrams, either the scalar DM or the fermionic mediator has to be flavoured, such as in the case of a sneutrino DM or a neutrino mediator. This property has to be taken into account in any specific model and it will decide on the actual existence of a t-channel diagram. For definiteness, throughout our discussion, we suppose that the scalar DM particle carries a flavour. Our conclusions are as well applicable to the case in which the fermionic mediator is flavoured.

We consider a fermionic mediator, whose left and right components can transform under $SU(2)_L$ as singlets, doublets or triplets. If the fermionic mediator is an $SU(2)_L$ singlet, $[\phi_{f;1}]_{L,R}$, the following interaction terms are allowed:

$$\mathcal{L}_{\chi\phi\nu}^{(1,1)} = \mathcal{T}_{\alpha k}^{(1,1)}\,\overline{\nu_R^\alpha}\,\chi_{s;1}^k\,[\phi_{f;1}]_L \;+\; h.c.\,, \tag{4.30}$$

$$\mathcal{L}_{\chi\phi\nu}^{(2,1)} = \mathcal{T}_{\alpha k}^{(2,1)}\,\overline{L_L^\alpha}\,\tilde{\chi}_{s;2}^k\,[\phi_{f;1}]_R \;+\; h.c.\,, \tag{4.31}$$

where $\mathcal{T}_{\alpha k}^{(i,j)}$ are trilinear couplings, with α being an index in flavour space and k being the index that denotes the lightest scalar particle. In general, indeed, different flavoured states of the scalar particle $\chi_{s;1}^{\beta}$ can exist. The DM particle will then be identified as the lightest particle among the mass eigenstates, $\chi_{s;1}^{k} = W_{k\beta}\chi_{s;1}^{\beta}$, with W being a rotation matrix. The indices (i, j) are, respectively, the $SU(2)_L$ representations of the DM and of the fermionic mediator. If the DM is a singlet scalar, it will only couple to sterile neutrinos, while, if it is the neutral component of a doublet, active neutrinos can be produced.

If the fermionic mediator is an $SU(2)_L$ doublet, $[\phi_{f;2}]_{L,R}$, the interaction terms that lead to a coupling between the DM particle and the neutrino are:

$$\begin{aligned}
\mathcal{L}_{\chi\phi\nu}^{(1,2)} &= \mathcal{T}_{\alpha k}^{(1,2)}\, \overline{L_L^{\alpha}}\, [\phi_{f;2}]_R\, \chi_{s;1}^{k} \;+\; h.c.\,, \\
\mathcal{L}_{\chi\phi\nu}^{(2,2)} &= \mathcal{T}_{\alpha k}^{(2,2)}\, \overline{\nu_R^{\alpha}} (i\sigma_2 \chi_{s;2}^{k})^T\, [\phi_{f;2}]_L \;+\; h.c.\,, \\
\mathcal{L}_{\chi\phi\nu}^{(3,2)} &= \mathcal{T}_{\alpha k}^{(3,2)}\, \overline{(L_L^{\alpha})^C} (i\sigma_2 \chi_{s;3}^{k})\, [\phi_{f;2}]_L \;+\; h.c.
\end{aligned} \tag{4.32}$$

In this case a singlet and a triplet scalar DM can couple to active neutrinos, while only sterile neutrinos will be produced if the DM is an $SU(2)_L$ doublet.

Finally, if the fermionic mediator is an $SU(2)_L$ triplet, $[\phi_{f;3}]_{L,R}$, we can have the following couplings:

$$\begin{aligned}
\mathcal{L}_{\chi\phi\nu}^{(2,3)} &= \mathcal{T}_{\alpha k}^{(2,3)}\, \overline{L_L^{\alpha}}\, [\phi_{f;3}]_R\, \chi_{s;2}^{k} \;+\; h.c.\,, \\
\mathcal{L}_{\chi\phi\nu}^{(3,3)} &= \mathcal{T}_{\alpha k}^{(3,3)}\, \mathrm{Tr}\left\{ \overline{\nu_R^{\alpha}}\, [\phi_{f;3}]_L\, \chi_{s;3}^{k} \right\} \;+\; h.c.
\end{aligned} \tag{4.33}$$

Active neutrinos arise from a doublet scalar DM, while a triplet scalar DM couples only to sterile neutrinos. Moreover, if the fermion mediator is an $SU(2)_L$ triplet with $Y = 0$, it can also couple to a scalar DM triplet with $Y = 0$ and to a right-handed neutrino. This coupling would produce only sterile neutrinos and thus lead to a negligible flux.

As in the case of scalar DM pair-annihilations into neutrinos through a scalar exchange, the couplings involved in the t-channel process are subject to experimental limits, coming in particular from lepton flavour violation processes (LFV). For example, if active neutrinos are produced and if the fermionic mediator belongs to a doublet or triplet representation of $SU(2)_L$, the couplings involved in the t-channel diagram will also contribute to the $\mu \to e\gamma$ decay. Another experimental constraint that could be present is on the actual existence of the fermion particle mediating the process. We will comment on these topics in Sect. 4.3.2.

4.2.2 Fermionic Dark Matter

In this Section we consider the DM as fermionic particle and, in analogy to the scalar case, we allow for $SU(2)_L$ singlet $[\chi_{f;1}]_{L,R} \sim (\mathbf{1}, \mathbf{1}, 0)$, doublet $[\chi_{f;2}]_{L,R} \sim (\mathbf{1}, \mathbf{2}, -1)$ and triplet $[\chi_{f;3}]_{L,R} \sim (\mathbf{1}, \mathbf{3}, -2)$ representations.

Scalar mediator, s-channel

For the s-channel, the considerations for the neutrino vertex are exactly the same as in the scalar DM case. Therefore, in the following we will focus on the DM vertex only. An intermediate scalar singlet $\phi_{s;1}$ could couple to all types of fermionic DM under consideration:

$$\mathcal{L}^{(1,1)}_{Y_{\chi;1}} = -Y^{(1,1)}_{\chi;1}\,\overline{[\chi_{f;1}]_L}\,[\chi_{f;1}]_R\,\phi_{s;1} + h.c.\,, \tag{4.34}$$

$$\mathcal{L}^{(2,2)}_{Y_{\chi;1}} = -Y^{(2,2)}_{\chi;1}\,\overline{[\chi_{f;2}]_L}\,[\chi_{f;2}]_R\,\phi_{s;1} + h.c.\,, \tag{4.35}$$

$$\mathcal{L}^{(3,3)}_{Y_{\chi;1}} = -Y^{(3,3)}_{\chi;1}\,\mathrm{Tr}\left\{\overline{[\chi_{f;3}]_L}\,[\chi_{f;3}]_R\right\}\phi_{s;1} + h.c. \tag{4.36}$$

In all the above cases, the left and right components of the DM particle belong to the same representation of $SU(2)_L$, i.e. the DM is a vector-like fermion. Note that another possible expression can be obtained replacing $\overline{[\chi_{f;1}]_L}$ with $\overline{[\chi_{f;1}]_R}^{\,C}$. The interaction term obtained in this way is associate with Majorana DM particles, since it can induce a Majorana mass term. As in the scalar DM case, the problem arises at the neutrino vertex, since only sterile neutrinos can be produced by a scalar singlet.

If the scalar mediator is an $SU(2)_L$ doublet, $\phi_{s;2}$, we could have the following couplings to the DM particle:

$$\mathcal{L}^{(1,2)}_{Y_{\chi;2}} = -Y^{(1,2)}_{\chi;2}\,\overline{[\chi_{f;1}]_L}(i\sigma_2\phi_{s;2})^T\,[\chi_{f;2}]_R + h.c\,, \tag{4.37}$$

$$\mathcal{L}^{(3,2)}_{Y_{\chi;2}} = -Y^{(3,2)}_{\chi;2}\,\phi^\dagger_{s;2}\overline{[\chi_{f;3}]_L}\,[\chi_{f;2}]_R + h.c. \tag{4.38}$$

These possibilities will only be present if the left and right components of the DM particle belong to different representations of $SU(2)_L$, i.e. the DM is a chiral fermion. As for the scalar DM case, the situation in which $\phi_{s;2}$ has a nonzero vev can be neglected, since the Yukawa couplings would be proportional to the neutrino mass or the tiny mixing angle θ between the heavy and light neutrinos would be present.

If the scalar mediator is a triplet under $SU(2)_L$, $\phi_{s;3}$, the following terms are allowed:

$$\mathcal{L}^{(2,2)}_{Y_{\chi;3}} = -Y^{(2,2)}_{\chi;3}\,\overline{[\chi_{f;2}]_L}^{\,C}(i\sigma_2\phi_{s;3})\,[\chi_{f;2}]_L + h.c\,, \tag{4.39}$$

$$\mathcal{L}^{(1,3)}_{Y_{\chi;3}} = -Y^{(1,3)}_{\chi;3}\,\mathrm{Tr}\left\{\overline{[\chi_{f;1}]_L}\phi_{s;3}\,[\chi_{f;3}]_R\right\} + h.c\,, \tag{4.40}$$

where the first term will be present if the DM particle is a vector-like fermion, while the second one will be there if it is a chiral fermion. An analogous expression to Eq. (4.39) can be obtained by exchanging the subscripts "L" with "R" and considering a new Yukawa coupling $Y'^{(2,2)}_{\chi;3}$. Notice that, if Eq. (4.39) holds, the triplet scalar mediator in the s-channel is associated only with Majorana DM (as well as Majorana neutrinos), since it leads to terms that violate lepton number. If the scalar triplet acquires a nonzero vev, a see-saw type II situation is induced, in analogy to the scalar DM case, to which we refer for more details. Remember that, in principle also a DM coupling to a triplet scalar with zero hypercharge is possible, but this would not lead to a coupling to neutrinos.

Z-boson mediator, s-channel

A fermionic DM particle can couple to the Z-boson, if it is a doublet or a triplet under $SU(2)_L$. The corresponding couplings arise from the following gauge-kinetic terms in the Lagrangian:

$$\begin{aligned}
\mathcal{L}^{\rm kin}_{\chi;2} &= \overline{[\chi_{f;2}]_L} i\gamma^\mu D_\mu [\chi_{f;2}]_L \\
&\to -\frac{g}{2\cos\theta_W}(\cos^2\theta_W - Y\sin^2\theta_W)\overline{[\chi_{f;2}]^0_L}\gamma^\mu [\chi_{f;2}]^0_L Z_\mu + h.c., \qquad (4.41)\\
\mathcal{L}^{\rm kin}_{\chi;3} &= {\rm Tr}\left\{\overline{[\chi_{f;3}]_L} i\gamma^\mu D_\mu [\chi_{f;3}]_L\right\} \\
&\to -\frac{g}{2\cos\theta_W}(2\cos^2\theta_W - Y\sin^2\theta_W)\overline{[\chi_{f;2}]^0_L}\gamma^\mu [\chi_{f;2}]^0_L Z_\mu + h.c., \qquad (4.42)
\end{aligned}$$

and analogous expressions can be written for the right-handed components $[\chi_{f;2}]_R$ and $[\chi_{f;3}]_R$ of the DM particle.

Scalar mediator, t&u-channels

As in the case of scalar DM, for the t and u-channel diagrams, either the fermionic DM or the scalar mediator has to be flavoured, such as in the case of a heavy neutrino DM or a sneutrino scalar mediator. For definiteness, throughout the discussion of this Section we will suppose that the scalar mediator carries a flavour. Our conclusions are as well applicable to the case in which the DM is flavoured.

If the scalar mediator is an $SU(2)_L$ singlet $\phi_{s;1}$, the following interaction terms are allowed:

$$\mathcal{L}^{(2,1)}_{\chi\phi\nu} = \mathcal{T}^{(2,1)}_{\alpha k}\,\overline{L^\alpha_L}\,[\chi_{f;2}]_R\,\phi^k_{s;1} + h.c., \qquad (4.43)$$

$$\mathcal{L}^{(1,1)}_{\chi\phi\nu} = \mathcal{T}^{(1,1)}_{\alpha k}\,\overline{\nu^\alpha_R}\,[\chi_{f;1}]_L\,\phi^k_{s;1} + h.c., \qquad (4.44)$$

where $\mathcal{T}^{(i,j)}_{\alpha k}$ are trilinear couplings, with α being an index in flavour space and k being the index that denotes the mass eigenstate of the scalar mediator. The indices (i,j) are, respectively, the $SU(2)_L$ representations of the DM particle and of the scalar mediator. In order not to produce only sterile neutrinos, the right-handed component of the fermionic DM particle has to be an $SU(2)_L$ doublet.

If, instead, the scalar mediator is an $SU(2)_L$ doublet, $\phi_{s;2}$, the interaction terms are:

$$\begin{aligned}
\mathcal{L}^{(1,2)}_{\chi\phi\nu} &= \mathcal{T}^{(1,2)}_{\alpha k}\,\overline{L^\alpha_L}\tilde{\phi}^k_{s;2}\,[\chi_{f;1}]_R + h.c.,\\
\mathcal{L}^{(2,2)}_{\chi\phi\nu} &= \mathcal{T}^{(2,2)}_{\alpha k}\,\overline{\nu^\alpha_R}\,(i\sigma_2\phi^k_{s;2})^T\,[\chi_{f;2}]_L + h.c., \qquad (4.45)\\
\mathcal{L}^{(3,2)}_{\chi\phi\nu} &= \mathcal{T}^{(3,2)}_{\alpha k}\,\overline{L^\alpha_L}\,[\chi_{f;3}]_R\,\phi^k_{s;2} + h.c.,
\end{aligned}$$

among which only the ones involving a singlet or a triplet fermionic DM lead to active neutrinos in the final state. One specific example falling in this category would be a slight

extension of the MSSM, with an additional singlet chiral superfield, whose fermionic component acts as DM particle, while the sneutrino is the scalar mediator.

Finally, if the scalar mediator is an $SU(2)_L$ triplet, $\phi_{s;3}$, we have

$$\begin{aligned}\mathcal{L}^{(2,3)}_{\chi\phi\nu} &= \mathcal{T}^{(2,3)}_{\alpha k}\,\overline{(L^{\alpha}_{L})^{C}}(i\sigma_2\phi^{k}_{s;3})\,[\chi_{f;2}]_R \,+\, h.c.\,,\\ \mathcal{L}^{(3,3)}_{\chi\phi\nu} &= \mathcal{T}^{(3,3)}_{\alpha k}\,\mathrm{Tr}\left\{\overline{\nu^{\alpha}_{R}}\,\phi^{k}_{s;3}\,[\chi_{f;3}]_L\right\} \,+\, h.c.\,,\end{aligned} \tag{4.46}$$

where, only in the case of a doublet fermionic DM particle, the production of active neutrinos is possible.

In our analysis of the t-channel diagram for fermionic DM, we have decided to neglect the possibility that the intermediate scalar mediator acquires a nonzero vev. In this case, a mixing between the DM particle and the neutrino is induced. The corresponding constraints on the Yukawa couplings become strongly model dependent and general considerations will not be possible anymore.

As in the case of scalar DM pair-annihilations, the couplings involved in the t-channel process could be subject to the experimental limits coming from LFV processes. We refer to Sect. 4.3.2 for more details.

4.3 Discussion of unsuppressed cases

A summary of our results can be found in Table 4.1 and Table 4.2, respectively, for the case of scalar DM and of fermionic DM. In these tables, we explicitly divide between the s, t and u annihilation channels, and we consider different possible $SU(2)_L$ representations for the DM and the mediator particle. Moreover, different neutrino scenarios are considered.

In Appendix C we give the explicit expressions of the annihilation cross sections for the different cases. The results are reported in a model independent way and, therefore, can be used for any specific model.

For a scalar DM particle, the s-channel annihilation diagram can be relevant only in the presence of a triplet scalar mediator with zero vev. Moreover, this case is present only for Majorana neutrinos. The explicit expression of the annihilation cross section can be found using Eq. (C.3). Another promising situation for neutrino production is given by a t-channel diagram with a singlet, a doublet or a triplet fermion exchange. In the first case the DM particle should be a doublet under $SU(2)_L$, in the second case a singlet or a triplet and in the third case a doublet. For the t-channel diagram, the annihilation cross section will be determined mainly by the mass of the mediator, see Eq. (C.5) and Eq. (C.6).

For a fermionic DM particle, a triplet scalar exchange in an s-channel diagram can give rise to a sizable neutrino production if the left-handed or right-handed components of the DM particle transform as a doublet under $SU(2)_L$ and if the neutrinos are Majorana particles. For a chiral fermion DM, the s-channel diagram might be relevant if the scalar mediator is a doublet or a triplet under $SU(2)_L$. The first case can be present if the

Annihilation channels	Internal mediator	Dark Matter $SU(2)_L$-rep.	Dirac neutrino	Majorana neutrino	See-saw type I	See-saw type II
s	Scalar **1**	**1, 2, 3**	$\not{L}$	-	R, θ^2	R, θ^2
s	Scalar **3**	**2**	$\not{L}$	☑	☑	☑
s	Scalar **1** with vev	**1, 2, 3**	$\not{L}$	-	R, θ^2	R, θ^2
s	Scalar **2** with vev	**1, 2, 3**	m_ν	-	θ	θ
s	Scalar **3** with vev	**1, 2, 3**	$\not{L}$	m_ν	-	f.t.
s	Z-boson	**2, 3**	$\boxtimes(p)$	$\boxtimes(p)$	$\boxtimes(p)$	$\boxtimes(p)$
t, u	Fermion **1**	**1**	R	-	R, θ^2	R, θ^2
t, u	Fermion **1**	**2**	☑	☑	☑	☑
t, u	Fermion **2**	**1, 3**	☑	☑	☑	☑
t, u	Fermion **2**	**2**	R	-	R, θ^2	R, θ^2
t, u	Fermion **3**	**2**	☑	☑	☑	☑
t, u	Fermion **3**	**3**	R	-	R, θ^2	R, θ^2

Table 4.1: Summary table for scalar Dark Matter. ☑: potentially unsuppressed in at least one channel; $\boxtimes(p)$: suppressed for non-relativistic Dark Matter (p-wave term); f.t.: fine tuning required between two couplings to get a sizable rate; $\not{L}$: LNV terms are present; - : a see-saw type I and/or type II situation is present; R: yields only right-handed neutrinos; θ^n: suppressed by the n-th power of the mixing angle between heavy and light neutrinos; m_ν: the Yukawa coupling involved is proportional to the light neutrino mass.

neutrinos are Dirac particles, while the second one can be there if they are Majorana particles. The explicit expression for the annihilation cross section can be found using Eq. (C.7). As in the case of scalar DM, another promising case for neutrino production is given by the t-channel diagram with a singlet, doublet or triplet scalar exchange. In the first case, the DM particle should be a doublet under $SU(2)_L$, in the second case a singlet or a triplet, while in the third case it must be a doublet. Other unsuppressed t-channel diagrams require explicitly a chiral fermion DM, see Table 4.2. For the t-channel diagram, the annihilation cross section will be determined mainly by the mass of the DM particle, see Eq. (C.10) and Eq. (C.11). Moreover, if the DM was a Dirac fermion, also the s-channel diagram with the Z-boson exchange could lead to sizable neutrino production. In this case, the annihilation cross section will be proportional to the mass of the DM particle, see Eq. (C.8). However, particles with strong couplings to the Z-boson are constrained by DM direct detection experiments [104].

For definiteness, we focus on two different typologies of unsuppressed cases: one involving an s-channel diagram, in Sect 4.3.1, and one with a t-channel diagram, in Sect. 4.3.2. For the first possibility, we consider a triplet scalar exchange with null vev and a DM particle that transforms as a doublet under $SU(2)_L$. We explicitly distinguish between the case of scalar and Majorana DM. Remember that a triplet scalar exchange in an s-channel diagram is associated to Majorana neutrinos only. For the t-channel diagram,

Annihilation channels	Internal mediator	Dark Matter $SU(2)_L$-rep.	Dirac neutrino	Majorana neutrino	See-saw type I	See-saw type II
s	Scalar **1**	**1, 2, 3**	$\not{L}$	-	R, θ^2	R, θ^2
s	Scalar **2**	**(1,2) ,(2,3)**	☑	-	θ	θ
s	Scalar **3**	$\mathbf{2}^a$	$\not{L}$	☑	☑	☑
s	Scalar **3**	**(1,3)**	$\not{L}$	☑	☑	☑
s	Scalar **1** with vev	**1, 2, 3**	$\not{L}$	-	R, θ^2	R, θ^2
s	Scalar **2** with vev	**(1,2) ,(2,3)**	m_ν	-	θ	θ
s	Scalar **3** with vev	$\mathbf{2}^a$	$\not{L}$	m_ν	-	f.t.
s	Scalar **3** with vev	**(1,3)**	$\not{L}$	m_ν	-	f.t.
s	Z-boson	**2, 3**	☑/⊠(p)	☑/⊠(p)	☑/⊠(p)	☑/⊠(p)
$t\,(u)$	Scalar **1**	**1**	R	-	R, θ^2	R, θ^2
$t\,(u)$	Scalar **1**	**2**	☑	☑	☑	☑
$t\,(u)$	Scalar **1**	**(1,2)**	☑	-	θ	θ
$t\,(u)$	Scalar **2**	**1, 3**	☑	☑	☑	☑
$t\,(u)$	Scalar **2**	**2**	R	-	R, θ^2	R, θ^2
$t\,(u)$	Scalar **2**	**(1,2)**	☑	-	θ	θ
$t\,(u)$	Scalar **2**	**(1,3)**	☑	☑	☑	☑
$t\,(u)$	Scalar **3**	**2**	☑	☑	☑	☑
$t\,(u)$	Scalar **3**	**3**	R	-	R, θ^2	R, θ^2
$t\,(u)$	Scalar **3**	**(2,3)**	☑	-	θ	θ

Table 4.2: Summary table for chiral and vector-like fermionic Dark Matter. ☑: potentially unsuppressed in at least one channel; ⊠(p): suppressed for non-relativistic Dark Matter (p-wave term); f.t.: fine tuning required between two couplings to get a sizable rate; $\not{L}$: LNV terms are present; - : a see-saw type I and/or type II situation is present; R: yields only right-handed neutrinos; θ^n: suppressed by the n-th power of the mixing angle between heavy and light neutrinos; m_ν: the Yukawa coupling involved is proportional to the light neutrino mass; x/y: applies for Dirac DM/applies for Majorana DM; ^{a}the coupling is present for Majorana DM only.

we also consider a DM particle that is a doublet under $SU(2)_L$. In the context of a scalar DM, we focus on the possibility of a Majorana singlet mediator, while in the case of Majorana DM we consider a scalar singlet mediator. As an example, we consider the case of Majorana neutrinos for the t-channel diagrams.

4.3.1 s-channel: the triplet scalar mediator

The couplings involved in an s-channel diagram with a triplet scalar exchange will not be connected to the neutrino mass, if the triplet has a null vev. However, the entries of the Yukawa coupling matrix $Y_{\nu;3}$ are constrained by different experimental results, in

particular by the limits on μ and τ decays, and by the values of the electron and the muon anomalous magnetic moments. In the following, we summarize these bounds.

Experimental constraints

The singly charge triplet component $\phi^-_{s;3}$ might transmit a lepton number violating muon decay with one μ^--$\overline{\nu}_\mu$-$\phi^-_{s;3}$ and one e^--$\overline{\nu}_e$-$\phi^-_{s;3}$ vertex. Considering the experimental uncertainty on G_F of about 10^{-10} GeV^{-2} [89], obtained through μ-decay measurements, the corresponding diagonal entries of $Y_{\nu;3}$ are set to be:

$$|Y^{ee}_{\nu;3}|^2\,|Y^{\mu\mu}_{\nu;3}|^2 \lesssim 0.1\left(\frac{10^{-10}m^2_\phi}{\text{GeV}^2}\right)^2 . \tag{4.47}$$

In general, also the electrically neutral component $\phi^0_{s;3}$ of the Higgs triplet will mediate μ-decay. However, the corresponding diagram involves the LFV coupling $Y^{\mu e}_{\nu;3}$, that is constrained stronger by the experimental limit on the branching ratio for $\mu \to 3e$ (see later).

The singly charged triplet component $\phi^-_{s;3}$ might transmit a lepton number violating tau decay with one τ^--$\overline{\nu}_\tau$-$\phi^-_{s;3}$ and one e^--$\overline{\nu}_e$-$\phi^-_{s;3}$ or μ^--$\overline{\nu}_\mu$-$\phi^-_{s;3}$ vertex. Therefore, the diagonal elements of $Y_{\nu;3}$ receive bounds also from the experimental limit on the τ lifetime. Taking into account that the uncertainty on Γ_τ is roughly 0.1% [89], we find

$$|Y^{\tau\tau}_{\nu;3}|^2\left(|Y^{ee}_{\nu;3}|^2 + |Y^{\mu\mu}_{\nu;3}|^2\right) \lesssim 0.1\left(\frac{10^{-5}m^2_\phi}{\text{GeV}^2}\right)^2 . \tag{4.48}$$

If the Yukawa coupling matrix $Y_{\nu;3}$ contains off-diagonal terms, the triplet will also have LFV couplings. In this case, the strongest constraint arises from $\mu \to 3e$ decay. Indeed, this process can be mediated at tree-level by the doubly charged component of the triplet $\phi^{--}_{s;3}$ with one μ^--e^+-$\phi^{--}_{s;3}$ and one e^--e^--$\phi^{--}_{s;3}$ vertex. From the experiment SINDRUM I [178], we know that $BR(\mu \to 3e) \lesssim 10^{-12}$ at 90% confidence level. Therefore, the bound on the off-diagonal entries reads

$$|Y^{e\mu}_{\nu;3}|^2\,|Y^{ee}_{\nu;3}|^2 \lesssim 5.4\left(\frac{10^{-11}m^2_\phi}{\text{GeV}^2}\right)^2 . \tag{4.49}$$

Note that the $\mu \to e\gamma$ process naturally arises only at 1-loop level and is therefore suppressed with respect to the $\mu \to 3e$ decay. The branching ratio of the τ decay into three leptons l (with l=e,μ) is, instead, constrained from the BELLE experiment [179] to be $BR(\tau \to lll) \lesssim (2-4)\times 10^{-8}$ at 90% confidence level. This implies the following limit on the off-diagonal τ Yukawa entries:

$$|Y^{l\tau}_{\nu;3}|^2\,|Y^{ll}_{\nu;3}|^2 \lesssim 0.6\left(\frac{10^{-9}m^2_\phi}{\text{GeV}^2}\right)^2 . \tag{4.50}$$

The Yukawa entries $Y^{ee}_{\nu;3}$ and $Y^{\mu\mu}_{\nu;3}$ are also subject to constraints coming from measurements of the electron and the muon anomalous magnetic moments [180]:

$$|Y^{ee}_{\nu;3}| \lesssim \mathcal{O}(10^{-4}) \left(\frac{m_\phi}{\text{MeV}}\right) , \tag{4.51}$$

$$|Y^{\mu\mu}_{\nu;3}| \lesssim \mathcal{O}(10^{-6}) \left(\frac{m_\phi}{\text{MeV}}\right) . \tag{4.52}$$

If we suppose that the diagonal elements $Y^{ee}_{\nu;3}$ and $Y^{\mu\mu}_{\nu;3}$ are of the same magnitude, Eq. (4.47) and Eq. (4.48) imply that the only sizable diagonal Yukawa entry is given by the element $Y^{\tau\tau}_{\nu;3}$:

$$|Y^{\tau\tau}_{\nu;3}|^2 \lesssim \min\left(1, \frac{10^{-1} m_\phi^2}{\text{GeV}^2}\right) , \tag{4.53}$$

where we have explicitly imposed that the Yukawa coupling is at most of order one. Since in our numerical analysis we always consider $m_\phi \gtrsim 100$ GeV, we have that $|Y^{\tau\tau}_{\nu;3}|^2 \lesssim 1$. For simplicity, we neglect the contributions coming from the off-diagonal terms of the Yukawa matrix $Y_{\nu;3}$.

In the case of scalar DM, the coupling between the DM particles and the scalar triplet mediator $\phi_{s;3}$ in the s-channel arises from a trilinear term in the potential, see Eq. (4.17). The existence of this coupling and at the same time the possibility for the scalar triplet to have a null vev will depend on the actual form of the scalar potential. In a particular model, one has to check that these two conditions are fulfilled.

In the case of vector-like fermionic DM, the coupling between the DM particles and the scalar triplet mediator $\phi_{s;3}$ in the s-channel can arise from two different Yukawa couplings: $Y^{(2,2)}_{\chi;3}$, which is related to the DM left-handed components, and $Y'^{(2,2)}_{\chi;3}$, which is connected to the DM right-handed components. In case these two couplings result to be of the same order, the s-wave contribution to the annihilation cross section will vanish, see Eq. (C.7). However, there is no a priori reason for them to be of the same magnitude. Therefore, we will suppose in our analysis that one of the Yukawa couplings, $Y^{(2,2)}_{\chi;3}$, dominates over the other one, $Y'^{(2,2)}_{\chi;3}$.

We want to stress that, even though the scalar triplet can be associated also to a chiral DM (see Table 4.2), we neglect this possibility, since strong bounds from electroweak precision measurements apply on new chiral fermions beyond the SM ones. Indeed, a new multiplet of degenerate fermions will contribute to the value of the S parameter in the following way [89]:

$$S = N_C \sum_i (t_{3L}(i) - t_{3R}(i))^2 / 3\pi \, , \tag{4.54}$$

where $t_{3L}(i)$ and $t_{3R}(i)$ are the third components of weak isospins of the left-handed and the right-handed components of the fermion i and N_C is the number of colors. Considering a SM Higgs mass $M_H = 117$ GeV, the new physics contribution to the S parameter is constrained to be $\lesssim 0.06$ at 95% C.L. [89].

To be consistent with direct searches at collider experiments, we consider the mass of the triplet scalar mediator in the s-channel to be $\gtrsim 100$ GeV [181].

The annihilation cross section

Using the Lagrangian terms of Eq. (4.16) and Eq. (4.17) and the expression of the annihilation cross section given in Eq. (C.3), we find that

$$\sigma_{\text{ann}} v = \frac{1}{8\pi} \frac{\left(\gamma_{\chi\phi}^{(2,3)}\right)^2 |Y_{\nu;3}^{\tau\tau}|^2}{(4m_\chi^2 - m_\phi^2)^2} + \mathcal{O}(v^2) \quad \text{for scalar DM,} \tag{4.55}$$

where we have assumed for simplicity that the DM particle and the lightest neutral scalar mediator correspond to the real components of $\chi_{s;2}^0$ and $\phi_{s;3}^0$, respectively. The parameter $\gamma_{\chi\phi}^{(2,3)}$ is set to be real. Considering, instead, Eq. (4.39) and Eq. (C.7), we conclude that

$$\sigma_{\text{ann}} v = \frac{1}{4\pi} \frac{|Y_\chi|^2 |Y_{\nu;3}^{\tau\tau}|^2}{(4m_\chi^2 - m_\phi^2)^2} m_\chi^2 + \mathcal{O}(v^2) \quad \text{for Majorana DM,} \tag{4.56}$$

with

$$Y_\chi = Y_{\chi;3}^{(2,2)} + \left[Y_{\chi;3}^{(2,2)}\right]^* . \tag{4.57}$$

We have assumed the Yukawa coupling $Y_{\chi;3}^{(2,2)}$ to dominate over $Y_{\chi;3}^{\prime(2,2)}$. If these two couplings are of the same order, instead, the first nonzero contribution to the annihilation cross section would be given by a p-wave term. Moreover, we have considered the imaginary component of the $\phi_{s;3}^0$ as exchanged particle. The real component would, indeed, have a zero s-wave due to parity conservation.

The expressions reported above refer to the production of tau neutrinos. The DM annihilation into neutrinos with different flavours would be more suppressed, because of the bound reported in Eq. (4.47), and can therefore be neglected.

In Fig. 4.1, we show the behaviour of the annihilation cross section into tau neutrinos for the case of scalar DM (left panel) and of Majorana DM (right panel). The annihilation cross sections result to be of the order of the value expected for a thermal relic for a wide range of the parameter space. From our plots, it is possible to identify which are the values of the Yukawa couplings and of the triplet and DM mass in which the neutrino production might be relevant. This can then be applied to specific model, in which a triplet scalar without vev is present.

In general, we can say that the neutrino flux from the galactic center (GC), generated by the triplet scalar exchange, might be accessible to neutrino telescopes only in the resonant region, in which $m_\chi \simeq m_\phi$. Indeed a boost factor of order 100 or more is required to overcome the atmospheric neutrino background [152]. In this case, however, a DM production mechanism different from the thermal one is necessary. Moreover, the CMB measurements of the WMAP satellite impose stringent limits on DM models with very large annihilation cross section, as has been pointed out in Refs. [182, 183]. Remember that even a DM particle that annihilates mainly into neutrinos will generally produce electromagnetic final states by loop diagrams [177]. In considering specific DM models, the CMB bounds of Refs. [182, 183] must be imposed.

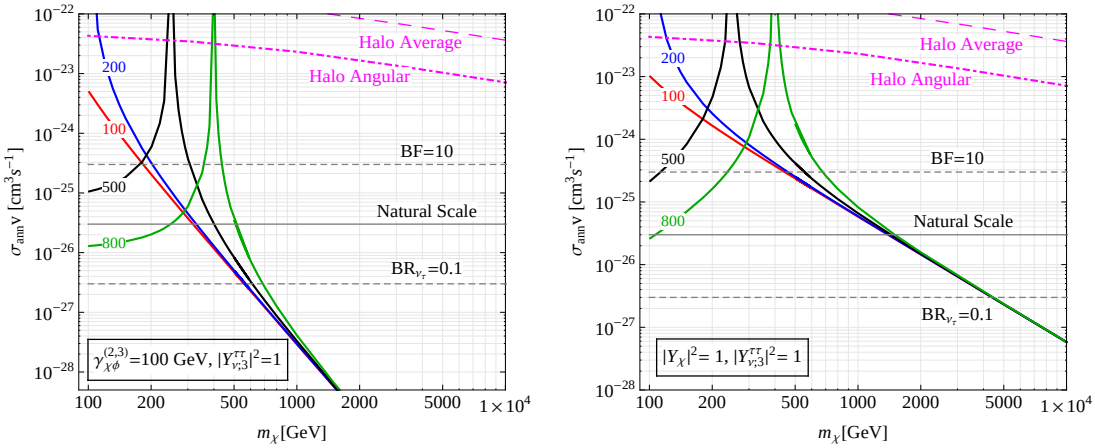

Figure 4.1: Dark Matter annihilation cross sections into tau neutrinos through the exchange of a scalar triplet with null vev, in an s-channel diagram. Left panel: scalar Dark Matter. Right panel: Majorana Dark Matter. The numbers next to each curve denote the different values of the scalar triplet mass (in GeV). The Halo Angular and the Halo Average lines represent bounds from neutrino searches, see text for more details. The gray solid line indicates the standard value of $\sigma_{\rm ann}v$ for a thermal relic (natural scale), while the gray dashed lines mark the values for a 10% branching ratio into tau neutrinos (BR$_{\nu_\tau}$) and for a boost factor (BF) equal to ten (where the natural scale is taken as reference).

The signals from the Sun and the Earth could, instead, be detected for a wide range of the parameters, depending on the value of the DM scattering cross section. For the Sun a 5σ discovery, after one year of data taking with the IceCube detector, can be achieved if $\sigma_p BR_\nu \simeq 6 \times 10^{-7}$ pb for $m_\chi \simeq 200$ GeV or if $\sigma_p BR_\nu \simeq 10^{-5}$ pb for $m_\chi \simeq 1$ TeV, where σ_p is assumed to be dominated by spin-dependent interactions and where BR_ν is the branching ratio into neutrinos of all flavours [184, 185]. For the Earth, assuming equilibrium between the capture and the annihilation rate, the 5σ discovery can be reached if $\sigma_p^{SI} BR_\nu \simeq 9 \times 10^{-10}$ pb for $m_\chi \simeq 200$ GeV and if $\sigma_p^{SI} BR_\nu \simeq 3 \times 10^{-9}$ pb for $m_\chi \simeq 1$ TeV [184, 185]

In the plots we also report the limits on the annihilation cross section $\sigma_{\rm ann}v$, as derived by the authors of Ref. [150] comparing the energy spectrum produced by DM pair-annihilation into neutrinos with the atmospheric neutrino background measured by the Super-Kamiokande, Frejus and AMANDA detectors. The Halo Angular bound corresponds to a cone half-angle of about 30° around the GC and to a value of the J-factor, see Eq. (3.25), of 25. The Halo Average bound is associated, instead, to $J \simeq 5$, which is an average value for the whole sky. As can be seen from the figures, these constraints are not really strong and exclude only a small fraction of the parameter space in the resonance region.

Note that, for the case of Majorana DM, the scalar triplet could also induce a neutrino production through a t-channel diagram. For simplicity, we show in Fig. 4.1 only the s-channel annihilation cross sections.

4.3.2 t-channel: the singlet fermionic and scalar mediator

The couplings involved in a t-channel diagram are subject to experimental bounds, since they induce LFV processes at one loop. A summary of these experimental limits is given in the following, considering for definiteness the case of a singlet vector-like fermionic mediator $\phi_{f;1}$ (for a doublet scalar DM) and of a singlet scalar mediator $\phi_{s;1}$ (for a doublet vector-like DM). Bounds from measurements of the anomalous magnetic moments of the electron and the muon also apply.

Experimental constraints

In the case of a scalar DM particle that is a doublet under $SU(2)_L$, the $\mu \to e\gamma$ process can be mediated by the charged scalar $\chi^-_{s;2}$ and the fermionic singlet $\phi_{f;1}$. Instead, for a doublet vector-like DM, the $\mu \to e\gamma$ process can be induced by the charged fermion $\chi^-_{f;2}$ and the scalar singlet $\phi_{s;1}$. Using the limit on the $BR(\mu \to e\gamma)$ provided by the MEGA experiment [186], we can write

$$3.2 \times 10^9 \, \frac{m_\mu^2/\mathrm{GeV}^2}{m_s^4/\mathrm{GeV}^4} \, \xi_1^4 \, H^2(t) \lesssim 1.2 \times 10^{-11} \,, \tag{4.58}$$

where m_μ is the muon mass. We have defined $\xi_1^2 = \mathcal{T}_{ek}^{(2,1)} \left[\mathcal{T}_{k\mu}^{(2,1)}\right]^*$ and $t = m_f^2/m_s^2$, with m_f and m_s being, respectively, the mass of the fermion and the scalar particles involved in the loop process. The function $H(t)$ is given by [187]

$$H(t) = \begin{cases} \frac{2t^2+5t-1}{12\,(t-1)^3} - \frac{t^2 \ln t}{2\,(t-1)^4} & \text{for scalar DM,} \\ \frac{t^2-5t-2}{12\,(t-1)^3} + \frac{t \ln t}{2\,(t-1)^4} & \text{for fermionic DM.} \end{cases} \tag{4.59}$$

In analogy, we find the following constraint on the couplings involved in the $\tau \to \mu\gamma$ process:

$$2.1 \times 10^6 \, \frac{m_\tau^2/\mathrm{GeV}^2}{m_s^4/\mathrm{GeV}^4} \, \xi_2^4 \, H^2(t) \lesssim 4.5 \times 10^{-8} \,, \tag{4.60}$$

where m_τ is the tau mass. We have defined $\xi_2^2 = \mathcal{T}_{ek}^{(2,1)} \left[\mathcal{T}_{k\tau}^{(2,1)}\right]^*$ and we have used the experimental limit on the $BR(\tau \to \mu\gamma)$ as provided by the BELLE experiment [188]. Finally, the last bound is given by the BaBar [189] experimental limit on the $BR(\tau \to e\gamma)$:

$$2.1 \times 10^6 \, \frac{m_\tau^2/\mathrm{GeV}^2}{m_s^4/\mathrm{GeV}^4} \, \xi_3^4 \, H^2(t) \lesssim 1.1 \times 10^{-7} \,, \tag{4.61}$$

where in this case we have $\xi_3^2 = \mathcal{T}_{\mu k}^{(2,1)} \left[\mathcal{T}_{k\tau}^{(2,1)}\right]^*$. Moreover, the couplings $\mathcal{T}_{ek}^{(2,1)}$ and $\mathcal{T}_{\mu k}^{(2,1)}$ are also subject to constraints coming from measurements of the electron and the muon anomalous magnetic moments [180]:

$$|\mathcal{T}_{ek}^{(2,1)}| \lesssim \mathcal{O}(10^{-4}) \left(\frac{m_\phi}{\text{MeV}}\right) , \tag{4.62}$$

$$|\mathcal{T}_{\mu k}^{(2,1)}| \lesssim \mathcal{O}(10^{-6}) \left(\frac{m_\phi}{\text{MeV}}\right) . \tag{4.63}$$

For simplicity, in our numerical examples we consider the situation in which $\mathcal{T}_{ek}^{(2,1)} \simeq \mathcal{T}_{\mu k}^{(2,1)} \ll \mathcal{T}_{\tau k}^{(2,1)}$. In this case, using Eq. (4.58) and Eq. (4.60), we find the following constraint:

$$|\mathcal{T}_{\tau k}^{(2,1)}|^2 \lesssim \min\left(1,\, 8.7 \times 10^{-4} \frac{m_s^2/\text{GeV}^2}{m_\tau/\text{GeV}} \frac{1}{H(t)}\right) , \tag{4.64}$$

where we have explicitly imposed that the trilinear coupling is at most of order one.

For the t-channel diagram, we restrict our analysis to a singlet Majorana mediator and to a singlet scalar mediator with masses $\gtrsim 100$ GeV. We use the limit of Eq. (4.64) in the numerical evaluation, considering also that in the case of scalar DM $m_s \simeq \mathcal{O}(m_\chi)$ and $m_f = m_\phi$, while in the case of fermionic DM $m_s = m_\phi$ and $m_f \simeq \mathcal{O}(m_\chi)$. We finally wish to add that, in the case of a chiral mediator $\phi_{f;1}$ or of a chiral DM $\chi_{f;2}$, the constraints from LFV processes might be much stronger. In particular, in Eq. (4.64), we would have the mass of the fermionic particle exchanged in the loop instead of the tau mass. This can be related to a chirality flip in the fermionic line.

The annihilation cross section

Using the Lagrangian term of Eq. (4.31) and the expression of the annihilation cross section given in Eq. (C.6), we find that

$$\sigma_{\text{ann}} v = \frac{1}{8\pi} \frac{|\mathcal{T}_{\tau k}^{(2,1)}|^4}{(m_\chi^2 + m_\phi^2)^2} m_\phi^2 + \mathcal{O}(v^2) \quad \text{for scalar DM,} \tag{4.65}$$

where we have assumed that the fermionic mediator is a Majorana particle and that the DM is the real component of $\chi_{s;2}^0$. This can be, for example, the case of sneutrino annihilation through a neutralino exchange. Considering, instead, Eq. (4.43) and Eq. (C.11), we conclude that

$$\sigma_{\text{ann}} v = \frac{1}{64\pi} \frac{|\mathcal{T}_{\tau k}^{(2,1)}|^4}{(m_\chi^2 + m_\phi^2)^2} m_\chi^2 + \mathcal{O}(v^2) \quad \text{for Majorana DM,} \tag{4.66}$$

where we have considered the real component of $\phi_{s;1}$ to be the lightest scalar mediator. Remember that, if the Majorana particle is the supersymmetric neutralino, the couplings $\mathcal{T}_{\tau k}^{(2,1)}$ will be proportional to the neutrino mass and thus the annihilation cross section into neutrinos will be negligible, see the discussion after Eq. (C.14). In a more general

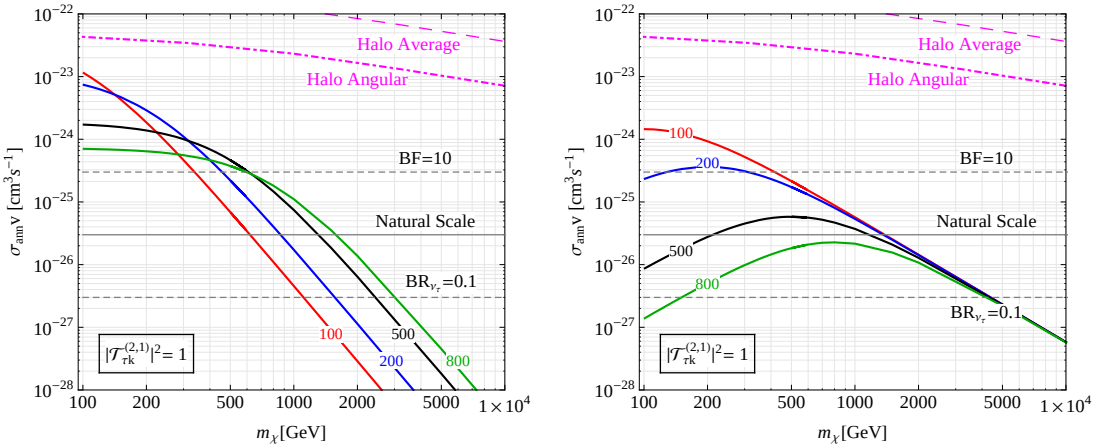

Figure 4.2: Dark Matter annihilation cross section into tau neutrinos through the exchange of a singlet mediator, in a t-channel diagram. Left panel: scalar Dark Matter and Majorana mediator. Right panel: Majorana Dark Matter and scalar mediator. The numbers next to each curve denote the different values of the singlet mediator mass (in GeV). The Halo Angular and the Halo Average lines represent bounds from neutrinos searches, see text for more details. The gray solid line indicates the standard value of $\sigma_{\rm ann} v$ for a thermal relic (natural scale), while the gray dashed lines mark the values for a 10% branching ratio into tau neutrinos (BR$_{\nu_\tau}$) and for a boost factor (BF) equal to ten (where the natural scale is taken as reference).

model, however, the couplings are not fixed and the neutrino production can be sizable, even if the DM particle is Majorana. This possibility is often overlooked in the literature.

The expressions reported above refer to the production of tau neutrinos, which we have assumed to be the dominant channel. Depending on the structure of the matrix $\mathcal{T}_{\alpha k}$, the other neutrino flavours could lead to sizable contributions. Nevertheless, the total annihilation cross section into neutrinos would be of the same order as the one obtained considering the tau neutrino as the dominant flavour channel.

The behaviour of the annihilation cross sections into tau neutrinos is reported in Fig. 4.2 for the cases of scalar DM (left panel) and Majorana DM (right panel). For a wide range of the parameter space, the annihilation cross sections can cover the order of magnitudes expected for a standard WIMP. In our specific examples, the experimental limits on LFV processes reported in Eq. (4.64) result to be quite weak and do not restrict the allowed parameter space in the interesting region of $\sigma_{\rm ann} v$. However, we want to remind that in the cases of a chiral mediator, for scalar DM, or of a chiral DM, the bounds from LFV processes might be much stronger. In the plots we also report the Halo Angular and Halo Average bounds [150], which partially limit the regions of the annihilation cross section under consideration.

The neutrino signal from the GC, generated by a t-channel singlet exchange, could be

hardly accessible to neutrino telescopes, since a cross section of the order of $\gtrsim 10^{-24}$ cm^3 s^{-1} is almost never reached. The signal from the Sun and the Earth, instead, might be detected, depending on the value of the scattering cross section, as we have explained in Sect. 4.3.1.

5 Indirect versus direct Dark Matter detection

Indirect evidence of DM particles in our halo by measurements of upward-going muons at neutrino detectors has been the subject of many investigations in the past, see for instance Refs. [9, 10, 11, 12].

Recently, a number of papers appeared where possible signals at neutrino telescopes are discussed. These consider either a generic DM particle with assumed dominance of specific annihilation channels [190, 191] or discuss specific DM candidates, like WIMPless DM or mirror DM [191]. Also DM particles which directly annihilate into neutrinos have been analyzed [192].

In Sect. 5.1, we present the neutrino constraints coming from DM searches at the Super-Kamiokande detector in the framework of the leptophilic DM, while, in Sect. 5.2, we calculate the muon fluxes expected for the neutralino DM. The constraints from direct DM detection experiments, in particular the DAMA experiment, are implemented for both the leptophilic and the neutralino DM.

5.1 Leptophilic Dark Matter

The leptophilic DM model has been proposed in Ref. [193] to reconcile the DAMA results with the absence of a signal in experiments like CDMS and XENON, that search for nuclear recoils from DM scattering, see Sect. 2.4.3. Indeed, while electronic events will contribute to the scintillation light signal in the DAMA detectors, most of the other DM experiments reject pure electron events by aiming at a (close to) background free search for nuclear recoils. As shown in Ref. [193], DM scattering off electrons at rest cannot provide enough energy to be seen in a detector. However, exploiting the tail of the momentum distribution of electrons bound in an atom may lead to a scintillation

light signal in DAMA of order few keVee. The signal in direct detection experiments from DM-electron scattering has been considered recently also in Ref. [194].

Such a framework, where DM recoils against electrons bound in atoms, might be also motivated by recent cosmic ray anomalies [4, 79, 85] observed in electrons/positrons, but not in anti-protons. A simple model for leptophilic DM has been presented in Ref. [128], see in this context for example also Refs. [195, 196].

In this work, we consider the hypothesis that DM has tree-level interactions only with leptons and has no direct couplings to quarks. We use an effective field theory approach to perform a model independent analysis. In Sect. 5.1.1 we introduce the effective Lagrangian for DM-lepton interactions, considering all possible Lorentz structures. In Sect. 5.1.2 we analyze the scattering on electrons in more details, while the possible experimental signatures of leptophilic DM in direct detection experiments are discussed in Sect. 5.1.3.

Even in such a leptophilic DM scenario, in many cases a DM-quark interaction is induced at one or two-loop level by photon exchange. In Sect. 5.1.4, we identify the Lorentz structures for which the loop induced coupling to quarks is present. For these cases, the DM-nucleon scattering dominates over DM-electron scattering, since the latter is suppressed by the bound state wave function.

Sect. 5.1.5 contains a summary of the possible Lorentz structures and their relative cross sections. We identify only one possible Lorentz structure, the axial vector type coupling, where DM-electron scattering dominates, since the loop diagram vanishes, and the scattering cross section is not additionally suppressed by small quantities. The expressions for the event rates in direct detection experiments are given in Sect. 5.1.6.

The Super-Kamiokande bounds on neutrinos from leptophilic DM annihilations inside the Sun are presented in Sect. 5.1.7. We show how the constraints on the scattering cross section, provided by this indirect detection method, disfavour the possibility of the leptophilic DM as viable explanation of the DAMA annual modulation signal.

5.1.1 Effective Dark Matter interactions

In this Section, we pursue a model independent analysis of the leptophilic DM candidate, using an effective interaction description. In the case of fermionic DM, the most general dimension six four-Fermi effective interactions are, shown pictorially also in Fig. 5.1 (right diagram),

$$\mathcal{L}_{\text{eff}} = \sum_i G\,(\bar{\chi}\Gamma^i_\chi\chi)\,(\bar{\ell}\Gamma^i_\ell\ell) \qquad \text{with} \qquad G = \frac{1}{\Lambda^2}\,, \tag{5.1}$$

where Λ is the cut-off scale for the effective field theory description, while the sum is over different Lorentz structures. A complete set consists of scalar (S), pseudo-scalar (P), vector (V), axial-vector (A), tensor (T), and axial-tensor (AT) currents. The four-Fermi

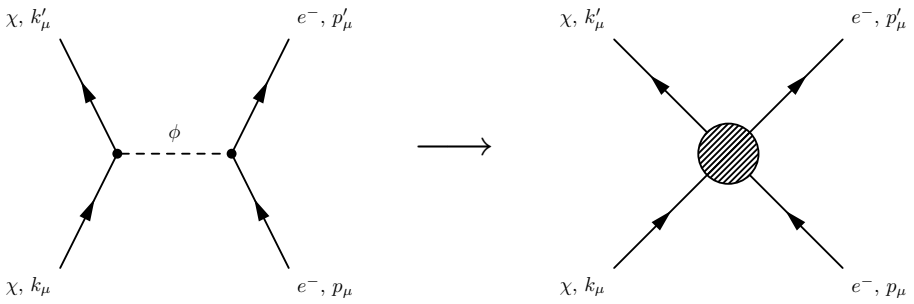

Figure 5.1: Example for generating an effective local DM-electron interaction vertex (right diagram) as used in our analysis by the exchange of a heavy intermediate particle ϕ (left diagram).

operators can thus be classified to be of

$$\begin{array}{lll} \text{scalar-type:} & \Gamma_\chi = c_S^\chi + ic_P^\chi\gamma_5, & \Gamma_\ell = c_S^\ell + ic_P^\ell\gamma_5, \\ \text{vector-type:} & \Gamma_\chi^\mu = (c_V^\chi + c_A^\chi\gamma_5)\gamma^\mu, & \Gamma_{\ell\mu} = (c_V^\ell + c_A^\ell\gamma_5)\gamma_\mu, \\ \text{tensor-type:} & \Gamma_\chi^{\mu\nu} = (c_T + ic_{AT}\gamma_5)\sigma^{\mu\nu}, & \Gamma_{\ell\mu\nu} = \sigma_{\mu\nu}, \end{array} \tag{5.2}$$

where $\sigma_{\mu\nu} = \frac{i}{2}[\gamma_\mu, \gamma_\nu]$.[1] If DM is a Majorana particle, vector and tensor like interactions vanish, i.e., $c_V^\chi = c_T^\chi = c_{AT}^\chi = 0$.

In our work we do not rely on any specific realization of the effective interaction. The simplest example would just be assuming that the interaction is induced by the exchange of an intermediate particle, whose mass is much larger than the recoil momenta, that are of order a few MeV/c. The intermediate particle can then be integrated out leaving an effective point interaction. Let us look at the χ-lepton interaction mediated by a scalar field ϕ, shown in Fig. 5.1. It gives an amplitude

$$ig_S^\chi(\bar{u}_\chi u_\chi)\,\frac{i}{q^2 - m_\phi^2 + i\epsilon}\,ig_S^\ell(\bar{u}_\ell u_\ell) \quad\longrightarrow\quad i\,\frac{g_S^\chi g_S^\ell}{m_\phi^2}\,(\bar{u}_\chi u_\chi)(\bar{u}_\ell u_\ell)\,, \tag{5.3}$$

where on the right-hand side we have neglected the momentum transfer $q^2 = (p' - p)^2 \ll m_\phi^2$. The same amplitude is obtained from a local operator $(\bar{\chi}\chi)\,(\bar{\ell}\ell)$ with a Wilson coefficient $g_S^\chi g_S^\ell/m_\phi^2$ (in the notation used in Eqs. (5.1), (5.2) we have $c_S^\chi = g_S^\chi, c_S^\ell = g_S^\ell, \Lambda = m_\phi$).

In the case of scalar DM, there is only one dimension five operator. The effective Lagrangian is given by

$$\mathcal{L}_{\text{eff}} = G_5(\chi^\dagger\chi)\left[\bar{\ell}(d_S + id_P\gamma_5)\ell\right] \qquad \text{with} \qquad G_5 = \frac{1}{\Lambda}\,. \tag{5.4}$$

[1] The relation $\sigma^{\mu\nu}\gamma_5 = \frac{i}{2}\epsilon^{\mu\nu\alpha\beta}\sigma_{\alpha\beta}$ implies that the $AT \otimes AT$ coupling is equivalent to $T \otimes T$, and $T \otimes AT = AT \otimes T$.

5.1.2 Dark Matter scattering on electrons

To simplify the discussion, we investigate the DM scattering on electrons at rest. This will enable us to see for which types of Lorentz structures in the effective DM-lepton Lagrangian, Eq. (5.1), this interaction is relevant. We comment in Sect. 5.1.6 on the complications introduced by the fact that electrons are actually bound in atoms.

We consider a DM particle χ of mass m_χ scattering elastically on a free electron at rest, assuming that all the particles are non-relativistic. The scattering cross sections for fermionic DM are then:

$$\text{scalar-type:} \qquad \sigma = \sigma_e^0 \left\{ (c_S^\chi c_S^e)^2 + \left[(c_S^\chi c_P^e)^2 + (c_P^\chi c_S^e)^2 \frac{m_e^2}{m_\chi^2} \right] \frac{v^2}{2} + \right. \\ \left. + \frac{(c_P^\chi c_P^e)^2}{3} \frac{m_e^2}{m_\chi^2} v^4 \right\} , \tag{5.5}$$

$$\text{vector-type:} \qquad \sigma = \sigma_e^0 \left\{ (c_V^\chi c_V^e)^2 + 3\,(c_A^\chi c_A^e)^2 + \left[(c_V^\chi c_A^e)^2 + 3\,(c_A^\chi c_V^e)^2 \right] \frac{v^2}{2} \right\} , \tag{5.6}$$

$$\text{tensor-type:} \qquad \sigma = \sigma_e^0 \left\{ 12\, c_T^2 + 6\, c_{AT}^2 v^2 \right\} . \tag{5.7}$$

In the above expressions there are two suppression factors, the DM velocity in our halo $v \sim 10^{-3} c$ and the ratio m_e/m_χ. The cross section for each Lorentz structure is given to leading order in these expansion parameters. Up to the velocity or electron mass suppression the typical size of the scattering cross section is

$$\sigma_e^0 \equiv \frac{G^2 m_e^2}{\pi} = \frac{m_e^2}{\pi \Lambda^4} \approx 3.1 \times 10^{-39}\,\mathrm{cm}^2 \left(\frac{\Lambda}{10\,\mathrm{GeV}} \right)^{-4} . \tag{5.8}$$

For scalar DM the χe scattering cross section is induced by the dimension 5 operator, Eq. (5.4), giving

$$\sigma = \sigma_{e,5}^0 \left(d_S^2 + \frac{d_P^2}{2} v^2 \right) , \tag{5.9}$$

with

$$\sigma_{e,5}^0 \equiv \frac{G_5^2}{4\pi} \frac{m_e^2}{m_\chi^2} = \frac{1}{4\pi \Lambda^2} \frac{m_e^2}{m_\chi^2} = 7.7 \times 10^{-42}\,\mathrm{cm}^2 \left(\frac{\Lambda}{10\,\mathrm{GeV}} \right)^{-2} \left(\frac{m_\chi}{100\,\mathrm{GeV}} \right)^{-2} . \tag{5.10}$$

Compared to fermionic DM two powers of Λ are replaced by m_χ which typically is larger than Λ. The scalar DM scattering cross section is thus further suppressed compared to the fermionic case for given Λ. The results of Eqs. (5.5)÷(5.7) and (5.9) are summarized in the middle column of Tab. 5.1.

5.1.3 Signals in direct detection experiments

When a leptophilic DM particle interacts in a detector, it is possible to have the following types of signals (see also Ref. [194]):

	fermionic DM		
$\Gamma_\chi \otimes \Gamma_\ell$	$\sigma(\chi e \to \chi e)/\sigma_e^0$	$\sigma(\chi N \to \chi N)/\sigma_N^1$	
$S \otimes S$	1	$\alpha_{\rm em}^2$	[2-loop]
$S \otimes P$	$\mathcal{O}(v^2)$	–	
$P \otimes S$	$\mathcal{O}(r_e^2 v^2)$	$\alpha_{\rm em}^2 v^2$	[2-loop]
$P \otimes P$	$\mathcal{O}(r_e^2 v^4)$	–	
$V \otimes V$	1	1	[1-loop]
$V \otimes A$	$\mathcal{O}(v^2)$	–	
$A \otimes V$	$\mathcal{O}(v^2)$	v^2	[1-loop]
$A \otimes A$	3	–	
$T \otimes T$	12	q_ℓ^2	[1-loop]
$AT \otimes T$	$\mathcal{O}(v^2)$	$q_\ell^2 v^{-2}$	[1-loop]
	scalar DM		
Γ_ℓ	$\sigma(\chi e \to \chi e)/\sigma_{e,5}^0$	$\sigma(\chi N \to \chi N)/\sigma_{N,5}^1$	
S	1	$\alpha_{\rm em}^2$	[2-loop]
P	$\mathcal{O}(v^2)$	–	

Table 5.1: Scattering cross section suppression by small parameters for DM-electron scattering and loop induced DM-nucleon scattering for all possible Lorentz structures. Here, $v \sim 10^{-3}c$ is the DM velocity, $r_e = m_e/m_\chi$, and $q_\ell = m_\ell/m_N$ ($\ell = e, \mu, \tau$). The reference cross sections σ_e^0, $\sigma_{e,5}^0$, σ_N^1, $\sigma_{N,5}^1$ are defined in Eqs. (5.8), (5.10), (5.24). The couplings c^χ, c^ℓ, d have been set to one. The entries for $\chi N \to \chi N$ are orders of magnitude estimates.

1. *WIMP–electron scattering* (WES): The whole recoil is absorbed by the electron that is then kicked out of the atom to which it was bound.

2. *WIMP–atom scattering* (WAS): The electron on which the DM particle scatters remains bound and the recoil is taken up by the whole atom. The process can either be elastic (el-WAS) in which case the electron wave function remains the same, or inelastic (ie-WAS), in which case the electron is excited to an outer shell.

3. Loop induced *WIMP–nucleus scattering* (WNS): Although per assumption DM couples only to leptons at tree level, an interaction with quarks is induced at loop level, by coupling a photon to virtual leptons, see Fig. 5.2. This will lead to scattering of the DM particle off nuclei.

The WES produces a prompt electron and possibly additional Auger electrons or X-rays. This leads to a signal in scintillation detectors such as DAMA, but is rejected in nuclear recoil experiments like CDMS and XENON. In the other two cases, instead, the signal consists of a scattered nucleus and shows up in all direct detection experiments searching for DM nuclear recoils. Note that quenching and channeling (see Sect. 2.3.1) is

relevant in DAMA in the cases of WAS and WNS , while the scattered electrons in the case of WES produce unquenched scintillation light.

The event rate in direct detection experiments is proportional to the differential cross section $d\sigma/dE_R$, where

$$E_R = E_\chi - E'_\chi \,, \tag{5.11}$$

is the energy deposited by the WIMP in the detector. The DAMA annual modulation signal is observed at $E_R \simeq 3$ keVee. Also for other direct detection experiments typical values are in the few to tens of keVee range. Just from kinematics the cross section is proportional to

$$\frac{d\sigma}{dE_R} \propto G^2 m_e \, (G^2 m_N) \quad \text{for} \quad \text{WES}\,(\text{WAS}, \text{WNS})\,, \tag{5.12}$$

where G is defined in Eq. (5.1) and m_e (m_N) is the electron (nucleus) mass. This suppresses the WES induced event rate by a factor m_e/m_N with respect to WAS and WNS.

In order for WES to deposit $\sim$ keV energy in the detector, the electron that a WIMP scatters off has to have quite a high momentum. Indeed, the maximal detectable energy from DM scattering on electrons at rest is $2m_e v^2$, with typical DM velocities of $v \sim 10^{-3}c$. Hence, the maximal detectable energy is of order eV, far too low to be relevant for the DAMA signal at few keV. Therefore, one has to explore the scattering off bound electrons with non-negligible momentum [193]. In this case, the energy transfer to the detector is $E_R \sim \mathcal{O}(pv)$, and an electron momentum $p \sim$ MeV is required to obtain $E_R \sim$ keV. Since electrons are bound in the atom, there is a nonzero but small probability that it carries such high momentum. The detailed calculations of Ref. [14] show that the suppression factor from the wave function is given by the expression

$$\epsilon_{\text{WES}} = \sqrt{2m_e(E_R - E_B)}\,(2l+1) \int \frac{dp\, p}{(2\pi)^3} \, |\chi_{nl}(p)|^2 \sim 10^{-6}\,. \tag{5.13}$$

The integral is over MeV momenta, while $\chi_{nl}(p)$ is the momentum wave function of the shell nl with the binding energy E_B.

Similarly, ie-WAS is also suppressed by the overlap of atomic wave functions of the initial and final states of the electron [14]:

$$\epsilon_{\text{WAS}} = \sum_{nlm} \sum_{n'l'm'} |\langle n'l'm'|e^{i(\mathbf{k}-\mathbf{k'})\mathbf{x}}|nlm\rangle|^2 \sim 10^{-19}\,. \tag{5.14}$$

We will show in Sect. 5.1.6 that, for the cases in which WAS is relevant, the el-WAS can be safely neglected and only the ie-WAS should be taken into account.

Loop induced WNS does not suffer from any wave function suppression, but instead carries a loop factor. At 1-loop the suppression is of order $(\alpha_{\text{em}} Z/\pi)^2$, with Z being the charge number of the nucleus. Combining this with Eqs. (5.12), (5.13), (5.14), we obtain the following rough estimate for the ratios of ie-WAS, WES and WNS induced event rates (neglecting order-one factors but also possible different v dependences):

$$R^{\text{WAS}} : R^{\text{WES}} : R^{\text{WNS}} \sim \epsilon_{\text{WAS}} : \epsilon_{\text{WES}} \, \frac{m_e}{m_N} : \left(\frac{\alpha_{\text{em}} Z}{\pi}\right)^2 \sim 10^{-17} : 10^{-10} : 1\,, \tag{5.15}$$

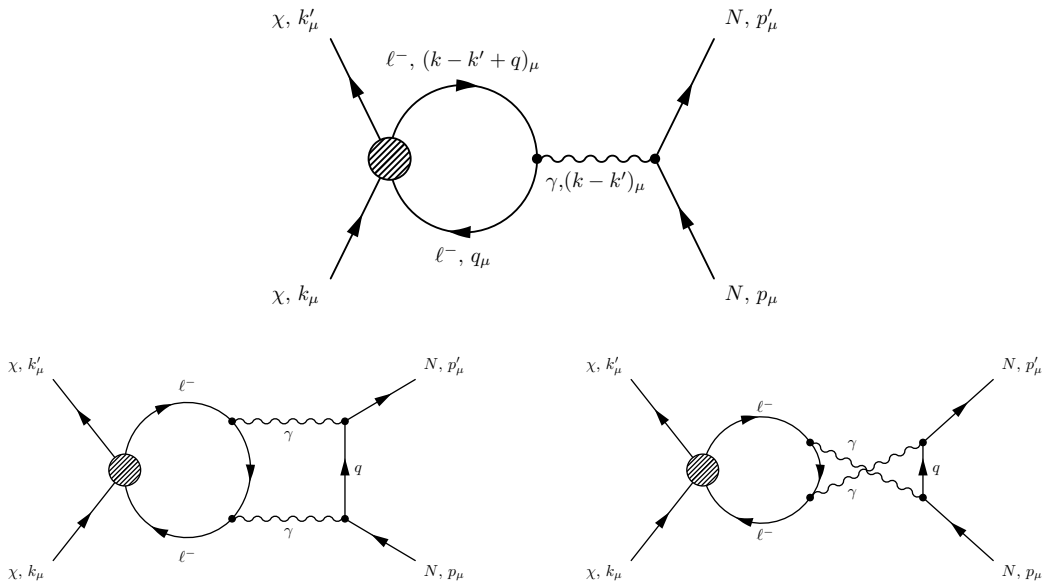

Figure 5.2: DM-nucleus interaction induced by a charged lepton loop and photon exchange at 1-loop (top) and 2-loop (bottom).

where in the last step we used $m_N = 100$ GeV and $Z = 53$. We conclude that whenever a loop induced cross section is present it will dominate the rate in direct detection experiments. This holds for 1-loop as well as 2-loop cross sections, since the latter will be suppressed by another factor $(\alpha_{\rm em} Z/\pi)^2 \simeq 5 \times 10^{-6} Z^2$ relative to 1-loop, and hence they are still much larger than the WES contribution.

5.1.4 Loop induced interactions

We have assumed that DM is leptophilic, so that at scale Λ only operators connecting DM to leptons, Eqs. (5.1), (5.2), (5.4), are generated. However, even under this assumption, at loop level one does induce *model independently* also couplings to quarks from photon exchange between virtual leptons and the quarks. The diagrams that can arise at one and two-loop order are shown in Fig. 5.2.[2] The lepton running in the loop can be either an electron or any other charged lepton to which the DM couples.

The one loop contribution involves the integral over loop momenta of the form

$$\int \frac{d^4q}{(4\pi)^4} \mathrm{Tr}\left[\Gamma_\ell \frac{\not{q}' + m_\ell}{q'^2 - m_\ell^2} \gamma^\mu \frac{\not{q} + m_\ell}{q^2 - m_\ell^2}\right], \tag{5.16}$$

[2]Similar diagrams with a photon replaced by a Z or a Higgs boson are power suppressed by $(k - k')^2/M_{Z,H}^2$ and thus negligible.

with $q' = k - k' + q$ and k, k' the incoming momenta as denoted in Fig. 5.2 and Γ_ℓ the Dirac structures given in Eqs. (5.2), (5.4). The one loop contribution is non-zero only for vector and tensor lepton currents, $\Gamma_\ell = \gamma_\mu, \sigma_{\mu\nu}$. For the scalar lepton current, $\Gamma_\ell = 1$, the loop integral vanishes, reflecting the fact that one cannot couple a scalar current to a vector current. The DM-quark interaction is then induced at two-loops through the diagrams shown in Fig. 5.2. In contrast for pseudo-scalar and axial vector lepton currents, $\Gamma_\ell = \gamma_5, \gamma_\mu\gamma_5$, the diagrams vanish to all loop orders. One insertion of γ_5 gives either zero or a fully anti-symmetric tensor $\epsilon^{\alpha\beta\nu\mu}$. Since there are only three independent momenta in a $2 \to 2$ process, two indices need to be contracted with the same momentum, yielding zero.

The cross section for scattering of a non-relativistic DM particle χ with mass m_χ on a nucleus at rest having a mass m_N is

$$\frac{d\sigma}{dE_R} = \frac{\overline{|\mathcal{M}|^2}}{32\pi m_N m_\chi^2 v^2}\,, \tag{5.17}$$

with $\mathcal{M}$ the matrix element for $\chi N \to \chi N$ scattering. For the explicit calculation of the 1-loop and 2-loop cross sections for all the non vanishing cases we refer to Ref. [14]. Here we will discuss only the case of the vector DM-lepton interaction, since is the only one important for the subsequent discussion.

For vector type interaction between leptons and DM, $\mathcal{L}_\ell = G(\bar\chi\Gamma^\mu_\chi\chi)(\bar\ell c^\ell_V\gamma_\mu\ell)$, with $\Gamma^\mu_\chi = (c^\chi_V + c^\chi_A\gamma_5)\gamma^\mu$, the matrix element for $\chi N \to \chi N$ scattering, generated through the one loop diagram of Fig. 5.2, is

$$\begin{aligned}\mathcal{M} &= \mathcal{C}_V^{(1)}(\mu)\big(\bar u'_\chi\Gamma^\mu_\chi u_\chi\big)\langle N(p')|\sum_i Q_i\big(\bar q_i\gamma_\mu q_i\big)|N(p)\rangle \\ &= \mathcal{C}_V^{(1)}(\mu)\big(\bar u'_\chi\Gamma^\mu_\chi u_\chi\big)ZF(E_R)\big(\bar u'_N\gamma_\mu u_N\big)\,.\end{aligned} \tag{5.18}$$

The sum is over the light quarks q_i with charges Q_i, $F(E_R)$ is the nuclear form factor, and $\mathcal{C}_V^{(1)}(\mu)$ is the 1-loop factor calculated in the $\overline{\text{MS}}$ scheme

$$\mathcal{C}_V^{(1)}(\mu) = \frac{2\alpha_{\text{em}}}{\pi}Gc^\ell_V\int_0^1 dx x(1-x)\log\left[\frac{-x(1-x)q^2 + m_\ell^2 - i0}{\mu^2}\right], \tag{5.19}$$

where $q^2 \simeq -\kappa^2$ with $\kappa = \sqrt{2m_N E_R}$ being the momentum transfer. In the calculation we set $\mu = \Lambda$, with $\Lambda \sim 10$ GeV, since this corresponds roughly to the scale Λ, where our effective theory is defined.

Even though in our numerical analysis we use the full 1-loop result, we give in the following also analytic result for the cross section in the case of the vector DM-lepton interaction, considering the "leading log" approximation, neglecting the remaining logarithmic dependence on momentum transfer. For $m_\ell \gg \kappa$ one can neglect the momentum transfer in the integral of Eq. (5.19), giving an approximate expression

$$\mathcal{C}_V^{\text{LL}}(\mu) = \frac{\alpha_{\text{em}}}{3\pi}Gc^\ell_V\log\left(m_\ell^2/\mu^2\right), \tag{5.20}$$

which is very precise for muon and tau running in the loop. It is quite precise also for the electron, even though $m_e \sim \kappa$. The reason is that there is still a hierarchy $m_e \ll \mu \simeq \Lambda$.

Expanding also in the χ velocity v to first non-zero order, the differential cross section $d\sigma/dE_R$ results

$$\frac{d\sigma}{dE_R} = \frac{d\sigma_N^1}{dE_R}\left[\log\left(\frac{m_\ell^2}{\mu^2}\right)\right]^2 \frac{1}{9}\left\{(c_V^\chi c_V^\ell)^2 + (c_A^\chi c_V^\ell)^2\left[v^2 + v_d^2\left(2 - \frac{m_N^2}{\mu_N^2}\right)\right]\right\} F^2(E_R)\,, \quad (5.21)$$

where the 1-loop cross section prefactor is

$$\frac{d\sigma_N^1}{dE_R} = \frac{m_N}{2\pi\, v^2}\left(\frac{\alpha_{\rm em} Z}{\pi} G\right)^2. \quad (5.22)$$

In the previous formula, the parameters m_N and Z are the nucleus mass and charge, respectively, while $\mu_N = m_N\, m_\chi/(m_N + m_\chi)$ is the reduced mass of the two-particle system. The two small parameters are the χ velocity v and the velocity of the recoiled nucleus, $v_d = \sqrt{2E_R/m_N}$. The kinetic recoil energy of the nucleus E_R in the $\chi N \to \chi N$ scattering, cf. Eq. 5.11, has a size $E_R \sim$ keVee.

We also report the result for the total $\chi N \to \chi N$ cross section, integrated over the recoil energy E_R. For simplicity we neglect the dependence on the nuclear form factors and set $F(E_R) = 1$ for this comparison, giving

$$\sigma = \sigma_N^1\left[\log\left(\frac{m_\ell^2}{\mu^2}\right)\right]^2 \frac{1}{9}\left\{(c_V^\chi c_V^\ell)^2 + (c_A^\chi c_V^\ell)^2 v^2\left[1 + \frac{1}{2}\frac{\mu_N^2}{m_N^2}\right]\right\}, \quad (5.23)$$

where σ_N^1 is the integral of the differential cross section of Eq. (5.22)

$$\sigma_N^1 = \frac{\mu_N^2}{\pi}\left(\frac{\alpha_{\rm em} Z}{\pi} G\right)^2 \approx 1.9 \times 10^{-32}\,{\rm cm}^2 \left(\frac{\Lambda}{10\,{\rm GeV}}\right)^{-4} \left(\frac{\mu_N}{10\,{\rm GeV}}\right)^2 \left(\frac{Z}{53}\right)^2. \quad (5.24)$$

The above result and the ones for the other interaction types (see Ref. [14] for the explicit calculations) are summarized in Table 5.1, facilitating comparison with χ scattering on free electrons. In Table 5.1 we took $\mu_N \sim m_N \sim m_\chi$, while the scaling for other values of nucleon and DM masses is easy to obtain from above results. In Table 5.1, we also report the case of scalar DM where $d\sigma_{N,5}^1/dE_R$ and $\sigma_{N,5}^1$ are given, respectively, by Eq. (5.22) and Eq. (5.24) with $G \to G_5/(2m_\chi)$.

5.1.5 Discussion of Lorentz structure

In Sect. 5.1.3, we have estimated a strong hierarchy between the three types of signals as $R^{\rm WAS} \ll R^{\rm WES} \ll R^{\rm WNS}$, see Eq. (5.15). These results imply that whenever WNS at 1-loop or 2-loop is generated, it dominates the event rate in direct detection experiments. The Lorentz structures for which this situation applies can be read off from Table 5.1. To be specific we will use as a representative example of this class the $V \otimes V$ coupling. From the table we also see that there is one case — the $A \otimes A$ coupling — where no χN

scattering is induced at loop level and moreover the WIMP-electron cross section is not additionally v and/or m_e/m_χ suppressed. Hence, we chose the $A \otimes A$ coupling as our second representative example to quantitatively discuss the case of a WES dominated event rate. The results from these two examples can be qualitatively extrapolated to other Lorentz structures using Table 5.1.

In the case of axial vector like DM-lepton coupling, the signal in DAMA will be dominated by WES. Then, WAS is still irrelevant for DAMA, but since WES will not contribute to the rate in CDMS and XENON, WAS might in principle lead to a signal in those experiments. The $\chi e \to \chi e$ cross section in the $A \otimes A$ case has to be very large (corresponding to $\Lambda \sim O(100\text{ MeV})$) in order to be relevant for the DAMA experiment. For the cases in Table 5.1 where σ_e^0 is further suppressed by small numbers, like for example $S \otimes P$ or $P \otimes P$, the scale Λ would have to be even lower, so that the effective field theory description would break down.

Finally, let us mention the tensor coupling $T \otimes T$, where the 1-loop cross section is suppressed by m_ℓ^2/m_N^2, while χe scattering is enhanced by a factor 12. If DM couples *only* to the electron and not to μ and τ the suppression of the loop is of order $m_e^2/m_N^2 \sim 10^{-10}$, and hence, WES and WNS rates can be of comparable size. However, in general one expects also a coupling to the μ and τ leptons. To be specific, in our numerical analysis of $V \otimes V$ and $A \otimes A$ cases we will assume equal couplings to all three leptons. For the tensor case the same choice would mean that WNS dominates.

5.1.6 Event rates

In this Section we provide the event rates in direct detection experiments. For WES and WAS we assume $A \otimes A$ coupling and for WNS we take $V \otimes V$. As argued above, the $A \otimes A$ and $V \otimes V$ cases are representative enough to cover qualitatively all possible Lorentz structures. Here we report the main important formulae, that have been used for the numerical fits to DAMA, CDMS, and XENON data, while technical details and supplementary information are given in Ref. [14]. In our numerical analysis we fix the local DM density to the standard value $\rho_\chi = 0.3$ GeV cm^{-3} and we consider a Maxwell-Boltzmann distribution with velocity dispersion $v_0 = 220$ km s^{-1}.

WIMP-electron scattering

To obtain an expression for the event rate in the case of WES it is necessary to take into account the fact that electrons are bound to the atoms. The kinematics of scattering off bound electrons has some important differences compared to scattering off free particles. The bound electron does not obey the free-particle dispersion relation $E_{e(\text{free})}^2 = p^2 + m^2$. Instead it has a fixed energy $E_e = m_e - E_B$, determined by the binding energy of the atomic shell, $E_B \geq 0$, whereas its momentum p follows a distribution which is given by the square of the Fourier transform of the bound state wave function corresponding to that shell. Energy conservation reads in this case $E_\chi + m_e - E_B = E'_\chi + E'_e$, or

$$E'_e = m_e + E_R - E_B\,. \tag{5.25}$$

After some algebra, it is possible to arrive at the following expression for E_R:

$$E_R \approx -\frac{p^2}{2m_\chi} - pv\cos\theta\,, \tag{5.26}$$

where[3] $\cos\theta = \mathbf{kp}/kp$. In the derivation we used the approximation $E_R \ll m_e \leq E_e \ll m_\chi$ and $v \sim 10^{-3}$. We see that to obtain detectable energies relevant for DAMA (E_R of few keV), electron momenta of order MeV are required.

Taking into account the peculiarities of scattering on bound electrons, the count rate for the axial vector Dirac structure, $\Gamma_\chi = \Gamma_e = A$, is (we also set $c_A^\chi = c_A^e = 1$ for simplicity) [14]:

$$\frac{dR^{\rm WES}}{dE_R} \simeq \frac{\eta}{\rho_{\rm det}}\frac{3\rho_\chi m_e G^2}{4\pi m_\chi}\sum_{nl}\sqrt{2m_e(E_R - E_{B,nl})}\,(2l+1)\int\frac{dp\,p}{(2\pi)^3}\,|\chi_{nl}(p)|^2\,I(v_{\rm min}^{\rm WES})\,, \tag{5.27}$$

where η is the number density of the target particles, $\rho_{\rm det}$ is the mass density of the detector, and $\chi_{nl}(p)$ is the momentum wave function of the electron. The function $I(v_{\rm min})$ is

$$I(v_{\rm min}) \equiv \int d^3v\frac{f(\mathbf{v})}{v}\,\theta(v - v_{\rm min})\,, \tag{5.28}$$

while the minimal velocity required to give detectable energy E_R follows from Eq. (5.26):

$$v_{\rm min}^{\rm WES} \approx \frac{E_R}{p} + \frac{p}{2m_\chi}\,. \tag{5.29}$$

For $m_\chi \gtrsim 10$ GeV and p of order MeV the first term dominates.

The sum in Eq. (5.27) is over the atomic shells of both iodine and sodium with quantum numbers nl, and $E_{B,nl}$ is the corresponding binding energy. The electron can only be kicked out of its atomic shell if its binding energy is smaller than the total energy deposited in the detector (cf. Eq. (5.25)):

$$E_R \geq E_{B,nl}\,. \tag{5.30}$$

Only the shells satisfying this requirement can contribute to the event rate in Eq. (5.27). The dominant contribution to WES in DAMA comes from the inner s-shells of iodine because these are largest at high p [14]. Electrons from the $1s, 2s, 2p$ shells do not contribute to the DAMA signal region of $E_R \simeq 2-4$ keVee since the binding energies are too large, respectively 33.2 keV, 5.2 keV, and 4.7 keV [197]. The shell dominating the signal in the 2-4 keVee region is the $3s$ shell of iodine, with a binding energy of about 1 keV. This has been overlooked in Ref. [193], while it has important consequences on the size of the needed cross section.

[3] We always denote the DM momentum with $\mathbf{k}$ and the electron (or nucleus) momentum with $\mathbf{p}$. Bold symbols refer to 3-vectors and $k \equiv |\mathbf{k}|$, and similar for p.

WIMP-atom scattering

We now consider the case when the electron on which the DM particle scatters remains bound and the recoil is taken up by the whole atom. We specialize to the case of axial vector coupling, $\Gamma^\mu_\chi = \Gamma^\mu_e = \gamma^\mu\gamma^5$ and set $c^\chi_A = c^e_A = 1$. We use non-relativistic spinors, which is certainly justified for u^r_χ and $u^{r'}_\chi$, and also for u^s_e except, perhaps, for electrons from the $1s$ shell of iodine. In this last case, relativistic corrections are of order 20%.

Let us first consider the case when the electron remains in its state, and hence the scattering on the atom is elastic (el-WAS). Then we have $s = s'$ and $nlm = n'l'm'$. Furthermore, we have to sum coherently over all shells and electron spins, since it is impossible in principle to identify on which electron the WIMP has scattered. It turns out that for the axial vector case the spin sum $\sum_s \bar{u}^s_e\gamma^\mu\gamma^5 u^s_e$ vanishes. This can be verified by using explicit expressions for the spinors u^s_e, and follows from the fact that the different signs due to γ_5 of right-handed and left-handed components of the electron cancel each other in case of a coherent sum over spins.[4] The elastic scattering may be relevant for other Lorentz structures where this cancellation does not occur. However, in Sec. 5.1.5 we have argued that the only case of practical relevance is the axial coupling, and therefore we will not consider el-WAS further.

We are left now with the case where the electron is excited to an outer free shell which corresponds to inelastic WIMP-atom scattering (ie-WAS). In this case the sum over all occupied electron states nlm, over all unoccupied states $n'l'm'$, and over WIMP and electron spins has to be incoherent because one can distinguish in principle different initial and final states, e.g. by x-ray spectroscopy. The corresponding expression for the counting rate is [14]

$$\frac{dR_N^{\text{ie-WAS}}}{dE_R} = \frac{\eta\, m_N}{\rho_{\text{det}}}\frac{3\rho_\chi G^2}{2\pi\, m_\chi}\sum_{nlm}\sum_{n'l'm'}|\langle n'l'm'|e^{i(\mathbf{k}-\mathbf{k'})\mathbf{x}}|nlm\rangle|^2\, I(v_{\text{min}}^{\text{ie-WAS}})\,, \tag{5.31}$$

with m_N the mass of the target nucleus. The function I is defined in Eq. (5.28), and the minimal velocity required to give detectable energy E_R follows from the kinematics implied by energy conservation, $E_R = E_\chi - E'_\chi = \delta E_B + m_N v_N^2/2$, and momentum conservation, $\mathbf{k} = \mathbf{k'} + m_N\mathbf{v}_N$:

$$v_{\text{min}}^{\text{ie-WAS}} = \frac{E_R(m_\chi + m_N) - m_N\delta E_B}{m_\chi\sqrt{2m_N(E_R - \delta E_B)}}\,, \tag{5.32}$$

where δE_B is the difference of the binding energies of the initial and final shells: $\delta E_B = E_{B,nlm} - E_{B,n'l'm'}$.

[4] This argument will not hold if an unpaired valence electron is available so that we cannot sum over spins. However, most chemically bound systems are formed in such a way that this does not happen. Even in this case el-WAS would be suppressed since scattering on outer electrons is highly suppressed by the smallness of the binding energy of these electrons compared to the transferred momentum.

Loop induced WIMP-nucleus scattering

The event rate for loop induced DM-nucleus scattering is given by [14]

$$\frac{dR^{\rm WNS}}{dE_R} = \frac{\rho_\chi}{m_\chi}\frac{\eta}{\rho_{\rm det}}\left(\frac{d\sigma_N}{dE_R}v^2\right) I(v_{\rm min}^{\rm WNS})\,. \tag{5.33}$$

In this case the minimal velocity to produce a detectable energy E_R is given for WIMP-nucleus elastic scattering by $v_{\rm min}^{\rm WNS} = \sqrt{E_R m_N/2\mu_N^2}$.

We now specialize to the $V\otimes V$ case. The event rate depends on the χ mass and the coupling constant of the effective operator G (we set $c_V^\chi = c_V^\ell = 1$ from now on). For easier comparison with previous works, it is useful to trade G for the total $\chi e \to \chi e$ cross section $\sigma_e^0 = G^2 m_e^2/\pi$, Eq. (5.8). For the $V\otimes V$ case, considering the leading log approximation, we have

$$\frac{d\sigma_N}{dE_R}v^2 = \sigma_e^0 \times \frac{m_N}{18 m_e^2}\left(\frac{\alpha Z}{\pi}\right)^2 F(E_R)^2\left[\log\left(\frac{m_\ell^2}{\mu^2}\right)\right]^2, \tag{5.34}$$

to be inserted in Eq. (5.33). Furthermore, we assume (somewhat arbitrarily) equal couplings to all three leptons. The logarithm in Eq. (5.34) implies then a relative contribution of $e:\mu:\tau \simeq 30:7:1$. Note that the rate is dominated by the contribution from the electron in the loop assuming equal couplings at the scale $\Lambda \sim 10$ GeV. Therefore, our results are conservative, in the sense that per assumption DM has to couple to the electron.

5.1.7 Super-Kamiokande constraints

Any DM candidate, that is considered in a theoretical model, has to fulfill the constraints on the upward through-going muons coming from water Cherenkov detectors, like Super-Kamiokande [5], and from neutrino telescopes [6, 166, 167]. Here, we reanalyze, in the framework of leptonically interacting DM, the bound on the muon flux coming from the DM annihilations inside the Sun, provided by the Super-Kamiokande experiment. We do not consider the possibility of annihilation inside the Earth, since in this case the equilibrium between capture and annihilation rate generally depends on the specific characteristics of the model, because of the weaker gravitational field with respect to the Sun.

For our calculations we initially assume that the capture and annihilation processes are in equilibrium, i.e. $\tau_A \ll t_\odot$, where $t_\odot$ is the age of the Sun. In this case, the annihilation rate is just half the capture rate and becomes independent of the annihilation cross section $\langle\sigma_{\rm ann} v\rangle$. We will later comment on the validity of the equilibrium limit for our model. As discussed in Sect. 3.1.1, the temperature effect on the capture rate can be neglected for scattering off heavier nuclei, which dominates the capture in the case of loop induced WNS, while it has to be considered when WES is dominant.

Since we are interested in annihilations into leptons, we consider the following four channels: $\tau\bar\tau$, $\nu_e\bar\nu_e$, $\nu_\mu\bar\nu_\mu$ and $\nu_\tau\bar\nu_\tau$. Note that annihilations into electrons do not provide

neutrinos, and muons are always stopped before decay, giving rise to neutrinos in the MeV energy range which is below the Super-Kamiokande threshold [198]. In the case of direct neutrino channels, the initial neutrino spectrum is simply a Dirac δ function centered at $E_\nu = m_\chi$, and we assume a flavour-blind branching ratio, i.e., $BR_{\nu_e} = BR_{\nu_\mu} = BR_{\nu_\tau} = 1/3$. The results do not depend strongly on this assumption, since flavours are mixed due to oscillations.[5] For the $\tau\bar{\tau}$ channel, we use the initial neutrino spectrum given in [140].

Using the SK limit on through-going muons of Eq. (3.39), an upper bound on the DM scattering cross section as a function of m_χ can be obtained. In Fig. 5.3 we display the bounds obtained for the case of loop induced WIMP-nucleus scattering (upper panel) and WIMP-electron scattering (lower panel). For the calculation of loop induced scattering we used $q^2 \simeq -\mathcal{O}(m_\chi^2 v^2)$. We show the limit for annihilations into $\tau\bar{\tau}$ and $\nu\bar{\nu}$ (assuming equal branchings into the 3 flavours) starting from $m_\chi \gtrsim 10$ GeV, since for lower masses a great part of the muon signal would be in the form of stopping muons and thus a more carefully calculation should be pursued.

In the case of WNS, annihilations into neutrinos exclude the region compatible with DAMA, while annihilations into tau leptons might be marginally consistent with it at 3σ. In contrast, in the case of WES the neutrino bound excludes the region indicated by DAMA by more than 6 orders of magnitude. This implies that if DM couples to electrons with a cross section as large as necessary to explain the DAMA results through WES , DM annihilation into neutrinos must be very strongly suppressed.

We now wish to comment on the validity of the equilibrium assumption, between WIMP captures and annihilations in the Sun. Let us first estimate the cut-off scale Λ for the effective theory description of the DM-lepton coupling. For the two examples of $V \otimes V$ and $A \otimes A$ couplings, the neutrino bounds are of order $\sigma_e^0 \sim 10^{-43}\,\mathrm{cm}^2$ and $10^{-38}\,\mathrm{cm}^2$, respectively, see Fig. 5.3. From Eq. (5.8) we can estimate the corresponding cut-off scales as $\Lambda_V \sim 100$ GeV and $\Lambda_A \sim 10$ GeV, where we took coupling constants c_i^χ to be of order $\mathcal{O}(1)$. In DM annihilations the four-momentum transfer squared is of order m_χ^2. For $m_\chi \sim 10$ GeV, relevant for WNS, the WIMP annihilations may then also be described by effective field theory. Using effective interactions in Eq. (5.1) (extending them to neutrinos), we find

$$\text{Vector:} \quad \langle \sigma_{\text{ann}} v \rangle \sim \frac{G^2 m_\chi^2}{\pi} = \sigma_e^0 \frac{m_\chi^2}{m_e^2} \sim 10^{-24}\,\mathrm{cm}^3\,\mathrm{s}^{-1} \left(\frac{\sigma_e^0}{10^{-43}\,\mathrm{cm}^2}\right) \left(\frac{m_\chi}{10\,\mathrm{GeV}}\right)^2 . \quad (5.35)$$

In the WES case, however, the effective theory typically cannot be applied since the momentum transfer for annihilations is above the cut-off scale. Therefore, in general we cannot make model independent statements about $\langle \sigma_{\text{ann}} v \rangle$ without specifying the

[5] There is some difference of the $\nu_\tau\bar{\nu}_\tau$-channel due to ν_τ regeneration effects [140, 141], which are important for high energies. Assuming annihilations with branching ratios equal to one for each of the three flavours we find that the muon neutrino flux at the Earth is practically the same for all three initial flavours up to $m_\chi \simeq 100$ GeV. For $m_\chi = 1$ TeV the ratio of the muon neutrino fluxes at Earth is roughly $1 : 3.5 : 6.4$ for annihilations into $\nu_e\bar{\nu}_e : \nu_\mu\bar{\nu}_\mu : \nu_\tau\bar{\nu}_\tau$.

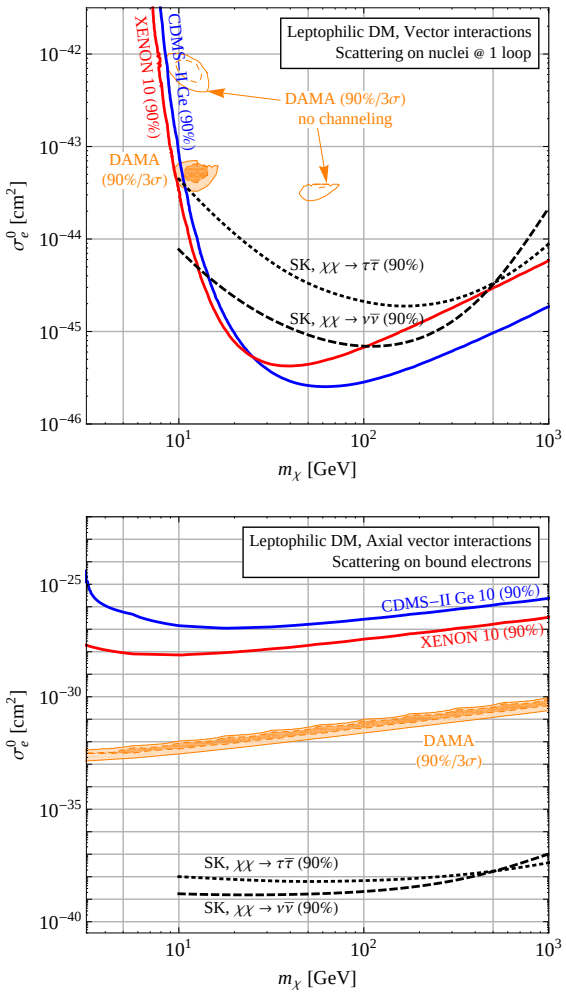

Figure 5.3: DAMA allowed region at 90% and 3σ C.L. in the case of 1-loop induced WIMP-nucleus scattering ($V \otimes V$ coupling) and in the case of WIMP-electron scattering ($A \otimes A$ coupling). The allowed region is shown in terms of the WIMP-electron cross section $\sigma_e^0 = G^2 m_e^2/\pi$, with and without taking into account the channeling effect. The bounds at 90% C.L. from CDMS-II and XENON10 are displayed. The dashed curves show the 90% C.L. constraints from the Super-Kamiokande limit on neutrinos from the Sun, by assuming annihilation into $\tau\bar{\tau}$ or $\nu\bar{\nu}$. Note how neutrino bounds are much stronger than the ones from direct detection experiments, in the case of $A \otimes A$ coupling.

UV completion of the effective $\chi\ell$ vertex. An order of magnitude estimate can still be obtained from dimensional analysis as

$$\text{Axial:} \qquad \langle \sigma_{\rm ann} v \rangle \sim \frac{g^4}{m_\chi^2} \sim 10^{-21}\,{\rm cm}^3\,{\rm s}^{-1} \times g^4 \left(\frac{m_\chi}{100\,{\rm GeV}}\right)^{-2}\,, \tag{5.36}$$

with g a typical coupling constant between leptons and the dark sector.

Equilibrium of WIMP capture and annihilations is obtained if $\tanh^2(t_\odot/\tau_A)$ is close to one, see Eq. (3.8). Fig. 5.4 shows the values of $\langle\sigma_{\rm ann}v\rangle$ for which $t_\odot/\tau_A = 1$ and 5 as a function of m_χ. The values of scattering cross sections σ_e^0 for $V\otimes V$ and $A\otimes A$ Lorentz structures were chosen to be above (but close to) the Super-Kamiokande bounds shown in Fig. 5.3. Since $\tanh^2 x \approx 1$ for $x \gtrsim 5$, WIMP capture and annihilations are in equilibrium in the Sun for values of $\langle\sigma_{\rm ann}v\rangle$ above the curve for $t_\odot/\tau_A = 5$. Comparing Eqs. (5.35) and (5.36) with the ranges shown in the figure we conclude that the assumption of equilibrium is very well justified in the cases of our interest.

In this study we have considered the hypothesis that DM has tree level couplings only to leptons but not to quarks and within this framework we have derived the bounds on the scattering cross sections coming from the indirect DM detection through neutrinos, carried out by the SK experiment.

By closing the lepton legs to a loop, we obtain a coupling to the charge of the nucleus by photon exchange. Whenever the Dirac structure of the DM-lepton coupling allows such a diagram at 1 or 2-loop, WIMP-nucleus scattering will dominate the event rate in direct detection experiments, since the scattering over electrons is highly suppressed by the high momentum tail of the bound state wave function. The WIMP capture by the Sun is also dominated by this induced coupling to nucleons and the capture rate on electrons is negligible, cf. also Fig. 3.2. Concerning the direct detection experiments, a DM-lepton vector like coupling leads to a situation very similar to the standard WIMP case, implying the well-known tension between the annually modulated scintillation signal in DAMA and the bounds from CDMS and XENON. In this case, the indirect detection in neutrinos provides limits that are competitive with the ones from direct detection experiments, see Fig. 5.3 .

If the DM-lepton coupling is axial vector like, no loop will be induced and hence the scattering proceeds only by the interaction with electrons bound to the atoms of the detector. This model is strongly disfavored by the indirect DM search with neutrinos, because the cross section required to explain the DAMA signal is ruled out by the Super-Kamiokande constraints by many orders of magnitude, see Fig. 5.3. Moreover, the predicted spectral shape of the modulated and/or unmodulated signal in DAMA provides a very bad fit to the data [14].

The applicability of the neutrino bounds depends of course on the assumption that neutrinos are produced by DM annihilations. Due to $SU(2)_L$ gauge symmetry, generically one expects that DM will couple to both, charged leptons and neutrinos, which would open the annihilation channel into $\nu\bar{\nu}$. If for some reason DM couples only to charged leptons, DM would generically also annihilate into $\tau\bar{\tau}$, leading again to the neutrino signal. In order to evade the Super-Kamiokande constraint one has to forbid the coupling of DM to neutrinos and to the tau lepton. Let us mention that the most generic way to avoid coupling to neutrinos is the chiral coupling only to right-handed leptons. Note, however, that such a chiral $V+A$ coupling involves a vector-like coupling which will induce DM-quark scattering via the loop diagram. In this way, the DAMA results will be again in tension with the other direct detection experiments. Moreover, annihi-

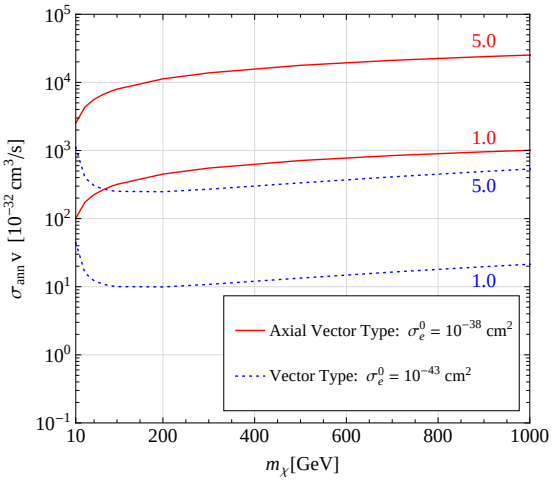

Figure 5.4: Contours of $t_\odot/\tau_A = 5$ and $t_\odot/\tau_A = 1$. For the case of vector (axial vector) coupling we have used a scattering cross section of $\sigma_e^0 = G^2 m_e^2/\pi = 10^{-43}(10^{-38})\,\mathrm{cm}^2$, motivated by the results of the Super-Kamiokande bound. For values of $\langle\sigma_{\mathrm{ann}} v\rangle$ above the curve for $t_\odot/\tau_A = 5$, WIMP capture and annihilations are in equilibrium in the Sun.

lation into charged leptons generates almost model independently also annihilation into neutrinos from W-boson exchange at 1-loop. Thus annihilation into neutrinos is typically suppressed by a loop factor of $\mathcal{O}(10^{-4})$ compared to annihilation into charged leptons, that however does not compensate the gap of more than 6 orders of magnitude between the DAMA region and the SK bounds. This consideration rules out all leptophilic DM models with dominant direct annihilation into leptons as an explanation of DAMA.

A possible realistic way to evade the bound from annihilations would be to assume that DM is not self-conjugate and postulate the presence of a large $\chi - \bar{\chi}$ asymmetry in our halo, see e.g. Refs. [199, 200, 201].

In conclusion, we have shown that the hypothesis of DM-interactions only with leptons does not provide a satisfactory solution to reconcile the DAMA annual modulation signal with constraints from other direct detection experiments. In the scenario of vector like coupling we recover the tension existing between DAMA and the other direct detection experiments, while in the case of axial vector coupling the bounds from indirect detection in neutrinos result extremely strong and hard to escape. However, even if the leptophilic DM candidate does not represent a successful explanation of the DAMA results, it is not ruled out as a whole. Indeed, it might still be a well motivated model to explain the PAMELA anomaly in the cosmic ray flux. In this case, our work provides a carefully description of its phenomenology for both direct detection experiments and indirect searches with neutrinos.

5.2 Neutralino Dark Matter

In the papers of Ref. [103] it was shown that light neutralinos with a mass in the range 7 GeV $\lesssim m_\chi \lesssim$ 50 GeV are interesting Dark Matter candidates, with events rates accessible by direct detection experiments. This population of light neutralinos arises in the MSSM when the unification of gaugino masses at the GUT scale is not assumed [202], see Sect. 5.2.1 for more details. In this supersymmetric framework the lower bound on the neutralino mass of about 7 GeV is set by a cosmological bound on the neutralino relic density [103]. This is at variance with the lower bound $m_\chi \gtrsim 50$ GeV, which is derived from the LEP2 lower limit on the chargino mass, within the MSSM with gaugino mass unification at the GUT scale, cf. Sect. 2.4.1.

It was proved in Refs. [57, 203] that the population of light neutralinos fitted very well the results from the DAMA/NaI experiment [53], independently of the possible presence of channeled events. This good agreement has been further confirmed in Ref. [58], using the DAMA/LIBRA combined data [3].

The neutrinos produced by pair-annihilations of light neutralinos captured in the Earth and the Sun were discussed in Ref. [204]. We reconsider that analysis, by implementing and extending it in various distinctive features.

In the calculation of the neutrino flux we include all the main processes that occur during the neutrino propagation, i.e. neutrino oscillations and neutrino incoherent interactions with matter. The muon events are then divided in through-going and stopping muons, using the geometry of the Super-Kamiokande detector. The last category of events was not considered before in the literature and, actually, this turns out to be the most promising possibility to constrain the parameter space.

In the evaluation of the signals, we take also into account the relevant particle-physics uncertainties in hadronic quantities and astrophysics uncertainties, which affect the capture rate of relic neutralinos by the celestial bodies. These effects are discussed in details in Sect. 5.2.2 and Sect. 5.2.3.

Our results are given in Sect. 5.2.4 for the whole population of light neutralinos, while the final analysis of Sect. 5.2.5 is focussed on the upward muon fluxes generated by those neutralino configurations which are able to explain the annual modulation data of the DAMA experiment [3]. In our study, we separate the case where the channeling effect is included from the one where this effect is neglected. For definiteness, we consider only the results from the DAMA experiment and we do not impose constraints coming from other DM detection experiments, like CDMS and XENON.

5.2.1 Theoretical model

The supersymmetric scheme we employ in this analysis is the one described in Refs. [58, 103]. It is an effective MSSM scheme (effMSSM) defined at the electroweak scale, with the following independent parameters: $M_1, M_2, \mu, \tan\beta, m_A, m_{\tilde{q}}, m_{\tilde{l}}$ and A. Notations are as follows: M_1 and M_2 are the $U(1)$ and $SU(2)$ gaugino masses (these parameters are taken here to be positive), μ is the Higgs mixing mass parameter, $\tan\beta$ the ratio of

the two Higgs vev's, m_A the mass of the CP-odd neutral Higgs boson, $m_{\tilde{q}}$ is a squark soft mass common to all squarks, $m_{\tilde{l}}$ is a slepton soft mass common to all sleptons, and A is a common dimensionless trilinear parameter for the third family, $A_{\tilde{b}} = A_{\tilde{t}} \equiv A m_{\tilde{q}}$ and $A_{\tilde{\tau}} \equiv A m_{\tilde{l}}$ (the trilinear parameters for the other families being set equal to zero). In our model, no gaugino mass unification at the GUT scale is assumed. The lightest neutralino is required to be the lightest supersymmetric particle and stable, because of R-parity conservation.

The numerical analysis is performed by a scanning of the supersymmetric parameter space, with the following ranges of the MSSM parameters: $1 \leq \tan\beta \leq 50$, $100\ \text{GeV} \leq |\mu| \leq 1000\ \text{GeV}$, $5\ \text{GeV} \leq M_1 \leq 500\ \text{GeV}$, $100\ \text{GeV} \leq M_2 \leq 1000\ \text{GeV}$, $100\ \text{GeV} \leq m_{\tilde{q}}, m_{\tilde{l}} \leq 3000\ \text{GeV}$, $90\ \text{GeV} \leq m_A \leq 1000\ \text{GeV}$, $-3 \leq A \leq 3$.

The supersymmetric parameter space is subjected to all available constraints due to accelerator data on supersymmetric and Higgs boson searches (CERN e^+e^- collider LEP2 [205] and Collider Detectors D0 and CDF at Fermilab [206]) and to other particle-physics precision results, as reported in Sect. 2.3.3.

Also included is the cosmological constraint that the neutralino relic abundance does not exceed the maximal allowed value for Cold Dark Matter, i.e. $\Omega_\chi h^2 \leq (\Omega_{CDM} h^2)_{\max}$, with $(\Omega_{CDM} h^2)_{\max} = 0.122$, as derived at the 2σ level from the results of Ref. [39]. We recall that this cosmological upper bound implies on the neutralino mass the lower limit of about 7 GeV [103].

For each neutralino configuration, we calculate the total neutrino flux summing, with the appropriate branching ratios, the neutrino spectra coming from the following annihilation channels: $b\bar{b}$, $\tau\bar{\tau}$, $c\bar{c}$, $q\bar{q}$ and gg. The annihilation of two neutralinos can also produce two Higgs bosons or one gauge and one Higgs boson in the final state, although these two channels (as well as the annihilation channels into $t\bar{t}$ and into two gauge bosons) are absent in our study, since we consider neutralinos with mass $m_\chi \leq 80$ GeV.

5.2.2 WIMP-nucleon cross section: hadronic uncertainties

In Ref. [207] it is stressed that the couplings between Higgs bosons (or squarks) with nucleons, which typically play a crucial role in the evaluation of the neutralino-nucleus cross section, suffer of large uncertainties [208]. Actually, these couplings are conveniently expressed in terms of three hadronic quantities: the pion-nucleon sigma term

$$\sigma_{\pi N} = \frac{1}{2}(m_u + m_d) < N|\bar{u}u + \bar{d}d|N > , \tag{5.37}$$

the quantity σ_0, related to the size of the $SU(3)$ symmetry breaking,

$$\sigma_0 \equiv \frac{1}{2}(m_u + m_d) < N|\bar{u}u + \bar{d}d - 2\bar{s}s|N > , \tag{5.38}$$

and the mass ratio $r = 2m_s/(m_u + m_d)$.

Because of a number of intrinsic theoretical and experimental problems, the determination of these hadronic quantities is rather poor. Conservatively, their ranges can be

hadronic set	$\sigma_{\pi N}$[MeV]	σ_0[MeV]	r
MIN	41	40	25
REF	45	30	29
MAX	73	30	25

Table 5.2: Set of values for the hadronic quantities considered in the numerical analysis.

summarized as follows (we refer to Refs. [58, 207] for details):

$$41 \text{ MeV} \lesssim \sigma_{\pi N} \lesssim 73 \text{ MeV}\,, \tag{5.39}$$

$$\sigma_0 = 30 \div 40 \text{ MeV}\,, \tag{5.40}$$

and

$$r = 29 \pm 7\,. \tag{5.41}$$

In the present paper, in order to display the influence of the uncertainties due to the hadronic quantities on the signals at neutrino detectors, we will report our results for three different sets of values for the quantities $(\sigma_{\pi N}\,, \sigma_0\,, r)$ as shown in Tab. 5.2. The set REF corresponds to the set of value referred to as *reference point* in Ref. [58]. The sets MIN and MAX listed in Tab. 5.2 bracket the range of hadronic uncertainties.

In the case where the neutralino-nucleus interaction is dominated by the exchange of Higgs bosons, it is straightforward to estimate by how much the capture rate C is affected by the hadronic uncertainties. Indeed, in this case the dominant term in the interaction amplitude of the neutralino-nucleus scattering is provided by coupling between the two CP-even Higgs bosons and the down-type quarks:

$$g_d = \frac{2}{27}\left(m_N + \frac{23}{4}\,\sigma_{\pi N} + \frac{23}{5}\,r\,(\sigma_{\pi N} - \sigma_0)\right)\,, \tag{5.42}$$

where m_N is the nucleon mass. Then:

$$C_{\rm MIN}/C_{\rm REF} \simeq (g_{d,\,\rm MIN}/g_{d,\,\rm REF})^2\,, \qquad C_{\rm MAX}/C_{\rm REF} \simeq (g_{d,\,\rm MAX}/g_{d,\,\rm REF})^2\,. \tag{5.43}$$

Using the values of Table 5.2 for the three sets of hadronic quantities, one finds for g_d: $g_{d,\,\rm MIN} = 99$ MeV, $g_{d,\,\rm REF} = 290$ MeV, $g_{d,\,\rm MAX} = 598$ MeV, respectively. We thus conclude that, because of the hadronic uncertainties, the capture rate in the case of set MIN is reduced by a factor ~ 9 as compared to the capture rate evaluated with the set REF, whereas C, evaluated with set MAX, is enhanced by a factor ~ 4.

The consequences over the annihilation rate $\Gamma_{\rm ANN}$ is more involved, since the capture rate C enters in $\Gamma_{\rm ANN}$ not only linearly but also through τ_A. When in the celestial body capture and annihilation are in equilibrium ($t \gtrsim \tau_A$), one has $\Gamma_{\rm ANN} \sim C/2$; then $\Gamma_{\rm ANN}$,

as a function of the hadronic quantities, rescales as C (see Eq. (5.43)); however, when the equilibrium is not realized, the uncertainties in $\Gamma_{\rm ANN}$ can be much more pronounced. For instance, for $t \ll \tau_A$, $\Gamma_{\rm ANN}$ is proportional to C^2, thus the rescaling factors for $\Gamma_{\rm ANN}$ are the squares of those in Eq. (5.43).

These estimates will be confirmed by the numerical analysis displayed in the following section.

5.2.3 Numerical evaluations

For the velocity distribution of relic neutralinos in the galactic halo we use, for definiteness, the standard isothermal distribution parametrized in terms of the local rotational velocity v_0 (model A1 in Ref. [51]). The local rotational velocity v_0 is set at three different representative values: the central value $v_0 = 220$ km s^{-1} and two extreme values $v_0 = 170$ km s^{-1} and $v_0 = 270$ km s^{-1} which bracket the v_0 physical range, cf. Sect. 2.2. Associated to each value of v_0 we take a value of ρ_0 within its physical range established according to the procedure described in Ref. [51]. In conclusion, we will provide the numerical results of our analysis for the following three sets of astrophysical parameters: 1) $v_0 = 170$ km s^{-1}, $\rho_0 = 0.20$ GeV cm^{-3}; 2) $v_0 = 220$ km s^{-1}, $\rho_0 = 0.34$ GeV cm^{-3}; 3) $v_0 = 270$ km s^{-1}, $\rho_0 = 0.62$ GeV cm^{-3}. Note that these values of ρ_0 correspond to the case of maximal amount of non halo components to DM in the galaxy [51].

It is however to be recalled that the actual distribution function could deviate sizably from the isothermal one [51] or even depend on non-thermalized effects [209]. Also the possible presence of a thick disk of DM could play a relevant role in the capture of DM by celestial bodies [210].

The density of neutralinos ρ_χ can be assumed equal to the local value of the total DM density ρ_0, when the neutralino relic abundance ($\Omega_\chi h^2$) turns out to be at the level of a minimal $(\Omega_{CDM} h^2)_{\rm min}$ consistent with ρ_0. On the contrary, when ($\Omega_\chi h^2$) is smaller than $(\Omega_{CDM} h^2)_{\rm min}$, the value to be assigned to ρ_χ has to be appropriately reduced. Thus we evaluate $\Omega_\chi h^2$ and we determine ρ_χ by adopting a standard rescaling procedure [9]:

$$\begin{aligned} \rho_\chi &= \rho_0 \,, && \text{when} \quad \Omega_\chi h^2 \geq (\Omega_{CDM} h^2)_{\rm min} \\ \rho_\chi &= \rho_0 \frac{\Omega_\chi h^2}{(\Omega_{CDM} h^2)_{\rm min}} \,, && \text{when} \quad \Omega_\chi h^2 < (\Omega_{CDM} h^2)_{\rm min} \end{aligned} \tag{5.44}$$

Here $(\Omega_{CDM} h^2)_{\rm min}$ is set to the value 0.098, as derived at 2σ level from the results of Ref. [39].

It is worth noticing that the neutralino density ρ_χ, evaluated according to Eq. (5.44), enters not only in the capture rate C but also in parameter τ_A (through C). Therefore the use of a correct value for ρ_χ (rescaled according to Eq. (5.44), when necessary) is important also in determining whether or not the equilibrium is already set in a macroscopic body.

Explicit calculations over the whole parameter space show that, whereas for the Earth the equilibrium condition depends sensitively on the values of the model parameters, in

the case of the Sun equilibrium between capture and annihilation is typically reached for the whole range of m_χ, due to the much more efficient capture rate implied by the stronger gravitational field [131, 132].

The left panel of Fig. 5.5 shows the scatter plots for the ratios of the capture rates $C_i^{\rm Earth}/C_{\rm REF}^{\rm Earth}$ (where i = set MIN, set MAX). One sees that, as anticipated in the previous section, the numerical values accumulate (most significantly for light masses), around the numerical factors shown in Eq. (5.43).

The scatter plots for the ratios $\Gamma_{{\rm ANN},i}^{\rm Earth}/\Gamma_{\rm ANN,REF}^{\rm Earth}$ (where i = set MIN, set MAX) are displayed in the right panel of Fig. 5.5. As expected and discussed before, these numerical values are much larger than those of Eq. (5.43), since many supersymmetric configurations are not able to provide a capture-annihilation equilibrium inside the Earth.

The dependence of the annihilation rate for the Sun, $\Gamma_{\rm ANN}^{\rm Sun}$ on the hadronic uncertainties is shown in Fig. 5.6. Since the capture-annihilation equilibrium is realized in the Sun for all supersymmetric configurations of our model, one has here that $\Gamma_{{\rm ANN},i}^{\rm Sun}/\Gamma_{\rm ANN,REF}^{\rm Sun} = C_i^{\rm Sun}/C_{\rm REF}^{\rm Sun}$, which implies that $\Gamma_{\rm ANN,MAX}^{\rm Sun}/\Gamma_{\rm ANN,REF}^{\rm Sun} \lesssim 4$ and $\Gamma_{\rm ANN,MIN}^{\rm Sun}/\Gamma_{\rm ANN,REF}^{\rm Sun} \gtrsim 1/9$. This is at variance with the case of the Earth which we have commented before.

Moreover, one notices from Fig. 5.6 that for many supersymmetric configurations $\Gamma_{\rm ANN}^{\rm Sun}$ depends very slightly (or negligibly) on the variations in the hadronic quantities. This is due to the fact that on many instances the capture of neutralinos from the Sun is dominated by spin-dependent cross-sections, due to squarks exchange.

5.2.4 Fluxes from the Earth and the Sun

For the case of neutralino annihilations in the Earth, we fix the angular opening to $-1.0 \leq \cos\theta_z \leq -0.9$, while, for the Sun, we divide the upward muons in stopping and through-going, using the Super-Kamiokande effective area averaged over the zenith angle. For simplicity, we neglect the ν_τ regeneration effect, since it provides only a negligible correction for the WIMPs mass range of our interest: $m_\chi \leq 80$ GeV.

The upper panel of Fig. 5.7 displays the scatter plots for the expected muon flux integrated over the muon energy for $E_\mu \geq 1.6$ GeV for the upward through-going muons. The three columns refer to the evaluation of the fluxes using in turn the three different set of hadronic quantities defined in Sect. 5.2.2.

The various peaks for $m_\chi \lesssim 40$ GeV are due to resonant capture of neutralinos on oxygen, magnesium and silicon; indeed, these elements are almost as abundant in Earth as iron, which is the most relevant target nucleus for the capture of neutralinos of higher mass. The dip at $m_\chi \sim 45$ GeV is a consequence of a depletion of the neutralino local density, implied by the rescaling recipe of Eq. (5.44) and a resonant effect in the (Z-exchange) neutralino pair annihilation when $m_\chi \lesssim m_Z/2$ (note that the neutralino relic abundance is inversely proportional to the neutralino pair-annihilation).

The fact that the muon signal for light neutralinos ($m_\chi \lesssim$ 25-30 GeV) is lower than the one at higher masses can be understood by considerations on the neutralino annihilation channels. Indeed, for light masses the branching ratio of the annihilation process into the $\tau\bar{\tau}$ final state, which is the one with the highest neutrino yield per annihilation, is

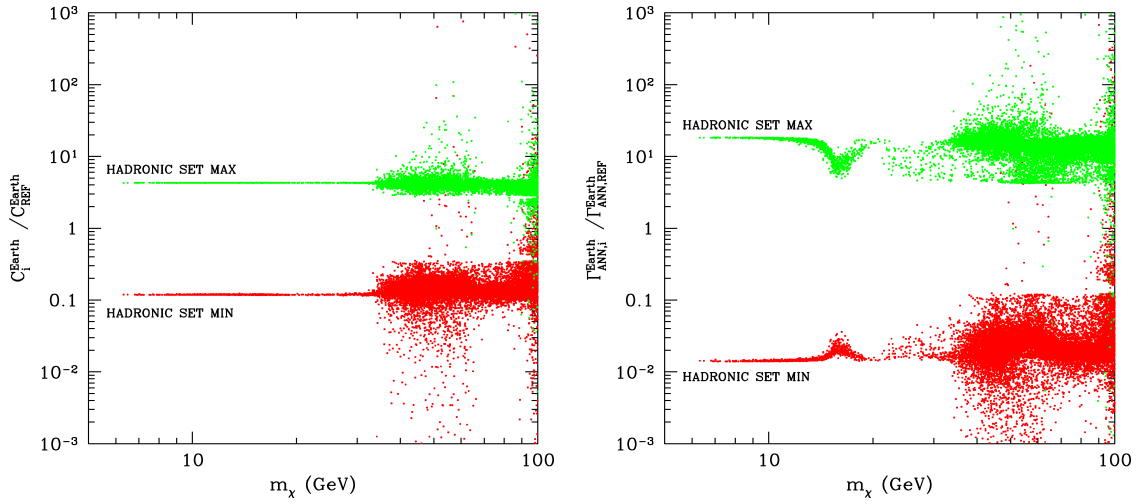

Figure 5.5: Ratios of capture rates (left panel) and annihilation rates (right panel), in the case of the Earth, calculated for the hadronic sets MIN and MAX with respect to the hadronic set REF. The local rotational velocity is set to its central value: $v_0 = 220$ km s^{-1} ($\rho_0 = 0.34$ GeV cm^{-3}).

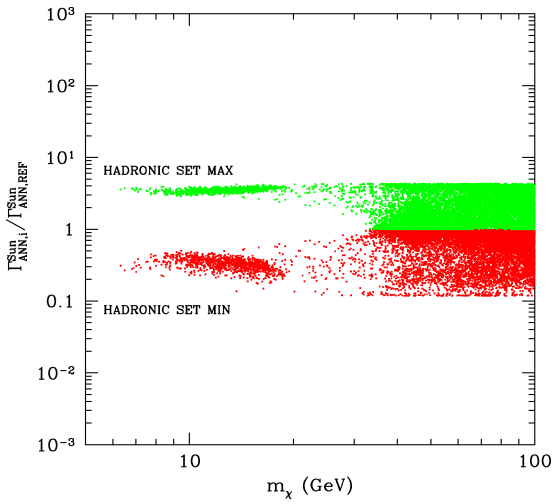

Figure 5.6: Ratios of annihilation rates, in the case of the Sun, calculated for the hadronic sets MIN and MAX with respect to the hadronic set REF. The local rotational velocity is set to its central value: $v_0 = 220$ km s^{-1} ($\rho_0 = 0.34$ GeV cm^{-3}).

suppressed. This last property being in turn due to the fact that, for these masses, the final state in $b\bar{b}$ in the annihilation cross section has to be the dominant one in order to keep the neutralino relic abundance below its cosmological upper bound [103]. Moreover, lower m_χ masses imply softer neutrino spectra, which entail fewer muons above threshold.

The comparison of the fluxes in the three columns shows how relevant can be the role of the size of the hadronic quantities on the final outputs. The suppression (enhancement) of the flux in the case of the set MIN (MAX) as compared to the flux for the set REF are set by the numerical factors previously discussed for $\Gamma_{\rm ANN}^{\rm Earth}$. This entails that, whereas the overall muon flux is completely below the present experimental bound in the case of the minimal set of the hadronic quantities, some part of the spectrum would emerge sizably above the limit for neutralino masses $m_\chi \gtrsim 50$ GeV for the other sets. In the case of set MAX, the neutralino configurations with masses $m_\chi \sim 15$ GeV or $m_\chi \sim$ 25-30 GeV would produce a neutrino signal higher than the SK experimental bound.

Since also the dependence of the muon signals on the astrophysical parameters v_0 and ρ_0 is important, in the lower panel of Fig. 5.7 we display the through-going fluxes for the three representative values of v_0 and ρ_0 which we discussed in Sect. 5.2.3. The overall increase in the fluxes in moving from left to right is essentially due to the increase in the value of the local DM density. In these scatter plots the hadronic quantities are set to the value REF.

The fluxes for upward stopping-muons from the Earth are given in Fig. 5.8. The scheme of this figure is the same as the one of the previous Fig. 5.7: the dependence of the fluxes on the hadronic quantities can be read in the upper panel, the one on the astrophysical parameters is displayed in the lower panel.

Because of the uncertainties affecting the evaluations of the muon fluxes, mainly due to the hadronic quantities, we cannot convert these results in terms of absolute constraints on supersymmetric configurations. However, we can conclude that the analysis of stopping muons from the Earth can have an interesting discovery potential not only for masses above 50 GeV, but also for light neutralinos with $m_\chi \sim 15$ GeV or $m_\chi \sim$ 25-30 GeV. Notice however that the neutralino configurations which provide the highest values of the muon fluxes, mainly at $m_\chi \sim$ 50-70 GeV, are actually disfavored by measurements of WIMP direct detection [211] which have their maximal sensitivity in this mass range.

The fluxes of upward through-going muons and of stopping muons from the Sun are provided in Fig. 5.9 and in Fig. 5.10, respectively: the dependence of the fluxes on the hadronic quantities can be read in the upper panels of Fig. 5.9 and Fig. 5.10, the one on the astrophysical parameters is displayed in the lower panels of the same figures.

From these results one notices that through-going muons can only be relevant for neutralinos with masses $m_\chi \gtrsim 50$ GeV or $m_\chi \sim$ 35-40 GeV, whereas stopping muons can potentially provide information also on some supersymmetric configurations with masses down to $m_\chi \sim 7$ GeV, in the favourable cases of high values of the hadronic quantities and of the astrophysical parameters.

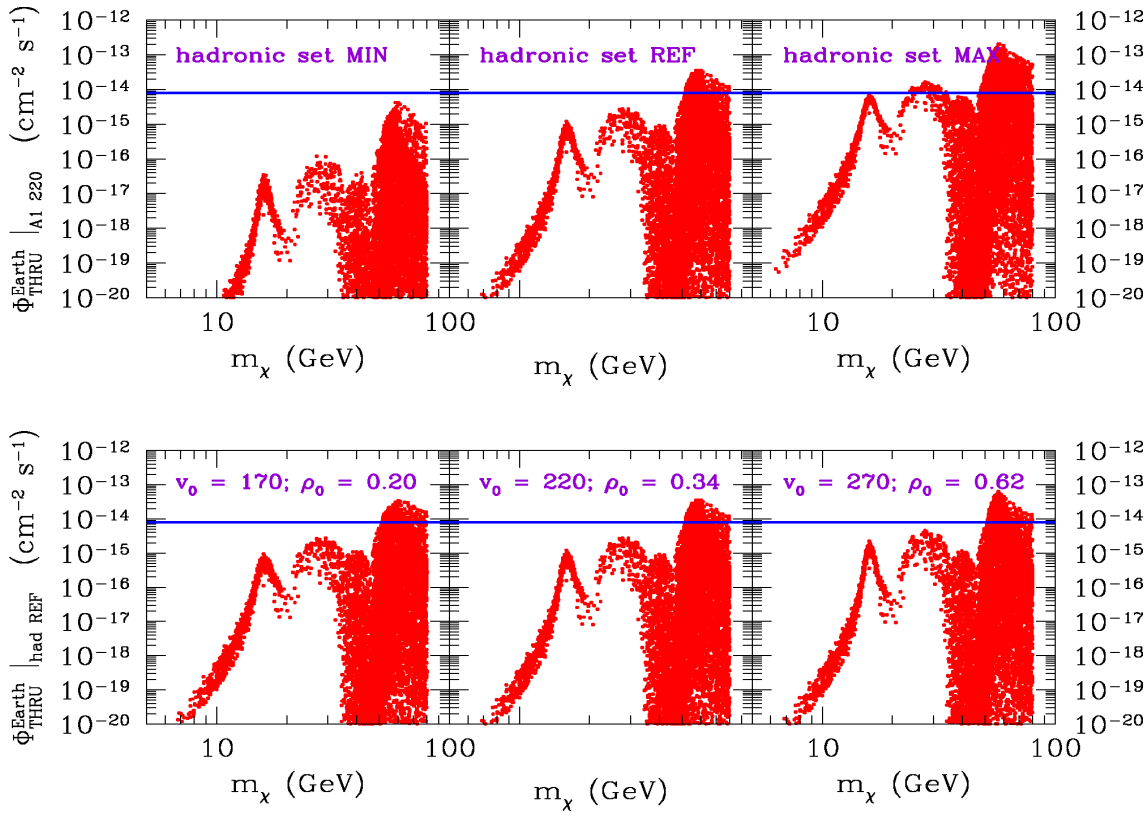

Figure 5.7: Upward through-going muon flux, generated by light neutralino pair-annihilation inside the Earth. The upper panel shows the dependence of the muon flux on the hadronic quantities, for fixed values of the astrophysical parameters: $v_0 = 220$ km s^{-1} and $\rho_0 = 0.34$ GeV cm^{-3}. The lower panel shows the dependence of the muon flux on the local rotational velocity v_0 and the total DM density ρ_0, for the hadronic set REF. The horizontal line represents the experimental limit on through-going muons from the Earth obtained using the SK data, see Eq. (3.41).

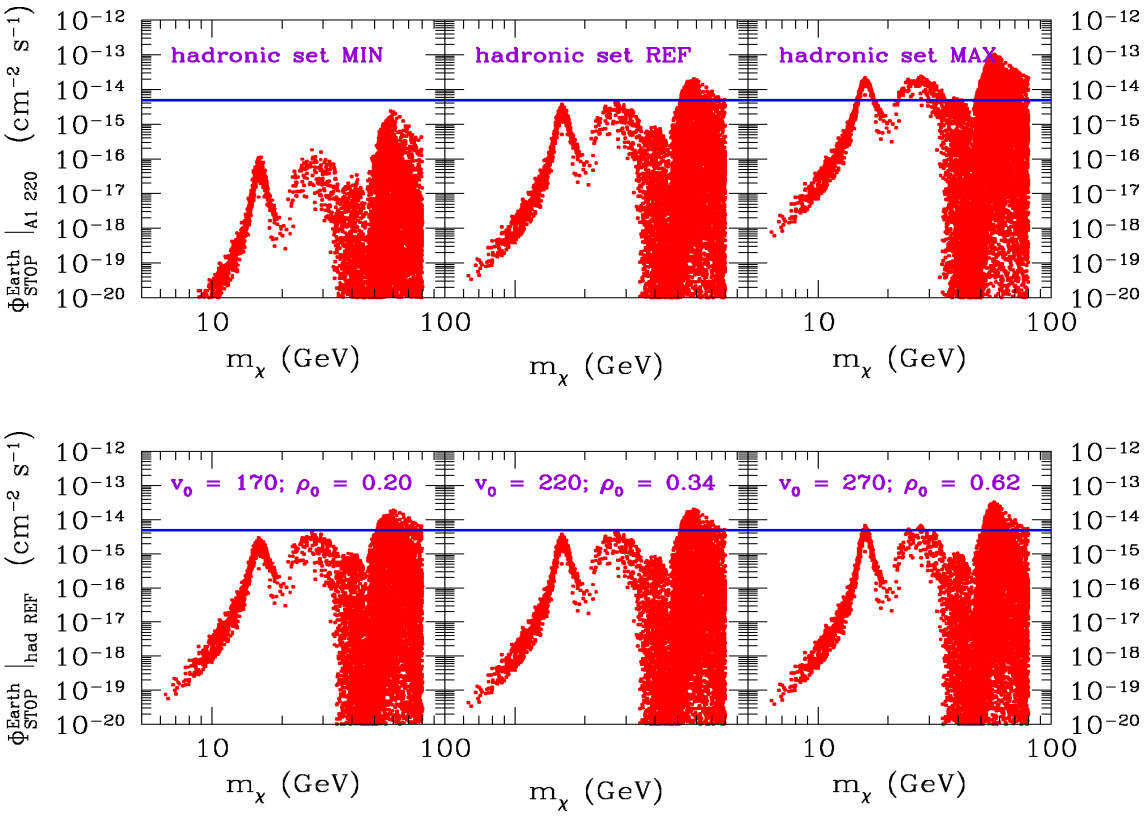

Figure 5.8: The same as Fig. 5.7, but in the case of light neutralino pair-annihilation inside the Earth and of upward stopping muons. In this case, the horizontal line refers to the experimental limit on stopping muons from the Earth obtained using the SK data, see Eq. (3.42).

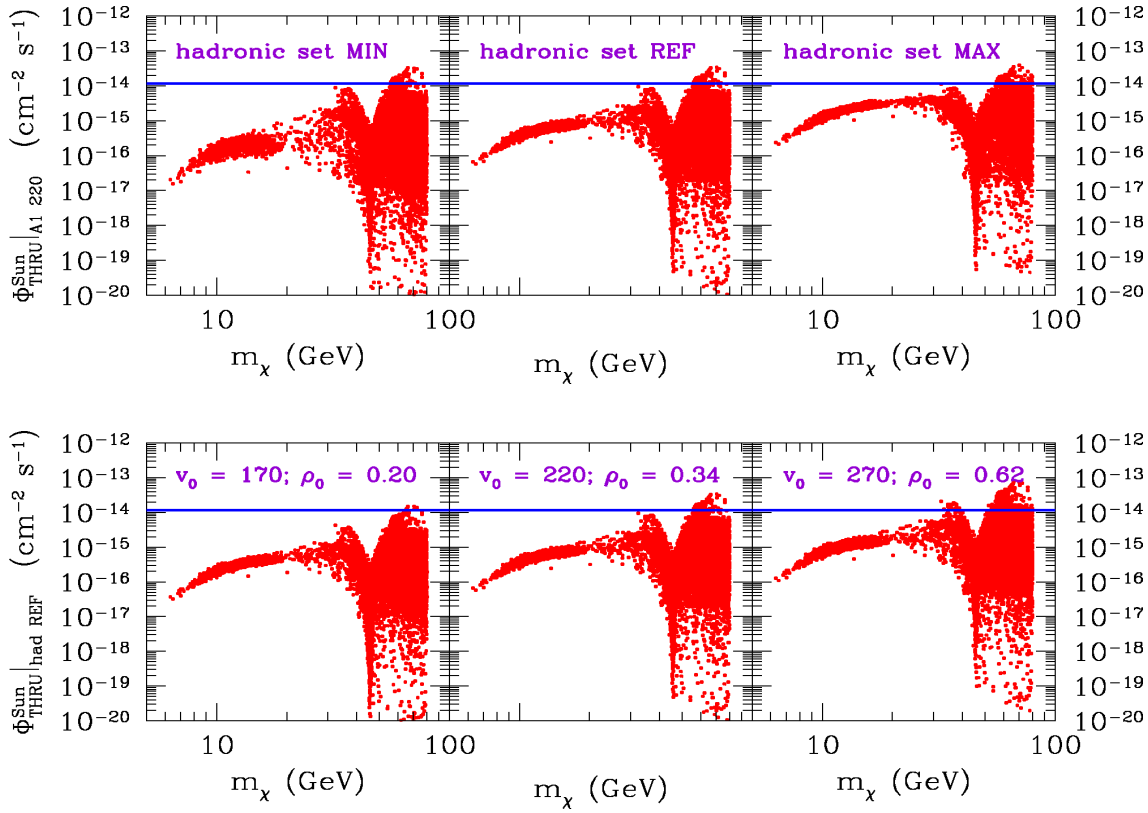

Figure 5.9: The same as Fig. 5.7, but in the case of light neutralino pair-annihilation inside the Sun. In this case, the horizontal line refers to the experimental limit on through-going muons from the Sun obtained using the SK data, see Eq. (3.39).

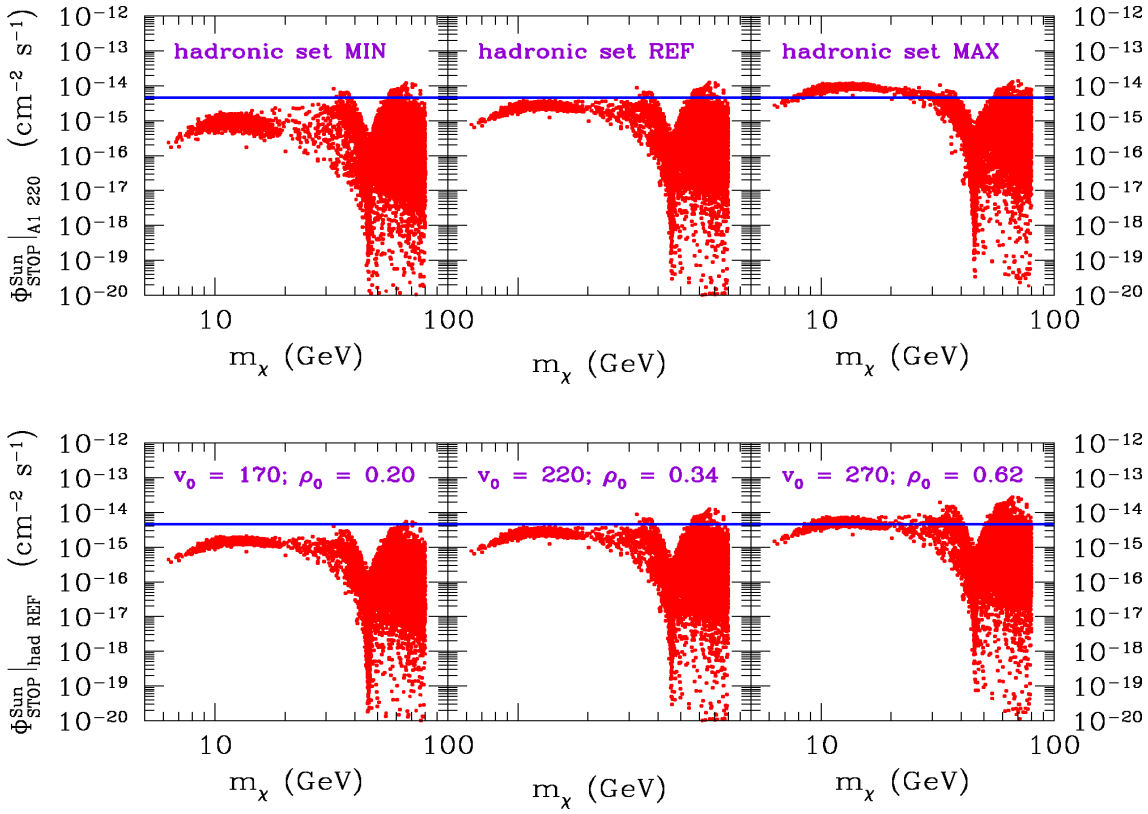

Figure 5.10: The same as Fig. 5.7, but in the case of upward stopping muons. In this case, the horizontal line refers to the experimental limit on stopping muons from the Sun obtained using the SK data, see Eq. (3.40).

5.2.5 Fluxes of stopping muons for configurations compatible with the DAMA results

Now we give the expected upward muon fluxes from the Earth and the Sun which would be produced by neutralino configurations which fit the annual modulation data of the DAMA experiment [3]. As before, for definiteness the analysis is performed in the framework of the isothermal sphere. The selection of the supersymmetric configurations is performed on the basis of the analysis carried out in Ref. [58]: for any set of astrophysical parameters and hadronic quantities, from the whole neutralino population are extracted the configurations which fit the experimental annual modulation data, and the relevant muon fluxes are evaluated. As for the yearly modulation data, we consider both outputs of the experimental analysis of the DAMA Collaboration: those where the channelling effect [68] is included as well as those where this effect is neglected. We recall that the way by which the channeling effect has to be taken into account in the analysis is still under study; thus the actual physical outputs in the analysis of the experimental data in terms of specific DM candidates could stay mid-way, between the case defined as channeling and the no-channeling one, respectively.

We only report the results for stopping muons, since, as we have seen above, this is the category of events which can provide the most sizable signals. The fluxes are calculated varying the hadronic quantities inside their allowed ranges. Fig. 5.11 displays the fluxes for the upward stopping muons expected from the Earth in case of no-channeling (upper panel) and in the case of channeling (lower panel). The corresponding fluxes from the Sun are shown in Fig. 5.12.

We note that depending on the role of channeling in the extraction of the physical supersymmetric configurations, the stopping muon fluxes can have a discovery potential with an interesting complementarity between the signals from the two celestial bodies: whereas the flux from the Earth cannot give insights into neutralino masses below about 15 GeV, the flux from the Sun would potentially be able to measure effects down to $m_\chi \sim 7$ GeV.

It is worth remarking that under favourable conditions provided by the actual values of the involved parameters, a combination of the annual modulation data and of measurements at neutrino detectors could help in pinning down the features of the DM particle and in restraining the ranges of the many quantities (of astrophysical and particle-physics origins) which enter in the evaluations and still suffer from large uncertainties. In general, we can affirm that, if the channeling effect is absent, light neutralinos might have better possibility to be discovered through measurements of stopping muons.

We stress once more that the present analysis, for definiteness, was performed only in the standard case of a halo DM distribution function given by an isothermal sphere. Use of different halo distributions, such as those described in Ref. [51], could modify the role of specific supersymmetric configurations.

We wish here to recall that indirect signals of light neutralinos could also be provided by future measurements of cosmic antideuterons in space [212] with forthcoming airborne experiments [87, 88]. Finally, investigations at the Large Hadron Collider will hopefully

provide a crucial test bench for the very existence of these light supersymmetric stable particles [213].

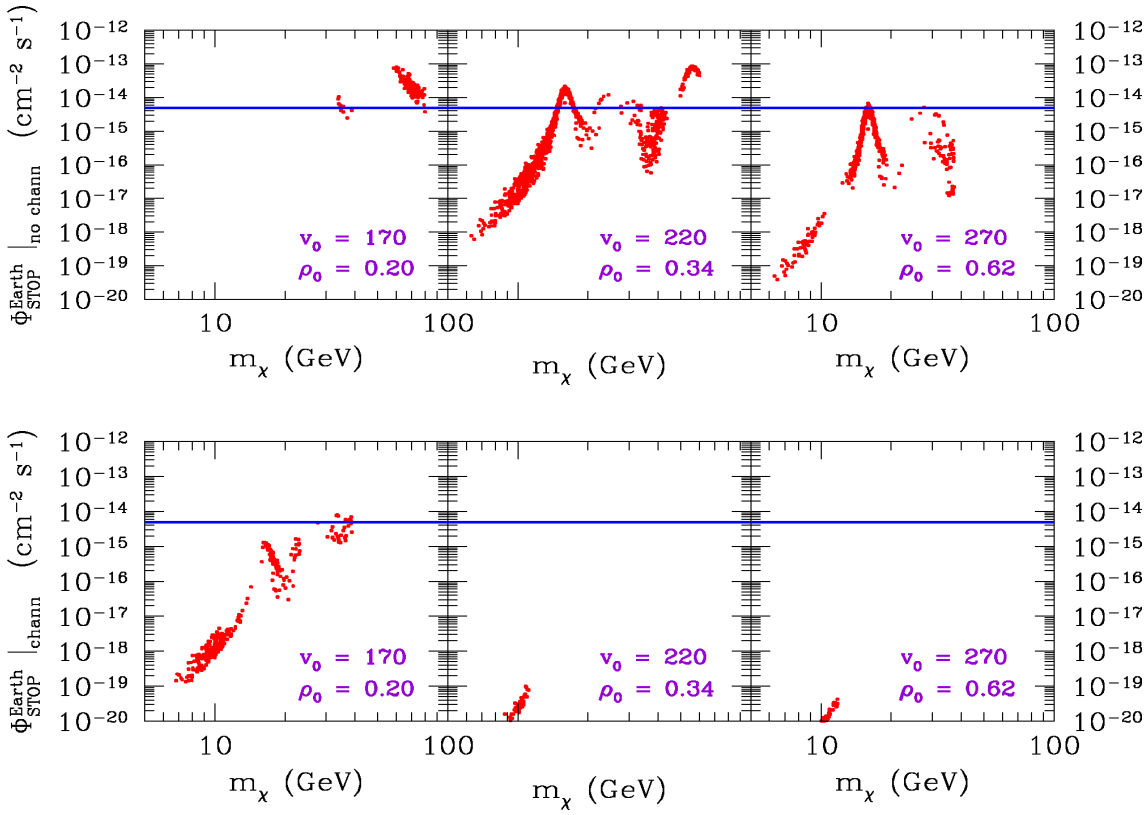

Figure 5.11: Upward stopping muon flux, generated by light neutralino pair-annihilation inside the Earth. The configurations displayed are only the ones compatible with the DAMA annual modulation region, obtained without including the channeling effect (upper panel) and including the channeling effect (lower panel). The three columns show the results for the different sets of astrophysical parameters, defined in Sect. 5.2.3. The horizontal line represents the experimental limit on stopping muons from the Earth obtained using the SK data, see Eq. (3.42).

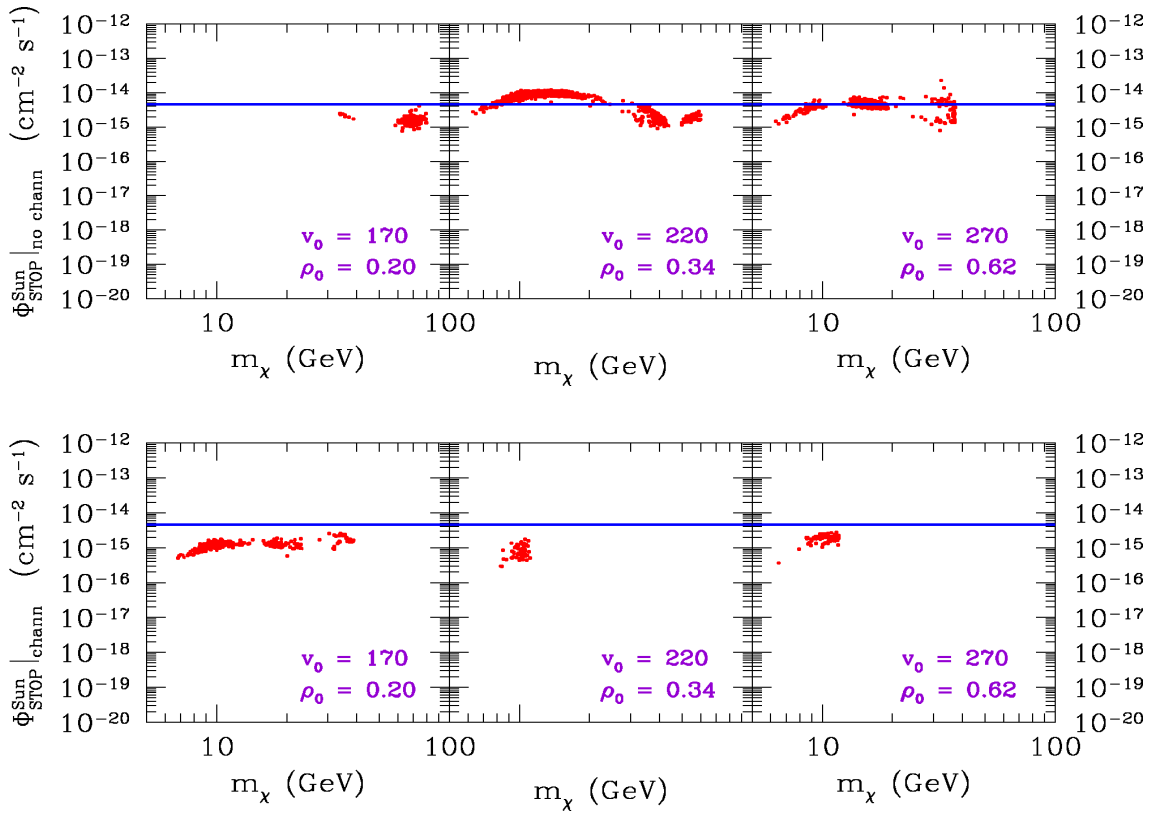

Figure 5.12: The same as Fig. 5.11, but in the case of light neutralino pair-annihilation inside the Sun. In this case, the horizontal line refers to the experimental limit on stopping muons from the Sun obtained using the SK data, see Eq. (3.40).

6

Summary and conclusions

A long time has passed since F. Zwicky in 1933 proposed for the first time the Dark Matter hypothesis. Several different and complementary experiments, carried out in the past decades, have confirmed the presence of an unknown form of matter at the level of galaxies and clusters. The most precise determination of its abundance is provided by the analysis of the Cosmic Microwave Background: roughly 84% of the mass of the Universe is in the form of a non-luminous unknown matter.

After compelling evidences from astrophysical and cosmological experiments, the Dark Matter concept is now commonly accepted by the whole physics community. However, despite these strong experimental hints, we know very little about the nature of the particle (or the particles) that constitute the Dark Matter. To overcome this poor knowledge, different types of experimental searches are necessary. A review on our current understanding of the Universe, on the Dark Matter detection methods and on the different Dark Matter candidates has been given in Chapter 2.

In this work, we have focused on a particular class of indirect Dark Matter detection methods: the search for neutrinos coming from Dark Matter annihilations. We have extensively explained in Chapter 3 how to calculate the neutrino flux in the case of annihilation inside celestial bodies or near the galactic center.

If the Dark Matter particles annihilate directly into neutrinos, the energy spectrum of the neutrinos will consist of a line centered at energy $E_\nu \simeq m_\chi$. This peculiar signal could certainly be distinguished from the background of atmospheric neutrinos. In Chapter 4, we have systematically investigated the different annihilation cross sections into neutrinos, identifying all the cases in which a non-negligible branching ratio might be present. With our analysis, we shed light on the main characteristics and criteria that have to be fullfilled to obtain a sizable neutrino production. The explicit behaviour of the annihilation cross section has also been shown for specific examples.

Most of the different theoretical models that arise from extentions of the Standard Model of particle physics contain a viable Dark Matter candidate. One possibility to

reduce this vast set of scenarios is to combine results coming from different Dark Matter searches. In Chapter 5, we have considered the interplay between indirect Dark Matter detection with neutrinos and the direct Dark Matter detection. In particular, we have focused on two different candidates: the leptophilic Dark Matter and the neutralino Dark Matter. In the first case, we have carefully described the phenomenology of the leptophilic Dark Matter for direct detection experiments and indirect detection with neutrinos. We have then shown how the Super-Kamiokande bounds on neutrinos from Dark Matter annihilations inside the Sun provide a strong constraint on the leptophilic candidate. Indeed, the cross section required to explain the DAMA data within this scenario is excluded by many orders of magnitude by the neutrino constraints.

In the case of neutralino Dark Matter, we have calculated the fluxes in through-going and stopping muons, as expected at the Super-Kamiokande detector, and we have compared them to the existing bounds. Depending on the category of events and on the values of the various astrophysics and particle physics parameters, we have derived the ranges of neutralino masses which could be explored at a water Cherenkov detector with a low muon energy threshold (around 1 GeV). Moreover, we have shown how stopping muons could be used to explore the low mass region in the allowed neutralino parameter space. For this category of events, we have also calculated the expected fluxes for the supersymmetric configurations selected by the DAMA annual modulation data.

We are in an important and exciting moment concerning the Dark Matter searches. A number of experiments that use direct or indirect detection techniques are now running and taking data, while others are under construction. Most notably, we should remember that new future results are expected from the Super-Kamiokande detector and that the IceCube neutrino telescope at the South Pole will soon be completed. Of strong importance for the analysis of the neutrino flux from the galactic center is the planned KM3Net neutrino telescope. Furthermore, the LHC collider experiment is expected to provide important information on the nature of Dark Matter, since most of the existing theoretical framework predicts particles with masses accessible to the energies that LHC will reach. Future LHC data will also be fundamental to constrain the existing models of New Physics and their Dark Matter candidates. Finally, we want to stress that the important task of identifying the nature of Dark Matter will require a joint effort between the astrophysics and the particle physics community, both on the theoretical and on the experimental side. Only with combined analyses that consider data form different experiments, we will be able to shed light on what has remained a mystery for about eighty years.

Acknowledgments

First of all I would like to thank my supervisor Prof. Manfred Lindner for giving me the possibility to come to Heidelberg and for accepting me as PhD student. Thanks for all the enthusiasm you put in physics and for all the interesting discussions we had. Thanks also for leaving me the freedom to find my way. I wish to thank Prof. Tilman Plehn for agreeing to be my second referee. Thanks also to Prof. Stephanie Hansmann-Menzemer and to Prof. Eva Grebel for accepting to take part in my exam.

A very big thank you to all the people that made this thesis possible: my collaborators. Thanks to Joachim Kopp for all the discussions we had together and for helping me throughout my doctorate. Thanks to Alexander Merle for constantly supervising me in the last period of my PhD. Thanks to Manfred Lindner, Thomas Schwetz, Jure Zupan and Thomas Underwood for the fruitful collaborations. A special thank you to the Astroparticle Physics group of the University of Torino. In particular I would like to express all my gratitude to Nicolao Fornengo for always finding the time to answer my questions, for guiding me during our research and for hospitality in Torino. Thanks also to Alessandro Bottino for all his passion towards physics and for the work we did together. I want to thank Werner Rodejohann and Sandhya Choubey, with whom I wrote my first paper. Thanks to Evgeny Akhmedov for giving me an interesting project to work on. A particular thank you also to Andreas Hohenegger for having always the solution to whatever computer-related problem. Thanks to my ex-officemate Mathias Garny to always have had an answer to my questions.

I am also grateful to Alexander Merle and to Joachim Kopp for proofreading my thesis. I want to thank all my colleagues (and ex-colleagues) from the Division on Particle and Astroparticle Physics for creating such an exciting working environment: Adisorn Adulpravitchai, Evgeny Akhmedov, Fedor Bezrukov, Alexander Blum, Mathias Garny, Claudia Hagedorn, Hans Hettmansperger, Andreas Hohenegger, Martin Holthausen, Alexander Kartavtsev, Alexander Merle, Werner Rodejohann, Michael Schmidt, Thomas Schwetz-Mangold, Tom Underwood and Elisa Resconi. Thanks to Anja Berneiser for helping me out with all the bureaucracy.

These years would have not been the same without having by my side wonderful people that made my stay in Heidelberg special. I am really thankful to Sara for all the time we spent together, for always being there to listen to my problems. It was great that you came here and that we shared also the PhD together. Thanks to Giulia for trying to make me feel at home here since the first time we met and for having always a good advice. Thanks to Claudia for being always full of ideas and for being an example for me. Thanks to Giovanna for all her sweetness and naivety. Thanks to Isabel for believing in friendship. Thanks also to Viví, Olga and Matteo. Thanks to Giovanni for being a good

friend (especially in the last period!) and thanks to Brian for all the good DVDs.

I would also like to thank Fede and Giulia for always being happy to see me each time I was coming back to Torino. It is such a great feeling to know that I have you as friends. Thanks also to Gianni, Andrea and Stefano for the funny time together.

Un grazie particolare alla mia famiglia: mamma, papá, Lavinia e Fabrizio. É stato difficile e doloroso stare cosí lontano in tutti questi anni e senza tutto il vostro supporto non sarei mai riuscita a finire questa tesi. Grazie per essermi stati vicino nei momenti piú difficili e per aver sempre creduto in me.

A

Neutrino interactions inside the Sun

In this Appendix, we report the explicit expressions for the neutral current and charged current terms, which appear in the evolution of the neutrino density matrix, see Eq. (3.14). We do not discuss the oscillatory term, since it has already been written explicitly in Eq. (3.15).

A.1 Neutral current interaction

The neutral current contribution to the density matrix equation is given by the sum of two terms that describe, respectively, the processes of neutrino energy loss and reinjection:

$$\left.\frac{d\rho}{dr}(E)\right|_{NC} = -\int_0^E dE' \frac{d\Gamma_{NC}}{dE'}(E,E')\,\rho(E) + \\ + \int_E^{m_\chi} dE' \frac{d\Gamma_{NC}}{dE}(E',E)\,\rho(E')\,, \tag{A.1}$$

where Γ_{NC} is defined as

$$\Gamma_{NC}(E,E') = \mathrm{diag}\left(\Gamma^e_{NC}(E,E'),\,\Gamma^\mu_{NC}(E,E'),\,\Gamma^\tau_{NC}(E,E')\right)\,, \tag{A.2}$$

with

$$\Gamma^l_{NC}(E,E') = N_p(r)\,\sigma(\nu_l p \to \nu'_l X) + N_n(r)\,\sigma(\nu_l n \to \nu'_l X)\,. \tag{A.3}$$

Since the neutral current cross sections are identical for the different flavours, the matrix $\Gamma_{NC}(E,E')$ is proportional to the unit matrix. The functions N_p and N_n represent the proton and neutron number densities of the medium in which the neutrinos are propagating. In the upper panel of Fig. A.1, we report the electron and neutron number

density as predicted by the Standard Solar Model of Ref. [214]. As a comparison, we also show the prediction of the approximate exponential density profile [215]:

$$\frac{N_e}{N_A} = 245 \ \exp(-10.54 \ x) \ \text{cm}^{-3} \,, \tag{A.4}$$

with N_e being the electron number density ($N_p = N_e$ for the Sun). The chemical composition of the ratio N_p/N_n varies from a value of ~ 7 in the outer region of the Sun to $N_p/N_n \sim 2$ in the central region, as displayed in the lower panel of Fig. A.1.

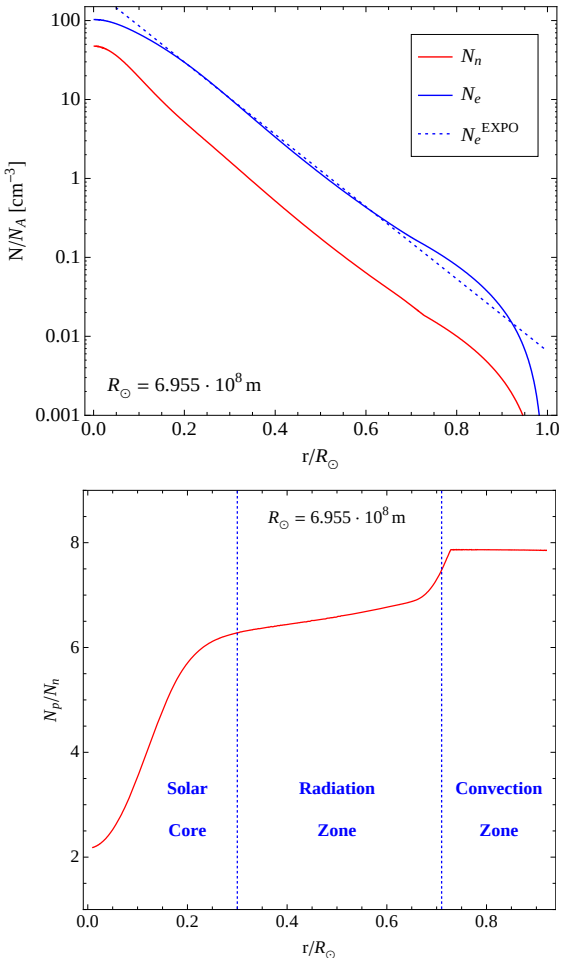

Figure A.1: Upper panel: neutron and electron number density inside the Sun, as predicted by the Standard Solar Model. We report also the exponential approximation of Eq. (A.4). Lower panel: ratio N_p/N_n as a function of the radius of the Sun.

A.2 Charged current interaction

For the charged current interaction contributions, we have to consider both the equations for the neutrino and antineutrino density matrix, since they are coupled by the regeneration processes due to tau decays after charged current interactions. Indeed, an initial ν_τ or $\bar{\nu}_\tau$ with energy $E^{\rm in}$ that undergoes charged current scatterings on nucleons can produce secondary neutrinos through the following decay chains:

$$\nu_\tau \to \tau^- \to \begin{cases} X + \nu_\tau \\ e^- + \bar{\nu}_e + \nu_\tau \\ \mu^- + \bar{\nu}_\mu + \nu_\tau \end{cases} \qquad \bar{\nu}_\tau \to \tau^+ \to \begin{cases} X + \bar{\nu}_\tau \\ e^+ + \nu_e + \bar{\nu}_\tau \\ \mu^+ + \nu_\mu + \bar{\nu}_\tau \end{cases}$$

The equations for the charged current terms read

$$\left.\frac{d\rho}{dr}\right|_{CC} = -\frac{\{\Gamma_{CC}, \rho\}}{2} + \int_E^{m_\chi} \frac{dE^{\rm in}}{E^{\rm in}} \left[\Pi_\tau\, \rho_{\tau\tau}(E^{\rm in})\, \Gamma^\tau_{CC}(E^{\rm in})\, f_{\tau\to\tau}(E^{\rm in}, E) + \right.$$
$$\left. + \Pi_{e,\mu}\, \bar{\rho}_{\tau\tau}(E^{\rm in})\, \bar{\Gamma}^\tau_{CC}(E^{\rm in})\, f_{\bar{\tau}\to e,\mu}(E^{\rm in}, E)\right] ,$$

$$\left.\frac{d\bar{\rho}}{dr}\right|_{CC} = -\frac{\{\bar{\Gamma}_{CC}, \bar{\rho}\}}{2} + \int_E^{m_\chi} \frac{dE^{\rm in}}{E^{\rm in}} \left[\Pi_\tau\, \bar{\rho}_{\tau\tau}(E^{\rm in})\, \bar{\Gamma}^\tau_{CC}(E^{\rm in})\, f_{\bar{\tau}\to\bar{\tau}}(E^{\rm in}, E) + \right.$$
$$\left. + \Pi_{e,\mu}\, \rho_{\tau\tau}(E^{\rm in})\, \Gamma^\tau_{CC}(E^{\rm in})\, f_{\tau\to\bar{e},\bar{\mu}}(E^{\rm in}, E)\right] ,$$

where Π_l is a diagonal matrix that projects onto the flavour ν_l, e.g. $\Pi_e = {\rm diag}(1,0,0)$. The matrix Γ_{CC} is defined as

$$\Gamma_{CC}(E) = {\rm diag}\left(\Gamma^e_{CC}(E),\, \Gamma^\mu_{CC}(E),\, \Gamma^\tau_{CC}(E)\right) , \tag{A.5}$$

and each component is given by:

$$\Gamma^l_{CC}(E) = N_p(r)\, \sigma(\nu_l p \to l X) + N_n(r)\, \sigma(\nu_l n \to l X) . \tag{A.6}$$

For antineutrinos, the function $\bar{\Gamma}^l_{CC}(E)$ is defined analogously to the above expression with the replacement of the neutrino cross sections by the ones of antineutrino. In Fig. A.2, we report the energy distribution function $f(E^{\rm in}, E)$ of the secondary neutrinos produced by ν_τ and $\bar{\nu}_\tau$ charged current scatterings on protons. The functions for the scatterings on neutrons are nearly the same.

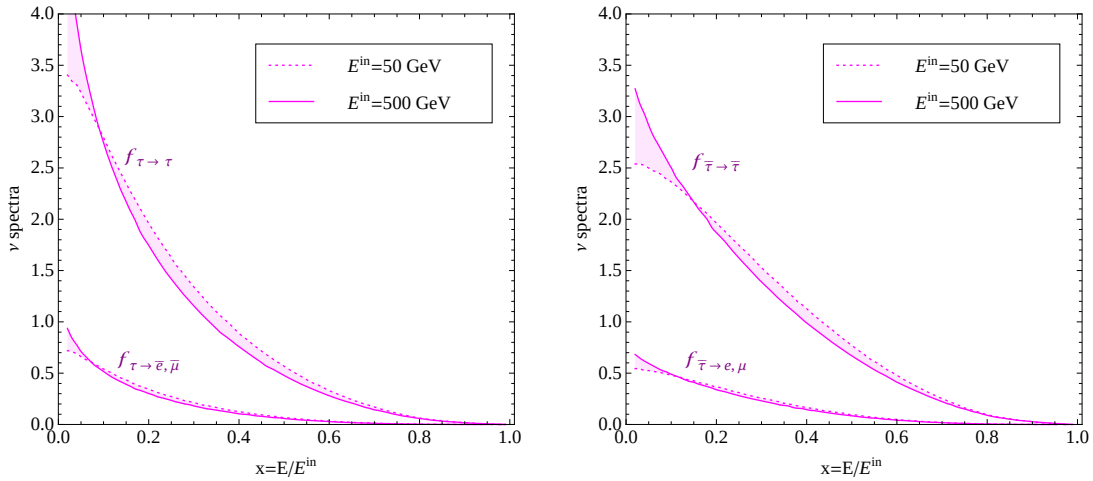

Figure A.2: Energy distributions of secondary neutrinos, generated by the decays of τ or $\bar{\tau}$, which are produced by ν_τ or $\bar{\nu}_\tau$ charged current scatterings on protons. We show the range of variability in case the initial neutrino energy $E^{\rm in}$ changes from 50 GeV to 500 GeV.

B

Neutrino cross sections

In this Appendix, we report the neutrino cross sections that have been used in the calculation of the neutrino spectra coming from Dark Matter annihilations as well as the corresponding muon flux. In Sect. B.1, we discuss the neutral current interactions, while in Sect. B.2 the charged current interactions are treated.

B.1 Neutral current cross sections

Throughout our analyses we have studied neutrinos and antineutrinos of energies of the order of GeV-TeV. In this range, the interaction with protons and neutrons is essentially dominated by deep inelastic scatterings.

As a good approximation, we can consider u and d as valence quarks, and $\bar{u}$ and $\bar{d}$ as sea quarks. The differential cross section for the neutral current process $\nu p \to \nu' X$ can be obtained by summing the differential cross sections for the parton processes, weighted by the quark distributions:

$$\frac{d\sigma}{dE'}(\nu p \to \nu' X) = \frac{2 m_p G_F^2}{\pi} \sum_{q=\{u,d\}} \Big[\langle q \rangle_p \left(g_{Lq}^2 + \tfrac{E'^2}{E^2} g_{Rq}^2 \right) + \\ + \langle \bar{q} \rangle_p \left(g_{Rq}^2 + \tfrac{E'^2}{E^2} g_{Lq}^2 \right) \Big] , \tag{B.1}$$

with:

$$\langle q \rangle = \int_0^1 dx \, x \, q(x) ,$$

where x is the fraction of the total momentum of the nucleon carried by the quark q and the function $q(x)$ is the probability that the quark q has a fraction of the total momentum equal to x. We have indicated by E the initial energy of the neutrino, while E' stands

for the final one. The coefficients g_L and g_R arise from the couplings between the quarks and the Z-boson:

$$g_{Lu} = \frac{1}{2} - \frac{2}{3}\sin^2\theta_W\,, \qquad g_{Ru} = -\frac{2}{3}\sin^2\theta_W\,,$$
$$g_{Ld} = -\frac{1}{2} + \frac{1}{3}\sin^2\theta_W\,, \qquad g_{Rd} = \frac{1}{3}\sin^2\theta_W\,,$$

where θ_W is the Weinberg angle:

$$\sin^2\theta_W = 0.237 \pm 0.006\,.$$

In the case of antineutrinos the cross section is given by:

$$\frac{d\sigma}{dE'}(\bar{\nu}p \to \bar{\nu}'X) = \frac{2m_pG_F^2}{\pi}\sum_{q=\{u,d\}}\Big[\langle q\rangle_p\left(g_{Rq}^2 + \tfrac{E'^2}{E^2}g_{Lq}^2\right) + \\ + \langle\bar{q}\rangle_p\left(g_{Lq}^2 + \tfrac{E'^2}{E^2}g_{Rq}^2\right)\Big]\,. \tag{B.2}$$

If we substitute m_p, $\langle q\rangle_p$ and $\langle\bar{q}\rangle_p$ by, respectively, m_n, $\langle q\rangle_n$ and $\langle\bar{q}\rangle_n$, we will obtain the cross section for the scattering on neutrons. The values that we have used in our work are:

$$\langle u\rangle_p = \langle d\rangle_n = 0.25\,, \tag{B.3}$$
$$\langle d\rangle_p = \langle u\rangle_n = 0.15\,, \tag{B.4}$$
$$\langle\bar{u}\rangle_p = \langle\bar{d}\rangle_n = 0.04\,, \tag{B.5}$$
$$\langle\bar{d}\rangle_p = \langle\bar{u}\rangle_n = 0.06\,. \tag{B.6}$$

We finally want to add that the expressions of the cross sections that we have reported in this Section are valid for energies $E_\nu \ll M_Z^2/(2\,m_p) \simeq 3600$ GeV, with M_Z being the mass of the Z-boson.

B.2 Charged current cross sections

In the case of charged current interaction, the intermediate boson that is exchanged between neutrinos and partons inside the proton is a W-boson. In this case, neutrinos and antineutrinos do not interact with all of the quarks, since the charge has to be conserved at each vertex of a Feynman diagram. The parton cross sections are given by the following expressions:

$$\frac{d\hat{\sigma}}{dy}(\nu_l d \to l u) = \frac{d\hat{\sigma}}{dy}(\bar{\nu}_l\bar{d} \to \bar{l}\bar{u}) = \frac{G_F^2\hat{s}}{\pi}\,, \tag{B.7}$$
$$\frac{d\hat{\sigma}}{dy}(\nu_l\bar{u} \to l\bar{d}) = \frac{d\hat{\sigma}}{dy}(\bar{\nu}_l u \to \bar{l}d) = \frac{G_F^2\hat{s}}{\pi}(1-y)^2\,. \tag{B.8}$$

After integrating over y, with $0 \leq y \leq 1$, we obtain the following total cross sections:

$$\hat{\sigma}(\nu_l d \to l u) \;=\; \hat{\sigma}(\bar{\nu}_l \bar{d} \to \bar{l}\bar{u}) = \frac{G_F^2 \hat{s}}{\pi}\,, \tag{B.9}$$

$$\hat{\sigma}(\bar{\nu}_l u \to \bar{l} d) \;=\; \hat{\sigma}(\nu_l \bar{u} \to l \bar{d}) = \frac{1}{3}\frac{G_F^2 \hat{s}}{\pi}\,, \tag{B.10}$$

where $\hat{s} = s\,x$ is the square of the total energy of the partonic process in the center-of-mass frame, while s is the one of the (anti)neutrino-nucleon process. Integrating over x, we can arrive at the final expressions for the cross sections:

$$\sigma(\nu_l p \to l X) \;=\; \int_0^1 dx\, \left[\, d_p(x)\, \hat{\sigma}(\nu_l d \to l u) \;+\; \bar{u}_p(x)\, \hat{\sigma}(\nu_l \bar{u} \to l \bar{d}) \,\right]$$

$$\Longrightarrow \sigma(\nu_l p \to l X) = \frac{G_F^2 s}{\pi}\left[\langle d \rangle_p + \frac{1}{3}\langle \bar{u} \rangle_p\right], \tag{B.11}$$

$$\sigma(\bar{\nu}_l p \to \bar{l} X) \;=\; \int_0^1 dx\, \left[\, \bar{d}_p(x)\, \hat{\sigma}(\bar{\nu}_l \bar{d} \to \bar{l}\bar{u}) \;+\; u_p(x)\, \hat{\sigma}(\bar{\nu}_l \bar{u} \to \bar{l} d) \,\right]$$

$$\Longrightarrow \sigma(\bar{\nu}_l p \to \bar{l} X) = \frac{G_F^2 s}{\pi}\left[\langle \bar{d} \rangle_p + \frac{1}{3}\langle u \rangle_p\right]. \tag{B.12}$$

Analogous expressions can be obtained for the scattering cross sections on neutrons.

The equations reported above refer to charged current conversions of a neutrino or antineutrino into an electron or a muon. The cross sections for the conversion into a tau lepton are slightly different than the ones derived before. Indeed, since we study neutrinos with energies of the order of m_τ, this will affect the range of variability of the Bjorken variables x and y. We implemented this correction following Ref. [216]. The behaviour of the charged current cross sections is reported in Fig. B.1.

The expressions of the cross sections that we have reported in this Section are valid up to energies $E_\nu \ll M_W^2/(2\,m_p) \simeq 3600$ GeV, with M_W being the mass of the W-boson.

Energy-differential charged current cross section

The energy-differential cross section for deep-inelastic scattering is given by

$$\frac{d\sigma}{dE_\mu} = \frac{1}{E_\nu}\frac{d\sigma}{dy}\,, \tag{B.13}$$

where $y = 1 - E_\mu/E_\nu$. Using Eq. (B.7) and Eq. (B.8), the explicit expressions for the energy-differential cross sections of neutrino and antineutrino scatterings off a proton

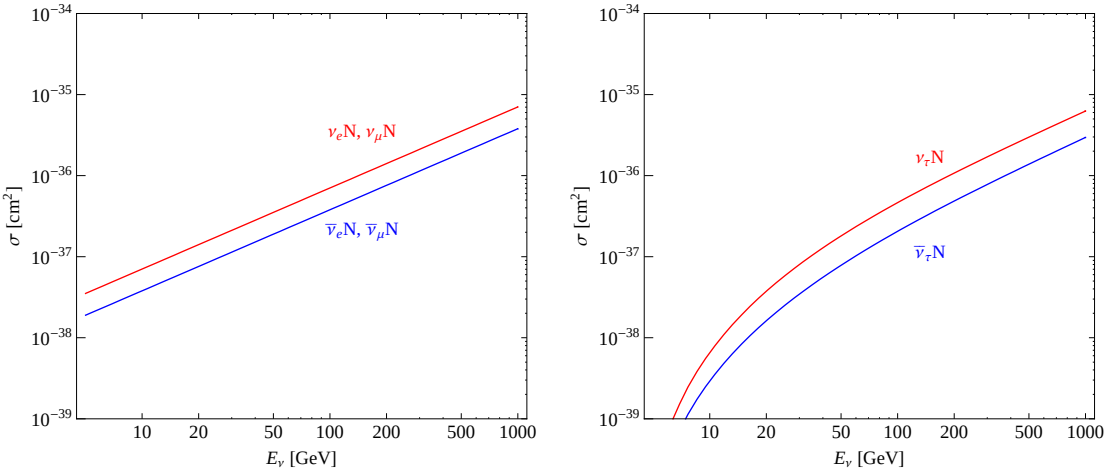

Figure B.1: Cross sections for the charged current interactions of ν and $\bar{\nu}$ on a nucleon N. Left panel: cross sections for $\nu_{e,\mu}$ and $\bar{\nu}_{e,\mu}$. Right panel: cross sections for ν_τ and $\bar{\nu}_\tau$. The effect of the τ mass is well visible at low energies.

are:

$$\frac{d\sigma}{dE_\mu}(\nu_l p \to l X) = \frac{2\, m_p\, G_F^2}{\pi} \left[\langle d \rangle_p + \langle \bar{u} \rangle_p \left(\frac{E_\mu}{E_\nu} \right)^2 \right] \simeq \tag{B.14}$$

$$\simeq \left[0.5 + 0.1 \left(\frac{E_\mu}{E_\nu} \right)^2 \right] 10^{-38}\ \text{cm}^2\ \text{GeV}^{-1}\,,$$

$$\frac{d\sigma}{dE_\mu}(\bar{\nu}_l p \to \bar{l} X) = \frac{2\, m_n\, G_F^2}{\pi} \left[\langle \bar{d} \rangle_p + \langle u \rangle_p \left(\frac{E_\mu}{E_\nu} \right)^2 \right] \simeq \tag{B.15}$$

$$\simeq \left[0.2 + 0.8 \left(\frac{E_\mu}{E_\nu} \right)^2 \right] 10^{-38}\ \text{cm}^2\ \text{GeV}^{-1}\,.$$

Analogous equations can be derived for scattering off a neutron.

C

Annihilation cross sections

The differential annihilation cross section of two DM particles χ into two neutrinos is given by [217]

$$v \frac{d\sigma_{\rm ann}}{d\cos\theta^*} = \frac{1}{16\pi} \frac{1}{s} \overline{|\mathcal{M}|^2}\,, \tag{C.1}$$

where v is the relative velocity between the two DM particles and θ^* is the scattering angle in the center-of-mass frame. In the previous formula we have neglected the neutrino mass and we have denoted by $\overline{|\mathcal{M}|^2}$ the spin-averaged matrix element:

$$\overline{|\mathcal{M}|^2} = \frac{1}{(2S_{\rm DM}+1)^2} \sum_{\rm spins} |\mathcal{M}|^2\,, \tag{C.2}$$

where $S_{\rm DM}$ is the spin of the DM particle.

Since we do not focus on a particular model, our results are general and can be applied to the calculation of the annihilation cross section into neutrinos for a specific DM candidate. Moreover, from our expressions it is easy to see which are the channels and the possible cases that could lead to a sizable DM branching ratio into neutrinos. For simplicity, throughout our analysis we consider only the Standard Model as gauge group. For the numerical calculation we use the `FeynCalc` package [218].

C.1 Scalar Dark Matter

For a scalar DM, the neutrino production can occur through a scalar and a Z-boson exchange in an s-channel diagram and through a fermion exchange in a t-channel diagram. In case the neutrinos are Majorana particles, also a u-channel diagram is present.

Scalar mediator, s-channel

Indicating the coupling of the scalar mediator to the DM with D and the coupling to Dirac neutrinos with $N_L P_L + N_R P_R$, with the projection operators defined as $P_{L,R} = (1 \mp \gamma_5)/2$, the total annihilation cross section can be written as

$$\sigma_{\text{ann}} v\,(\chi_s; \phi_s; s) = \frac{2^{-n}}{8\pi} |D|^2 \frac{|N_L|^2 + |N_R|^2}{(4m_\chi^2 - m_\phi^2)^2}\, 4^n \left(1 - \frac{2m_\chi^2}{(4m_\chi^2 - m_\phi^2)} v^2\right) + \mathcal{O}(v^4)\,, \quad \text{(C.3)}$$

where m_ϕ is the scalar mediator mass and $n = 0, 1$ for Dirac and Majorana neutrinos, respectively. In case of Majorana neutrinos, a factor $1/2$ is present to avoid double counting of identical particles in the final state and a factor 4 arises from the Feynman rule for the effective vertex, since the Majorana neutrinos are self-conjugate particles. Note that, for simplicity, we use the same form of the Yukawa couplings for Dirac and Majorana neutrinos. We want to stress that, in general, this is not the case, since Dirac and Majorana neutrinos usually couple to scalar mediators with different $SU(2)_L$ representations, see Table 4.1.

Z-boson mediator, s-channel

Indicating the coupling of the Z-boson to the DM generically as $D(k_1 - k_2)^\mu$, with k_1 and k_2 being the DM four momenta, and the coupling to the neutrinos with $N_L \gamma^\mu P_L$, the total annihilation cross section can be written as

$$\sigma_{\text{ann}} v\,(\chi_s; Z; s) = \frac{1}{12\pi} D^2 \frac{N_L^2}{(4m_\chi^2 - m_Z^2)^2}\, m_\chi^2 v^2 + \mathcal{O}(v^4)\,, \quad \text{(C.4)}$$

with D and N_L being real numbers. In this case the annihilation cross section is proportional to the DM velocity, as we would naively expect from angular momentum conservation. If the neutrinos are Majorana particles, the annihilation cross section is equivalent to the one given in Eq. (C.4). Indeed, it is well known that weak interactions mediated by the Z-boson do not distinguish between Dirac and Majorana neutrinos [219].

Fermionic mediator, t&u-channels

Indicating the coupling of the DM particle to the fermionic mediator and the neutrino with $F_L P_L + F_R P_R$ at one vertex, and with $G_L P_L + G_R P_R$ at the other vertex, the total annihilation cross section is given by

$$\begin{aligned} \sigma_{\text{ann}} v\,(\chi_s; \phi_f; t) \;=\; & \frac{1}{8\pi} \frac{|F_L|^2 |G_L|^2 + |F_R|^2 |G_R|^2}{(m_\chi^2 + m_\phi^2)^2} \left(m_\phi^2 - \frac{m_\phi^4}{\left(m_\chi^2 + m_\phi^2\right)^2} m_\chi^2 v^2\right) + \\ & + \frac{1}{48\pi} \frac{|F_R|^2 |G_L|^2 + |F_L|^2 |G_R|^2}{\left(m_\chi^2 + m_\phi^2\right)^2} m_\chi^2 v^2 + O\left(v^4\right)\,, \end{aligned} \quad \text{(C.5)}$$

where m_ϕ is the fermionic mediator mass. Notice that, in general, $G_L = F_R^*$ and $G_R = F_L^*$ for a Dirac mediator, while also $G_L = F_L$ and $G_R = F_R$ are allowed for a Majorana mediator. In the first case a pair of $\nu\bar{\nu}$ is produced, while in the second case $\nu\nu$ (or $\bar{\nu}\bar{\nu}$) are produced. If the DM particle is a real scalar, also a u channel is present. The corresponding cross section is equivalent to the one in Eq. (C.5).

In the case of Majorana neutrinos both, the t-channel and the u-channel diagram, must be considered and added together with a relative minus sign. The annihilation cross section is hence modified to

$$\begin{aligned}\sigma_{\text{ann}} v\left(\chi_s;\phi_f;t\&u\right) &= \frac{1}{4\pi}\frac{|F_L|^2|G_L|^2+|F_R|^2|G_R|^2}{\left(m_\chi^2+m_\phi^2\right)^2}\left(m_\phi^2-\frac{m_\phi^2\left(3m_\phi^2+m_\chi^2\right)}{3\left(m_\chi^2+m_\phi^2\right)^2}m_\chi^2v^2\right)+\\ &+ \frac{1}{48\pi}\frac{|F_RG_L-F_LG_R|^2}{\left(m_\chi^2+m_\phi^2\right)^2}m_\chi^2v^2+O\left(v^4\right)\,. \end{aligned} \tag{C.6}$$

C.2 Fermionic Dark Matter

For a fermionic DM, the neutrino production can occur through a Z-boson exchange in an s-channel diagram and through a scalar exchange in an s-channel or a t-channel diagram. In case the DM or the neutrinos are Majorana particles, also a u-channel diagram is present.

Scalar mediator, s-channel

Indicating the coupling of the Dirac DM particle to the scalar mediator with $D_LP_L + D_RP_R$ and the one of the Dirac neutrinos with $N_LP_L + N_RP_R$, the total annihilation cross section can be written as

$$\begin{aligned}\sigma_{\text{ann}} v\left(\chi_f;\phi_s;s\right) &= \frac{2^{-n}}{16\pi}\frac{|N_L|^2+|N_R|^2}{(4m_\chi^2-m_\phi^2)^2}4^n4^m\times\\ &\times\left(|D_L-D_R|^2m_\chi^2-\frac{m_\phi^2}{2\left(4m_\chi^2-m_\phi^2\right)}\left(|D_L|^2+|D_R|^2\right)m_\chi^2v^2+\right.\\ &\left.+\frac{m_\chi^2}{8\left(4m_\chi^2-m_\phi^2\right)}\left(D_LD_R^*+\,c.c.\right)m_\chi^2v^2\right)+\mathcal{O}(v^4)\,. \end{aligned} \tag{C.7}$$

where m_ϕ is the scalar mediator mass, n=0 (n=1) for Dirac (Majorana) neutrinos and m=0 (m=1) for Dirac (Majorana) DM. The factor 1/2 is present to avoid double counting of identical particles in the final state, while the factors 4 come from the Feynman rules for the effective vertex. For simplicity, we have used the same Yukawa couplings for Dirac and Majorana neutrinos. However, they generally couple to different scalar particles, see Table 4.2.

Note, that in case the DM couples to the scalar mediator through a scalar coupling (i.e. $D_L = D_R$), the cross section will be proportional to the DM velocity v. This is a consequence of parity conservation: a fermion-antifermion pair has a parity of (-1) and can therefore, in an s-wave configuration, only couple to a pseudoscalar particle (i.e. $D_L = -D_R$).

Z-boson mediator, s-channel

Indicating the coupling of the DM particle to the Z-boson with $\gamma^\mu(D_L P_L + D_R P_R)$ and the one of the neutrino with $N_L \gamma^\mu P_L$, the total annihilation cross section can be written as

$$\begin{aligned}\sigma_{\rm ann} v\,(\chi_f^D; Z; s) &= \frac{1}{8\pi}\frac{N_L^2}{(4m_\chi^2 - m_Z^2)^2} \times \\ &\times \left((D_L + D_R)^2\, m_\chi^2 - \frac{(m_Z^2 + 2m_\chi^2)}{3\,(4m_\chi^2 - m_Z^2)}(D_L^2 + D_R^2)\, m_\chi^2 v^2 - \right. \\ &\left. - \frac{4\, m_\chi^2}{(4m_\chi^2 - m_Z^2)}(D_L D_R)\, m_\chi^2 v^2 \right) + \mathcal{O}(v^4)\,. \end{aligned} \tag{C.8}$$

with D_L, D_R and N_L being real numbers. The cross section for Majorana neutrinos is equivalent to Eq. (C.8), since, as we have mentioned before, the weak interactions mediated by the Z-boson do not distinguish between Dirac and Majorana neutrinos [219].

If the DM particle is a Majorana fermion, the cross section reported above is drastically modified. Indeed, in an s-wave annihilation, the fermions in the initial state are forced to have opposite spins by the Pauli exclusion principle. As a consequence, since the Z-boson has a spin of one, we expect that the first non zero contribution to the annihilation cross section for Majorana DM is given by the p-wave term. Indeed, we find:

$$\sigma_{\rm ann} v\,(\chi_f^M; Z; s) = \frac{1}{12\pi}\frac{N_L^2}{(4\, m_\chi^2 - m_Z^2)^2}\,(D_L - D_R)^2\, m_\chi^2 v^2 + \mathcal{O}\left(v^4\right)\,, \tag{C.9}$$

where the same expression holds if the DM and the neutrinos are both Majorana particles.

Scalar mediator, t&u-channels

Indicating the coupling of the DM particle to the fermionic mediator and to the neutrino at one vertex with $F_L P_L + F_R P_R$ and at the other one with $G_L P_L + G_R P_R$, the total annihilation cross section is given by

$$\begin{aligned}\sigma_{\rm ann} v\,(\chi_f; \phi_s, t) &= \frac{1}{32\pi}\frac{(|F_L|^2 + |F_R|^2)(|G_L|^2 + |G_R|^2)}{(m_\chi^2 + m_\phi^2)^2} \times \\ &\times \left(m_\chi^2 + \frac{(m_\phi^4 - 3m_\chi^2 m_\phi^2 - m_\chi^4)}{3\,(m_\chi^2 + m_\phi^2)^2}\, m_\chi^2 v^2 \right) + \mathcal{O}(v^4)\,, \end{aligned} \tag{C.10}$$

where m_ϕ is the fermionic mediator mass. Note that, in general, $G_L = F_R^*$ and $G_R = F_L^*$ or $G_L = F_L$ and $G_R = F_R$. In the first case a pair of $\nu\bar{\nu}$ is produced, while in the second case $\nu\nu$ (or $\bar{\nu}\bar{\nu}$) are produced.

A t-channel and a u-channel diagram must be considered in the case of Majorana neutrinos and/or Majorana DM. The expression for the annihilation cross section is thus modified to

$$\begin{aligned}\sigma_{\rm ann} v\,(\chi_f;\phi_s;t\&u) &= \frac{1}{32\pi}\frac{1}{(m_\chi^2+m_\phi^2)^2}\,m_\chi^2\times\mathcal{A} - \\ &- \frac{1}{192\pi}\frac{1}{(m_\chi^2+m_\phi^2)^4}m_\chi^2 v^2\times\mathcal{B}+\mathcal{O}\left(v^4\right)\,, \end{aligned} \tag{C.11}$$

The functions $\mathcal{A}$ and $\mathcal{B}$ are given by the following expressions in the case of Majorana neutrinos:

$$\mathcal{A}_\nu = |F_L|^2|G_L|^2+|F_R|^2|G_R|^2+|F_LG_R-F_RG_L|^2\,, \tag{C.12}$$

$$\begin{aligned}\mathcal{B}_\nu &= \left(|F_L|^2|G_L|^2+|F_R|^2|G_R|^2\right)\left(m_\chi^4+4m_\chi^2m_\phi^2-3m_\phi^4\right)+\\ &+ \left(|F_L|^2|G_R|^2+|F_R|^2|G_L|^2\right)\left(m_\phi^4-3m_\chi^2m_\phi^2-m_\chi^4\right)-\\ &- 2\left(F_LF_R^*G_L^*G_R+\,c.c.\right)\left(3m_\phi^2+2m_\chi^2\right)m_\chi^2\,. \end{aligned} \tag{C.13}$$

In the case of Majorana DM, the corresponding expressions for $\mathcal{A}$ and $\mathcal{B}$ are given by

$$\mathcal{A}_\chi = 2\,|F_L|^2|G_L|^2+2\,|F_R|^2|G_R|^2\,, \tag{C.14}$$

$$\begin{aligned}\mathcal{B}_\chi &= 2\left(|F_L|^2|G_L|^2+|F_R|^2|G_R|^2\right)\left(3m_\phi^4-4m_\chi^2m_\phi^2-m_\chi^4\right)+\\ &+ 4\left(|F_L|^2|G_R|^2+|F_R|^2|G_L|^2\right)\left(m_\phi^4+m_\chi^4\right)\,. \end{aligned} \tag{C.15}$$

Notice that, for Majorana DM, terms proportional to F_LG_R or F_RG_L are not present in the s-wave. Indeed, due to the Pauli principle, two Majorana particles cannot have parallel spins if their relative angular momentum l is zero. The only nonzero contribution to the s-wave configuration will be present if $F_L \neq 0$ and $G_L \neq 0$. This situation can arise in supersymmetric models only in the presence of a mixing between the left and right sfermions. However, a mixing term between $\tilde{f}_L$ and $\tilde{f}_R$ is proportional to the fermion mass. For this reason, the annihilation cross section of a neutralino pair into fermions, through a t-channel sfermion exchange, is always proportional to the mass of the fermions produced. This conclusion does, in general, not hold when we consider a Majorana DM beyond a supersymmetric framework.

C.3 Vector Dark Matter

In this Section we report the annihilation cross sections for the case of vector DM, since in specific models, for example in Extra Dimensions, new vector particles can be present,

even without an extension of the Standard Model gauge group. The neutrino production can then occur through a scalar exchange in an s-channel diagram and through a fermion exchange in a t-channel diagram. In case the neutrinos are Majorana particles, also a u-channel diagram is present.

Scalar mediator, s-channel

Indicating the coupling of the scalar mediator to the DM particles with D and the one to the neutrinos with $N_L P_L + N_R P_R$, the total annihilation cross section can be written as

$$\sigma_{\rm ann} v\,(\chi_v;\phi_s;s) = \frac{2^{-n}}{24\pi} D^2 \frac{N_L^2+N_R^2}{(4m_\chi^2-m_\phi^2)^2}\,4^n\left(1-\frac{(2m_\chi^2+m_\phi^2)}{3\,(4m_\chi^2-m_\phi^2)}v^2\right)+\mathcal{O}(v^4)\,, \quad \text{(C.16)}$$

with D, N_L and N_R being real numbers and $n = 0, 1$ for Dirac and Majorana neutrinos, respectively. As in the previous cases, we have considered for simplicity the same couplings for Dirac and Majorana neutrinos.

Fermionic mediator, t&u-channels

Indicating the coupling of the DM particle to the fermionic mediator and to the neutrino at one vertex with $\gamma^\mu(F_L P_L + F_R P_R)$ and at the other one with $\gamma^\nu(G_L P_L + G_R P_R)$, the total annihilation cross section is given by

$$\begin{aligned}\sigma_{\rm ann} v\,(\chi_v;\phi_f;t) &= \frac{1}{72\pi}\frac{4m_\chi^2(F_L^2G_L^2+F_R^2G_R^2)+5m_\phi^2(F_R^2G_L^2+F_L^2G_R^2)}{(m_\chi^2+m_\phi^2)^2}+\\ &+ \frac{1}{432\pi}\frac{1}{(m_\chi^2+m_\phi^2)^4}\,v^2\times\mathcal{C}+\mathcal{O}\left(v^4\right)\,, \quad \text{(C.17)}\end{aligned}$$

with

$$\begin{aligned}\mathcal{C} &= 12\,m_\phi^6\,(F_L^2G_R^2+F_R^2G_L^2)+13\,m_\chi^6\,(F_L^2G_L^2+F_R^2G_R^2)+\\ &+ m_\chi^2\,m_\phi^4\,(13F_L^2G_L^2+13F_R^2G_R^2+2F_L^2G_R^2+2F_R^2G_L^2)+\\ &+ 2\,m_\chi^4\,m_\phi^2\,(F_L^2G_L^2+F_R^2G_R^2)+20\,m_\chi^4\,m_\phi^2\,(F_L^2G_R^2+F_R^2G_L^2)\,. \quad \text{(C.18)}\end{aligned}$$

Note that, in general, $G_L = F_L$ and $G_R = F_R$. For Majorana neutrinos, a t-channel and a u-channel diagram are present. The annihilation cross section is then modified to

$$\begin{aligned}\sigma_{\rm ann} v\,(\chi_v;\phi_f;t\&u) &= \frac{1}{36\pi}\frac{(G_L^2+G_R^2)(2m_\chi^2F_L^2+3m_\phi^2F_R^2)+4m_\chi^2\,G_LG_RF_LF_R}{(m_\chi^2+m_\phi^2)^2}+\\ &+ \frac{1}{432\pi}\frac{1}{(m_\chi^2+m_\phi^2)^4}\,v^2\times\mathcal{D}+\mathcal{O}\left(v^4\right)\,, \quad \text{(C.19)}\end{aligned}$$

with

$$\begin{aligned}\mathcal{D} &= 12\, m_\phi^6\,(F_L^2 G_R^2 + F_R^2 G_L^2) + 13\, m_\chi^6\,(F_L^2 G_L^2 + F_R^2 G_R^2) + \\ &+ 13\, m_\chi^2\, m_\phi^4\,(F_L^2 G_L^2 + F_R^2 G_R^2) - 4\, m_\chi^2\, m_\phi^4\,(F_L^2 G_R^2 + F_R^2 G_L^2) + \\ &+ 2\, m_\chi^4\, m_\phi^2\,(F_L^2 G_L^2 + F_R^2 G_R^2) + 16\, m_\chi^4\, m_\phi^2\,(F_L^2 G_R^2 + F_R^2 G_L^2) - \\ &- 2\, F_L F_R G_L G_R\,(9 m_\chi^4 + 10 m_\chi^2 m_\phi^2 - 7 m_\phi^4)\,. \end{aligned} \tag{C.20}$$

Bibliography

[1] E. Hubble, *A relation between distance and radial velocity among extra-galactic nebulae*, *Proceedings of the National Academy of Sciences of the United States of America* **15** (1929), no. 3 168–173, [http://www.pnas.org/content/15/3/168.full.pdf+html].

[2] S. Perlmutter and B. P. Schmidt, *Measuring Cosmology with Supernovae*, *Lect. Notes Phys.* **598** (2003) 195–217, [astro-ph/0303428].

[3] R. Bernabei *et. al.*, *First results from DAMA/LIBRA and the combined results with DAMA/NaI*, *Eur. Phys. J.* **C56** (2008) 333–355, [arXiv:0804.2741].

[4] O. Adriani *et. al.*, *An anomalous positron abundance in cosmic rays with energies 1.5.100 GeV*, *Nature* **458** (2009) 607–609, [arXiv:0810.4995].

[5] S. Desai *et. al.*, *Search for dark matter WIMPs using upward through-going muons in Super-Kamiokande*, *Phys. Rev.* **D70** (2004) 083523, [hep-ex/0404025].

[6] R. Abbasi *et. al.*, *Limits on a muon flux from neutralino annihilations in the Sun with the IceCube 22-string detector*, *Phys. Rev. Lett.* **102** (2009) 201302, [arXiv:0902.2460].

[7] J. A. Aguilar *et. al.*, *First results of the instrumentation line for the deep-sea ANTARES neutrino telescope*, *Astropart. Phys.* **26** (2006) 314–324, [astro-ph/0606229].

[8] Informations on the status of the project can be found at the web site http://www.km3net.org .

[9] T. K. Gaisser, G. Steigman, and S. Tilav, *Limits on Cold Dark Matter Candidates from Deep Underground Detectors*, *Phys. Rev.* **D34** (1986) 2206.

[10] M. Drees, G. Jungman, M. Kamionkowski, and M. M. Nojiri, *Neutralino annihilation into gluons*, *Phys. Rev.* **D49** (1994) 636–647, [hep-ph/9306325].

[11] J. Silk, K. A. Olive, and M. Srednicki, *The photino, the sun, and high-energy neutrinos*, *Phys. Rev. Lett.* **55** (1985) 257–259; K. Freese, *Can Scalar Neutrinos Or Massive Dirac Neutrinos Be the Missing Mass?*, *Phys. Lett.* **B167** (1986) 295; G. F. Giudice and E. Roulet, *Energetic neutrinos from supersymmetric Dark Matter*, *Nucl. Phys.* **B316** (1989) 429; G. B. Gelmini, P. Gondolo, and E. Roulet, *Neutralino dark matter searches*, *Nucl. Phys.* **B351** (1991) 623–644; M. Kamionkowski,

Energetic neutrinos from heavy neutralino annihilation in the sun, *Phys. Rev.* **D44** (1991) 3021–3042; F. Halzen, T. Stelzer, and M. Kamionkowski, *Signatures of dark matter in underground detectors*, *Phys. Rev.* **D45** (1992) 4439–4442; M. Mori *et. al.*, *Search for neutralino dark matter in Kamiokande*, *Phys. Rev.* **D48** (1993) 5505–5518; R. Gandhi, J. L. Lopez, D. V. Nanopoulos, K.-j. Yuan, and A. Zichichi, *Scrutinizing supergravity models through neutrino telescopes*, *Phys. Rev.* **D49** (1994) 3691–3703, [astro-ph/9309048]; L. Bergstrom, J. Edsjo, and P. Gondolo, *Indirect neutralino detection rates in neutrino telescopes*, *Phys. Rev.* **D55** (1997) 1765–1770, [hep-ph/9607237]; L. Bergstrom, J. Edsjo, and M. Kamionkowski, *Astrophysical-neutrino detection with angular and energy resolution*, *Astropart. Phys.* **7** (1997) 147–160, [astro-ph/9702037].

[12] A. Bottino, V. de Alfaro, N. Fornengo, G. Mignola, and M. Pignone, *Indirect search for neutralinos at neutrino telescopes*, *Phys. Lett.* **B265** (1991) 57–63; A. Bottino, N. Fornengo, G. Mignola, and L. Moscoso, *Signals of neutralino dark matter from earth and sun*, *Astropart. Phys.* **3** (1995) 65–76, [hep-ph/9408391]; V. Berezinsky *et. al.*, *Searching for relic neutralinos using neutrino telescopes*, *Astropart. Phys.* **5** (1996) 333–352, [hep-ph/9603342]; A. Bottino, F. Donato, N. Fornengo, and S. Scopel, *Combining the data of annual modulation effect in WIMP direct detection with measurements of WIMP indirect searches*, *Astropart. Phys.* **10** (1999) 203–210, [hep-ph/9809239]; A. Bottino, F. Donato, N. Fornengo, and S. Scopel, *Further investigation of a relic neutralino as a possible origin of an annual-modulation effect in WIMP direct search*, *Phys. Rev.* **D62** (2000) 056006, [hep-ph/0001309].

[13] Y. Ashie *et. al.*, *A measurement of atmospheric neutrino oscillation parameters by Super-Kamiokande I*, *Phys. Rev.* **D71** (2005) 112005, [hep-ex/0501064].

[14] J. Kopp, V. Niro, T. Schwetz, and J. Zupan, *DAMA/LIBRA and leptonically interacting Dark Matter*, *Phys. Rev.* **D80** (2009) 083502, [arXiv:0907.3159].

[15] V. Niro, A. Bottino, N. Fornengo, and S. Scopel, *Investigating light neutralinos at neutrino telescopes*, *Phys. Rev.* **D80** (2009) 095019, [arXiv:0909.2348].

[16] S. Choubey, V. Niro, and W. Rodejohann, *On Probing θ_{23} in Neutrino Telescopes*, *Phys. Rev.* **D77** (2008) 113006, [arXiv:0803.0423].

[17] E. K. Akhmedov and V. Niro, *An accurate analytic description of neutrino oscillations in matter*, *JHEP* **12** (2008) 106, [arXiv:0810.2679].

[18] J. Kopp, M. Lindner, V. Niro, and T. E. J. Underwood, *Consistency of Perturbativity and Gauge Coupling Unification*, *Phys. Rev.* **D81** (2010) 025008, [arXiv:0909.2653].

[19] G. D'Amico, M. Kamionkowski, and K. Sigurdson, *Dark Matter Astrophysics*, arXiv:0907.1912.

[20] D. Hooper, *TASI 2008 Lectures on Dark Matter*, arXiv:0901.4090.

[21] G. Bertone, D. Hooper, and J. Silk, *Particle dark matter: Evidence, candidates and constraints*, *Phys. Rept.* **405** (2005) 279–390, [hep-ph/0404175].

[22] L. Bergstrom, *Non-baryonic dark matter: Observational evidence and detection methods*, *Rept. Prog. Phys.* **63** (2000) 793, [hep-ph/0002126].

[23] F. Zwicky, *Die Rotverschiebung von extragalaktischen Nebeln*, *Helvetica Physica Acta* **6** (1933) 110–127.

[24] S. Smith, *The Mass of the Virgo Cluster*, *Astrophys. J.* **83** (Jan., 1936) 23–30.

[25] V. C. Rubin and W. K. Ford, Jr., *Rotation of the Andromeda Nebula from a Spectroscopic Survey of Emission Regions*, *Astrophys. J.* **159** (Feb., 1970) 379–404.

[26] M. S. Roberts and A. H. Rots, *Comparison of Rotation Curves of Different Galaxy Types*, *Astronomy and Astrophysics* **26** (Aug., 1973) 483–485.

[27] V. C. Rubin, W. K. J. Ford, and N. . Thonnard, *Rotational properties of 21 SC galaxies with a large range of luminosities and radii, from NGC 4605 R = 4kpc to UGC 2885 R = 122 kpc*, *Astrophys. J.* **238** (June, 1980) 471–487.

[28] T. S. van Albada, J. N. Bahcall, K. Begeman, and R. Sancisi, *The distribution of Dark Matter in the spiral galaxy NGC- 3198*, *Astrophys. J.* **295** (1985) 305–313; K. G. Begeman, *H I rotation curves of spiral galaxies. I - NGC 3198*, *Astron. Astrophys.* **223** (1989) 47–60; K. G. Begeman, A. H. Broeils, and R. H. Sanders, *Extended rotation curves of spiral galaxies: Dark haloes and modified dynamics*, *Mon. Not. Roy. Astron. Soc.* **249** (1991) 523.

[29] J. A. Tyson, G. P. Kochanski, and I. P. Dell'Antonio, *Detailed Mass Map of CL0024+1654 from Strong Lensing*, *Astrophys. J.* **498** (1998) L107, [astro-ph/9801193].

[30] D. M. Wittman, J. A. Tyson, D. Kirkman, I. Dell'Antonio, and G. Bernstein, *Detection of weak gravitational lensing distortions of distant galaxies by cosmic dark matter at large scales*, *Nature* **405** (2000) 143–149, [astro-ph/0003014].

[31] D. Clowe *et. al.*, *A direct empirical proof of the existence of dark matter*, *Astrophys. J.* **648** (2006) L109–L113, [astro-ph/0608407].

[32] M. Bradac *et. al.*, *Revealing the properties of dark matter in the merging cluster MACSJ0025.4-1222*, arXiv:0806.2320.

[33] G. Gamow, *Expanding universe and the origin of elements*, *Phys. Rev.* **70** (1946) 572–573.

[34] A. A. Penzias and R. W. Wilson, *A Measurement of Excess Antenna Temperature at 4080 Mc/s.*, *Astrophys. J.* **142** (July, 1965) 419–421.

[35] W. Hu, N. Sugiyama, and J. Silk, *The Physics of microwave background anisotropies*, *Nature* **386** (1997) 37–43, [astro-ph/9604166].

[36] D. J. Fixsen *et. al.*, *The Cosmic Microwave Background Spectrum from the Full COBE/FIRAS Data Set*, *Astrophys. J.* **473** (1996) 576, [astro-ph/9605054].

[37] J. C. Mather *et. al.*, *Measurement of the cosmic microwave background spectrum by the COBE FIRAS instrument*, *Astrophys. J.* **420** (Jan., 1994) 439–444.

[38] G. Hinshaw *et. al.*, *Five-Year Wilkinson Microwave Anisotropy Probe (WMAP) Observations: Data Processing, Sky Maps, and Basic Results*, *Astrophys. J. Suppl.* **180** (2009) 225–245, [arXiv:0803.0732].

[39] J. Dunkley *et. al.*, *Five-Year Wilkinson Microwave Anisotropy Probe (WMAP) Observations: Likelihoods and Parameters from the WMAP data*, *Astrophys. J. Suppl.* **180** (2009) 306–329, [arXiv:0803.0586].

[40] W. M. Yao *et. al.*, *Review of particle physics*, *J. Phys.* **G33** (2006) 1–1232.

[41] A list of publications of the SDSS collaboration can be found at the web site http://www.sdss.org/publications/index.html.

[42] A list of publications of the 2dFGRS collaboration can be found at the web site http://www2.aao.gov.au/2dFGRS/.

[43] D. H. Weinberg, R. Dave, N. Katz, and J. A. Kollmeier, *The Lyman-α Forest as a Cosmological Tool*, *AIP Conf. Proc.* **666** (2003) 157–169, [astro-ph/0301186].

[44] P. Gondolo and J. Silk, *Dark matter annihilation at the galactic center*, *Phys. Rev. Lett.* **83** (1999) 1719–1722, [astro-ph/9906391].

[45] D. Merritt, M. Milosavljevic, L. Verde, and R. Jimenez, *Dark matter spikes and annihilation radiation from the galactic center*, *Phys. Rev. Lett.* **88** (2002) 191301, [astro-ph/0201376]; D. Merritt, *Evolution of the Dark Matter Distribution at the Galactic Center*, *Phys. Rev. Lett.* **92** (2004) 201304, [astro-ph/0311594]; G. Bertone and D. Merritt, *Time-dependent models for dark matter at the Galactic center*, *Phys. Rev.* **D72** (2005) 103502, [astro-ph/0501555].

[46] P. Ullio, H. Zhao, and M. Kamionkowski, *A Dark-Matter Spike at the Galactic Center?*, *Phys. Rev.* **D64** (2001) 043504, [astro-ph/0101481].

[47] J. N. Bahcall and R. M. Soneira, *The Universe at faint magnetidues. 2. Models for the predicted star counts*, *Astrophys. J. Suppl.* **44** (1980) 73–110; G. Gentile, P. Salucci, U. Klein, D. Vergani, and P. Kalberla, *The cored distribution*

of dark matter in spiral galaxies, *Mon. Not. Roy. Astron. Soc.* **351** (2004) 903, [astro-ph/0403154]; P. Salucci *et. al.*, *The universal rotation curve of spiral galaxies. II: The dark matter distribution out to the virial radius*, *Mon. Not. Roy. Astron. Soc.* **378** (2007) 41–47, [astro-ph/0703115].

[48] J. F. Navarro, C. S. Frenk, and S. D. M. White, *The Structure of Cold Dark Matter Halos*, *Astrophys. J.* **462** (1996) 563–575, [astro-ph/9508025].

[49] B. Moore, T. R. Quinn, F. Governato, J. Stadel, and G. Lake, *Cold collapse and the core catastrophe*, *Mon. Not. Roy. Astron. Soc.* **310** (1999) 1147–1152, [astro-ph/9903164].

[50] A. W. Graham, D. Merritt, B. Moore, J. Diemand, and B. Terzic, *Empirical models for Dark Matter Halos. I. Nonparametric Construction of Density Profiles and Comparison with Parametric Models*, *Astron. J.* **132** (2006) 2685, [astro-ph/0509417]; J. F. Navarro *et. al.*, *The Diversity and Similarity of Cold Dark Matter Halos*, arXiv:0810.1522.

[51] P. Belli, R. Cerulli, N. Fornengo, and S. Scopel, *Effect of the galactic halo modeling on the DAMA/NaI annual modulation result: an extended analysis of the data for WIMPs with a purely spin-independent coupling*, *Phys. Rev.* **D66** (2002) 043503, [hep-ph/0203242].

[52] C. S. Kochanek, *The Mass of the Milky Way galaxy*, *Astrophys. J.* **457** (1996) 228, [astro-ph/9505068].

[53] R. Bernabei *et. al.*, *Dark matter search*, *Riv. Nuovo Cim.* **26N1** (2003) 1–73, [astro-ph/0307403]; G. B. Gelmini, *Search for Dark Matter*, *Int. J. Mod. Phys.* **A23** (2008) 4273–4288, [arXiv:0810.3733].

[54] P. Ullio, M. Kamionkowski, and P. Vogel, *Spin dependent WIMPs in DAMA?*, *JHEP* **07** (2001) 044, [hep-ph/0010036].

[55] Z. Ahmed *et. al.*, *Search for Weakly Interacting Massive Particles with the First Five-Tower Data from the Cryogenic Dark Matter Search at the Soudan Underground Laboratory*, *Phys. Rev. Lett.* **102** (2009) 011301, [arXiv:0802.3530].

[56] J. Angle *et. al.*, *First Results from the XENON10 Dark Matter Experiment at the Gran Sasso National Laboratory*, *Phys. Rev. Lett.* **100** (2008) 021303, [arXiv:0706.0039].

[57] A. Bottino, F. Donato, N. Fornengo, and S. Scopel, *Zooming in on light relic neutralinos by direct detection and measurements of galactic antimatter*, *Phys. Rev.* **D77** (2008) 015002, [arXiv:0710.0553].

[58] A. Bottino, F. Donato, N. Fornengo, and S. Scopel, *Interpreting the recent results on direct search for dark matter particles in terms of relic neutralino*, *Phys. Rev.* **D78** (2008) 083520, [arXiv:0806.4099].

[59] F. Petriello and K. M. Zurek, *DAMA and WIMP dark matter*, *JHEP* **09** (2008) 047, [arXiv:0806.3989].

[60] J. L. Feng, J. Kumar, and L. E. Strigari, *Explaining the DAMA Signal with WIMPless Dark Matter*, *Phys. Lett.* **B670** (2008) 37–40, [arXiv:0806.3746].

[61] S. Chang, A. Pierce, and N. Weiner, *Using the Energy Spectrum at DAMA/LIBRA to Probe Light Dark Matter*, arXiv:0808.0196.

[62] M. Fairbairn and T. Schwetz, *Spin-independent elastic WIMP scattering and the DAMA annual modulation signal*, *JCAP* **0901** (2009) 037, [arXiv:0808.0704].

[63] C. Savage, G. Gelmini, P. Gondolo, and K. Freese, *Compatibility of DAMA/LIBRA dark matter detection with other searches*, *JCAP* **0904** (2009) 010, [arXiv:0808.3607].

[64] A. Bottino, F. Donato, N. Fornengo, and S. Scopel, *Relic neutralinos and the two dark matter candidate events of the CDMS II experiment*, arXiv:0912.4025.

[65] E. Behnke *et. al.*, *Improved Spin-Dependent WIMP Limits from a Bubble Chamber*, *Science* **319** (2008) 933–936, [arXiv:0804.2886].

[66] H. S. Lee. *et. al.*, *Limits on WIMP-nucleon cross section with CsI(Tl) crystal detectors*, *Phys. Rev. Lett.* **99** (2007) 091301, [arXiv:0704.0423].

[67] S. Archambault *et. al.*, *Dark Matter Spin-Dependent Limits for WIMP Interactions on 19-F by PICASSO*, arXiv:0907.0307.

[68] R. Bernabei *et. al.*, *Possible implications of the channeling effect in NaI(Tl) crystals*, *Eur. Phys. J.* **C53** (2008) 205–213, [arXiv:0710.0288].

[69] E. M. Drobyshevski, *Channeling Effect and Improvement of the Efficiency of Charged Particle Registration with Crystal Scintillators*, arXiv:0706.3095.

[70] J. Graichen, K. Maier, J. Schuth, A. Siepe, and W. von Witsch, *Efficiency and directional effects in the detection of low-energy recoil nuclei in a NaI(Tl) single crystal*, *Nucl. Instrum. Meth.* **A485** (2002) 774–779.

[71] J. Kopp, T. Schwetz, and J. Zupan, *Global interpretation of direct Dark Matter searches after CDMS-II results*, arXiv:0912.4264.

[72] R. Foot, *Mirror dark matter and the new DAMA/LIBRA results: A simple explanation for a beautiful experiment*, *Phys. Rev.* **D78** (2008) 043529, [arXiv:0804.4518].

[73] E. Masso, S. Mohanty, and S. Rao, *Dipolar Dark Matter*, arXiv:0906.1979.

[74] Z. Ahmed *et. al.*, *Results from the Final Exposure of the CDMS II Experiment*, arXiv:0912.3592.

[75] M. Kuhlen *et. al.*, *Dark Matter Direct Detection with Non-Maxwellian Velocity Structure*, arXiv:0912.2358.

[76] J. Carr, G. Lamanna, and J. Lavalle, *Indirect detection of dark matter*, *Rept. Prog. Phys.* **69** (2006) 2475–2512.

[77] http://www.mpi-hd.mpg.de/hfm/HESS/.

[78] http://fermi.gsfc.nasa.gov/.

[79] J. Chang *et. al.*, *An excess of cosmic ray electrons at energies of 300-800 GeV*, *Nature* **456** (2008) 362–365.

[80] S. Torii *et. al.*, *High-energy electron observations by PPB-BETS flight in Antarctica*, arXiv:0809.0760.

[81] M. Cirelli, M. Kadastik, M. Raidal, and A. Strumia, *Model-independent implications of the e^+, e^-, anti-proton cosmic ray spectra on properties of Dark Matter*, *Nucl. Phys.* **B813** (2009) 1–21, [arXiv:0809.2409].

[82] S. Profumo, *Dissecting Pamela (and ATIC) with Occam's Razor: existing, well-known Pulsars naturally account for the 'anomalous' Cosmic-Ray Electron and Positron Data*, arXiv:0812.4457; D. Hooper, P. Blasi, and P. D. Serpico, *Pulsars as the Sources of High Energy Cosmic Ray Positrons*, *JCAP* **0901** (2009) 025, [arXiv:0810.1527].

[83] T. Delahaye *et. al.*, *Galactic secondary positron flux at the Earth*, *Astron. Astrophys.* **501** (2009) 821–833, [arXiv:0809.5268].

[84] H. E. S. S. C. F. Aharonian, *Probing the ATIC peak in the cosmic-ray electron spectrum with H.E.S.S*, arXiv:0905.0105.

[85] A. A. Abdo *et. al.*, *Measurement of the Cosmic Ray $e^+ + e^-$ spectrum from 20 GeV to 1 TeV with the Fermi Large Area Telescope*, *Phys. Rev. Lett.* **102** (2009) 181101, [arXiv:0905.0025].

[86] G. Bertone, M. Cirelli, A. Strumia, and M. Taoso, *Gamma-ray and radio tests of the $e^\pm$ excess from DM annihilations*, *JCAP* **0903** (2009) 009, [arXiv:0811.3744]; M. Cirelli, P. Panci, and P. D. Serpico, *Diffuse gamma ray constraints on annihilating or decaying Dark Matter after Fermi*, arXiv:0912.0663.

[87] C. J. Hailey *et. al.*, *Accelerator testing of the General Antiparticle Spectrometer, a novel approach to indirect dark matter detection*, *JCAP* **0601** (2006) 007, [astro-ph/0509587].

[88] V. Choutko and F. Giovacchini, *Cosmic Rays Antideuteron Sensitivity for AMS-02 Experiment*, in *International Cosmic Ray Conference*, vol. 4 of *International Cosmic Ray Conference*, pp. 765–768, 2008.

[89] C. Amsler *et. al.*, *Review of particle physics*, *Phys. Lett.* **B667** (2008) 1.

[90] E. Barberio *et. al.*, *Averages of b−hadron properties at the end of 2005*, hep-ex/0603003.

[91] http://www.g-2.bnl.gov/.

[92] V. M. Abazov *et. al.*, *Search for $B_s \to \mu^+\mu^-$ at D0*, *Phys. Rev.* **D76** (2007) 092001, [arXiv:0707.3997].

[93] B. K. Gjelsten, D. J. Miller, 2, and P. Osland, *Measurement of SUSY masses via cascade decays for SPS 1a*, *JHEP* **12** (2004) 003, [hep-ph/0410303].

[94] J. M. Smillie and B. R. Webber, *Distinguishing Spins in Supersymmetric and Universal Extra Dimension Models at the Large Hadron Collider*, *JHEP* **10** (2005) 069, [hep-ph/0507170].

[95] L. Bergstrom, *Dark Matter Candidates*, *New J. Phys.* **11** (2009) 105006, [arXiv:0903.4849].

[96] F. D. Steffen, *Dark Matter Candidates - Axions, Neutralinos, Gravitinos, and Axinos*, *Eur. Phys. J.* **C59** (2009) 557–588, [arXiv:0811.3347].

[97] L. Roszkowski, *Particle dark matter: A theorist's perspective*, *Pramana* **62** (2004) 389–401, [hep-ph/0404052].

[98] E. W. Kolb and M. S. Turner, *The early universe*. Frontiers in Physics, Addison-Wesley, 1994.

[99] S. P. Martin, *A Supersymmetry Primer*, hep-ph/9709356.

[100] H. E. Haber and G. L. Kane, *The Search for Supersymmetry: Probing Physics Beyond the Standard Model*, *Phys. Rept.* **117** (1985) 75–263; J. F. Gunion and H. E. Haber, *Higgs Bosons in Supersymmetric Models. 1*, *Nucl. Phys.* **B272** (1986) 1.

[101] G. Jungman, M. Kamionkowski, and K. Griest, *Supersymmetric dark matter*, *Phys. Rept.* **267** (1996) 195–373, [hep-ph/9506380].

[102] H. Baer, E.-K. Park, and X. Tata, *Collider, direct and indirect detection of supersymmetric dark matter*, *New J. Phys.* **11** (2009) 105024, [arXiv:0903.0555].

[103] A. Bottino, N. Fornengo, and S. Scopel, *Light relic neutralinos*, *Phys. Rev.* **D67** (2003) 063519, [hep-ph/0212379]; A. Bottino, F. Donato, N. Fornengo, and S. Scopel, *Lower bound on the neutralino mass from new data on CMB and implications for relic neutralinos*, *Phys. Rev.* **D68** (2003) 043506, [hep-ph/0304080].

[104] T. Falk, K. A. Olive, and M. Srednicki, *Heavy Sneutrinos as Dark Matter*, *Phys. Lett.* **B339** (1994) 248–251, [hep-ph/9409270].

[105] L. E. Ibanez, *The Scalar Neutrinos as the Lightest Supersymmetric Particles and Cosmology*, *Phys. Lett.* **B137** (1984) 160; J. S. Hagelin, G. L. Kane, and S. Raby, *Perhaps Scalar Neutrinos Are the Lightest Supersymmetric Partners*, *Nucl. Phys.* **B241** (1984) 638.

[106] C. Arina and N. Fornengo, *Sneutrino cold dark matter, a new analysis: Relic abundance and detection rates*, *JHEP* **11** (2007) 029, [arXiv:0709.4477].

[107] D. G. Cerdeno, C. Munoz, and O. Seto, *Right-handed sneutrino as thermal dark matter*, *Phys. Rev.* **D79** (2009) 023510, [arXiv:0807.3029]; D. G. Cerdeno and O. Seto, *Right-handed sneutrino dark matter in the NMSSM*, *JCAP* **0908** (2009) 032, [arXiv:0903.4677].

[108] F. Takayama and M. Yamaguchi, *Gravitino dark matter without R-parity*, *Phys. Lett.* **B485** (2000) 388–392, [hep-ph/0005214].

[109] T. Appelquist, H.-C. Cheng, and B. A. Dobrescu, *Bounds on universal extra dimensions*, *Phys. Rev.* **D64** (2001) 035002, [hep-ph/0012100]; D. Hooper and S. Profumo, *Dark matter and collider phenomenology of universal extra dimensions*, *Phys. Rept.* **453** (2007) 29–115, [hep-ph/0701197].

[110] G. Servant and T. M. P. Tait, *Is the lightest Kaluza-Klein particle a viable dark matter candidate?*, *Nucl. Phys.* **B650** (2003) 391–419, [hep-ph/0206071]; H.-C. Cheng, J. L. Feng, and K. T. Matchev, *Kaluza-Klein dark matter*, *Phys. Rev. Lett.* **89** (2002) 211301, [hep-ph/0207125].

[111] M. Perelstein, *Little Higgs models and their phenomenology*, *Prog. Part. Nucl. Phys.* **58** (2007) 247–291, [hep-ph/0512128]; M. Schmaltz and D. Tucker-Smith, *Little Higgs Review*, *Ann. Rev. Nucl. Part. Sci.* **55** (2005) 229–270, [hep-ph/0502182].

[112] A. Birkedal, A. Noble, M. Perelstein, and A. Spray, *Little Higgs dark matter*, *Phys. Rev.* **D74** (2006) 035002, [hep-ph/0603077].

[113] E. Komatsu *et. al.*, *Five-Year Wilkinson Microwave Anisotropy Probe (WMAP) Observations: Cosmological Interpretation*, *Astrophys. J. Suppl.* **180** (2009) 330–376, [arXiv:0803.0547].

[114] A. Boyarsky, O. Ruchayskiy, and M. Shaposhnikov, *The role of sterile neutrinos in cosmology and astrophysics*, *Ann. Rev. Nucl. Part. Sci.* **59** (2009) 191–214, [arXiv:0901.0011].

[115] C. Giunti and C. W. Kim, *Fundamentals of Neutrino Physics and Astrophysics*. Oxford, UK: Univ. Pr. (2007) 710 p.

[116] R. D. Peccei and H. R. Quinn, *CP Conservation in the Presence of Pseudoparticles*, *Phys. Rev. Lett.* **38** (Jun, 1977) 1440–1443; R. D. Peccei and H. R. Quinn, *Constraints imposed by CP conservation in the presence of pseudoparticles*, *Phys. Rev. D* **16** (Sep, 1977) 1791–1797.

[117] E. Zavattini *et. al.*, *Experimental observation of optical rotation generated in vacuum by a magnetic field*, *Phys. Rev. Lett.* **96** (2006) 110406, [hep-ex/0507107].

[118] E. Zavattini *et. al.*, *New PVLAS results and limits on magnetically induced optical rotation and ellipticity in vacuum*, *Phys. Rev.* **D77** (2008) 032006, [arXiv:0706.3419].

[119] D. Hooper and L.-T. Wang, *Possible evidence for axino dark matter in the galactic bulge*, *Phys. Rev. D* **70** (Sep, 2004) 063506.

[120] E. W. Kolb, D. J. H. Chung, and A. Riotto, *WIMPzillas!*, hep-ph/9810361.

[121] P. Blasi, R. Dick, and E. W. Kolb, *Ultrahigh-energy cosmic rays from annihilation of superheavy dark matter*, *Astropart. Phys.* **18** (2002) 57–66, [astro-ph/0105232].

[122] D. Tucker-Smith and N. Weiner, *Inelastic dark matter*, *Phys. Rev.* **D64** (2001) 043502, [hep-ph/0101138].

[123] J. March-Russell, C. McCabe, and M. McCullough, *Inelastic Dark Matter, Non-Standard Halos and the DAMA/LIBRA Results*, *JHEP* **05** (2009) 071, [arXiv:0812.1931]; S. Chang, G. D. Kribs, D. Tucker-Smith, and N. Weiner, *Inelastic Dark Matter in Light of DAMA/LIBRA*, *Phys. Rev.* **D79** (2009) 043513, [arXiv:0807.2250]; C. Arina, F.-S. Ling, and M. H. G. Tytgat, *The Inert Doublet Model and Inelastic Dark Matter*, arXiv:0907.0430.

[124] D. Tucker-Smith and N. Weiner, *The status of inelastic dark matter*, *Phys. Rev.* **D72** (2005) 063509, [hep-ph/0402065].

[125] D. B. Cline, W. Ooi, and H. Wang, *A Constrain on Inelastic Dark Matter Signal using ZEPLIN- II Results*, arXiv:0906.4119.

[126] G. Angloher *et. al.*, *Commissioning Run of the CRESST-II Dark Matter Search*, arXiv:0809.1829.

[127] Y. Cui, D. E. Morrissey, D. Poland, and L. Randall, *Candidates for Inelastic Dark Matter*, *JHEP* **05** (2009) 076, [arXiv:0901.0557].

[128] P. J. Fox and E. Poppitz, *Leptophilic Dark Matter*, *Phys. Rev.* **D79** (2009) 083528, [arXiv:0811.0399].

[129] N. Arkani-Hamed, D. P. Finkbeiner, T. R. Slatyer, and N. Weiner, *A Theory of Dark Matter*, *Phys. Rev.* **D79** (2009) 015014, [arXiv:0810.0713].

[130] A. H. G. Peter, *Dark matter in the solar system II: WIMP annihilation rates in the Sun*, arXiv:0902.1347.

[131] A. Gould, *Resonant Enhancements in WIMP Capture by the Earth*, *Astrophys. J.* **321** (1987) 571.

[132] A. Gould, *Direct and indirect capture of WIMPs by the Earth*, *Astrophys. J.* **328** (1988) 919–939; A. Gould, *Gravitational diffusion of solar system WIMPs*, *Astrophys. J.* **368** (Feb., 1991) 610–615.

[133] J. N. Bahcall, A. M. Serenelli, and S. Basu, *New solar opacities, abundances, helioseismology, and neutrino fluxes*, *Astrophys. J.* **621** (2005) L85–L88, [astro-ph/0412440].

[134] D. O'Sullivan, A. Thompson, J. Donnelly, L. O. Drury, and K. P. Wenzel, *The relative abundance of actinides in the cosmic radiation*, *Advances in Space Research* **27** (2001), no. 4 785 – 789.

[135] A. Gould, *Weakly interacting massive particle distribution in and evaporation from the sun*, *Astrophys. J.* **321** (oct, 1987) 560–570.

[136] G. Wikstrom and J. Edsjo, *Limits on the WIMP-nucleon scattering cross-section from neutrino telescopes*, *JCAP* **0904** (2009) 009, [arXiv:0903.2986].

[137] A. Menon, R. Morris, A. Pierce, and N. Weiner, *Capture and Indirect Detection of Inelastic Dark Matter*, arXiv:0905.1847; S. Nussinov, L.-T. Wang, and I. Yavin, *Capture of Inelastic Dark Matter in the Sun*, *JCAP* **0908** (2009) 037, [arXiv:0905.1333].

[138] K. Griest and D. Seckel, *Cosmic Asymmetry, Neutrinos and the Sun*, *Nucl. Phys.* **B283** (1987) 681.

[139] P. Schuster, N. Toro, N. Weiner, and I. Yavin, *High Energy Electron Signals from Dark Matter Annihilation in the Sun*, arXiv:0910.1839.

[140] M. Cirelli *et. al.*, *Spectra of neutrinos from dark matter annihilations*, *Nucl. Phys.* **B727** (2005) 99–138, [hep-ph/0506298].

[141] M. Blennow, J. Edsjo, and T. Ohlsson, *Neutrinos from WIMP Annihilations Using a Full Three- Flavor Monte Carlo*, *JCAP* **0801** (2008) 021, [arXiv:0709.3898].

[142] V. Barger, W.-Y. Keung, G. Shaughnessy, and A. Tregre, *High energy neutrinos from neutralino annihilations in the Sun*, *Phys. Rev.* **D76** (2007) 095008, [arXiv:0708.1325].

[143] J. Liu, P.-f. Yin, and S.-h. Zhu, *Neutrino Signals from Solar Neutralino Annihilations in Anomaly Mediated Supersymmetry Breaking Model*, *Phys. Rev.* **D77** (2008) 115014, [arXiv:0803.2164].

[144] T. Schwetz, M. Tortola, and J. W. F. Valle, *Three-flavour neutrino oscillation update*, *New J. Phys.* **10** (2008) 113011, [arXiv:0808.2016].

[145] N. Fornengo, L. Pieri, and S. Scopel, *Neutralino annihilation into gamma-rays in the Milky Way and in external galaxies*, *Phys. Rev.* **D70** (2004) 103529, [hep-ph/0407342]; G. Bertone, E. Nezri, J. Orloff, and J. Silk, *Neutrinos from dark matter annihilations at the galactic centre*, *Phys. Rev.* **D70** (2004) 063503, [astro-ph/0403322].

[146] L. Bergstrom, P. Ullio, and J. H. Buckley, *Observability of gamma rays from dark matter neutralino annihilations in the Milky Way halo*, *Astropart. Phys.* **9** (1998) 137–162, [astro-ph/9712318].

[147] G. D. Mack, T. D. Jacques, J. F. Beacom, N. F. Bell, and H. Yuksel, *Conservative Constraints on Dark Matter Annihilation into Gamma Rays*, *Phys. Rev.* **D78** (2008) 063542, [arXiv:0803.0157].

[148] V. Berezinsky, M. Kachelriess, and S. Ostapchenko, *Electroweak jet cascading in the decay of superheavy particles*, *Phys. Rev. Lett.* **89** (2002) 171802, [hep-ph/0205218].

[149] J. F. Beacom, N. F. Bell, and G. D. Mack, *General upper bound on the dark matter total annihilation cross section*, *Phys. Rev. Lett.* **99** (2007) 231301, [astro-ph/0608090].

[150] H. Yuksel, S. Horiuchi, J. F. Beacom, and S. Ando, *Neutrino Constraints on the Dark Matter Total Annihilation Cross Section*, *Phys. Rev.* **D76** (2007) 123506, [arXiv:0707.0196].

[151] A. E. Erkoca, M. H. Reno, and I. Sarcevic, *Muon Fluxes From Dark Matter Annihilation*, *Phys. Rev.* **D80** (2009) 043514, [arXiv:0906.4364].

[152] A. E. Erkoca, G. Gelmini, M. H. Reno, and I. Sarcevic, *Muon Fluxes and Showers from Dark Matter Annihilation in the Galactic Center*, arXiv:1002.2220.

[153] T. K. Gaisser, *Cosmic Rays and Particle Physics*. Cambridge, UK: Cambridge University Press, Jan., 1991; T. K. Gaisser and T. Stanev, *Neutrino induced muon flux deep underground and search for neutrino oscillations*, *Phys. Rev.* **D30** (1984) 985; T. K. Gaisser and T. Stanev, *Response of deep detectors to extraterrestrial neutrinos*, *Phys. Rev.* **D31** (1985) 2770.

[154] N. Fornengo, *Neutrino oscillation effect on the indirect signal of neutralino dark matter from the earth core*, hep-ph/9904351.

[155] P. H. Barrett, L. M. Bollinger, G. Cocconi, Y. Eisenberg, and K. Greisen, *Interpretation of cosmic-ray measurements far underground*, *Rev. Mod. Phys.* **24** (Jul, 1952) 133–178.

[156] P. Lipari and M. Lusignoli, *Comparison of $\nu_\mu \leftrightarrow \nu_\tau$ and $\nu_\mu \leftrightarrow \nu_s$ oscillations as solutions of the atmospheric neutrino problem*, *Phys. Rev.* **D58** (1998) 073005, [hep-ph/9803440].

[157] M. Honda, T. Kajita, K. Kasahara, and S. Midorikawa, *A new calculation of the atmospheric neutrino flux in a 3- dimensional scheme*, *Phys. Rev.* **D70** (2004) 043008, [astro-ph/0404457].

[158] G. Battistoni, A. Ferrari, T. Montaruli, and P. R. Sala, *The FLUKA atmospheric neutrino flux calculation*, *Astropart. Phys.* **19** (2003) 269–290, [hep-ph/0207035].

[159] G. D. Barr, T. K. Gaisser, P. Lipari, S. Robbins, and T. Stanev, *A three-dimensional calculation of atmospheric neutrinos*, *Phys. Rev.* **D70** (2004) 023006, [astro-ph/0403630].

[160] Y. Fukuda *et. al.*, *Measurements of the Solar Neutrino Flux from Super-Kamiokande's First 300 Days*, *Phys. Rev. Lett.* **81** (Aug, 1998) 1158–1162.

[161] Y. Fukuda *et. al.*, *Evidence for oscillation of atmospheric neutrinos*, *Phys. Rev. Lett.* **81** (1998) 1562–1567, [hep-ex/9807003]; Y. Fukuda *et. al.*, *Study of the atmospheric neutrino flux in the multi-GeV energy range*, *Phys. Lett.* **B436** (1998) 33–41, [hep-ex/9805006].

[162] C. Saji, *Study of upward-going muons in Super-Kamiokande*. PhD thesis, Niigata University, Mar, 2002.

[163] W. Lohmann, R. Kopp, and R. Voss, *Energy loss of muons in the energy range 1-GeV to 10000-GeV*, *CERN-85-03* (1985).

[164] Informations can be found on the web site http://nemoweb.lns.infn.it/.

[165] Informations can be found on the web site http://www.nestor.noa.gr/.

[166] A. Achterberg *et. al.*, *First year performance of the IceCube neutrino telescope*, *Astropart. Phys.* **26** (2006) 155–173, [astro-ph/0604450].

[167] M. Ackermann *et. al.*, *Limits to the muon flux from neutralino annihilations in the Sun with the AMANDA detector*, *Astropart. Phys.* **24** (2006) 459–466, [astro-ph/0508518]; R. Ehrlich, *The search for neutralino dark matter with the AMANDA neutrino telescope*. PhD thesis.

[168] G. Wikstrom, *A Search for solar dark matter with the IceCube neutrino telescope*. PhD thesis.

[169] E. Resconi and f. t. I. Collaboration, *Status and prospects of the IceCube neutrino telescope*, *Nucl. Instrum. Meth.* **A602** (2009) 7–13, [arXiv:0807.3891].

[170] A. Falkowski, J. Juknevich, and J. Shelton, *Dark Matter Through the Neutrino Portal*, arXiv:0908.1790.

[171] M. Blennow, H. Melbeus, and T. Ohlsson, *Neutrinos from Kaluza-Klein dark matter in the Sun*, arXiv:0910.1588.

[172] E. K. Akhmedov, *Neutrino physics*, hep-ph/0001264; W. Grimus, *Neutrino physics: Theory*, *Lect. Notes Phys.* **629** (2004) 169–214, [hep-ph/0307149].

[173] M. Beltran, D. Hooper, E. W. Kolb, and Z. C. Krusberg, *Deducing the nature of dark matter from direct and indirect detection experiments in the absence of collider signatures of new physics*, *Phys. Rev.* **D80** (2009) 043509, [arXiv:0808.3384].

[174] N. F. Bell, J. B. Dent, T. D. Jacques, and T. J. Weiler, *Electroweak Bremsstrahlung in Dark Matter Annihilation*, *Phys. Rev.* **D78** (2008) 083540, [arXiv:0805.3423].

[175] M. Kachelriess and P. D. Serpico, *Model-independent dark matter annihilation bound from the diffuse γ ray flux*, *Phys. Rev.* **D76** (2007) 063516, [arXiv:0707.0209].

[176] D. Hooper, *Constraining Supersymmetric Dark Matter With Synchrotron Measurements*, *Phys. Rev.* **D77** (2008) 123523, [arXiv:0801.4378].

[177] J. B. Dent, R. J. Scherrer, and T. J. Weiler, *Toward a Minimum Branching Fraction for Dark Matter Annihilation into Electromagnetic Final States*, *Phys. Rev.* **D78** (2008) 063509, [arXiv:0806.0370].

[178] U. Bellgardt *et. al.*, *Search for the Decay $\mu^+ \to e^+e^+e^-$*, *Nucl. Phys.* **B299** (1988) 1.

[179] K. Abe *et. al.*, *Search for Lepton Flavor Violating tau Decays into Three Leptons*, arXiv:0708.3272.

[180] P. Fayet, *U-boson production in e^+e^- annihilations, ψ and Υ decays, and light dark matter*, *Phys. Rev.* **D75** (2007) 115017, [hep-ph/0702176].

[181] A. Raspereza, *Higgs search results*, hep-ex/0209021.

[182] S. Galli, F. Iocco, G. Bertone, and A. Melchiorri, *CMB constraints on Dark Matter models with large annihilation cross-section*, *Phys. Rev.* **D80** (2009) 023505, [arXiv:0905.0003].

[183] T. R. Slatyer, N. Padmanabhan, and D. P. Finkbeiner, *CMB Constraints on WIMP Annihilation: Energy Absorption During the Recombination Epoch*, *Phys. Rev.* **D80** (2009) 043526, [arXiv:0906.1197].

[184] V. D. Barger, W.-Y. Keung, and G. Shaughnessy, *Monochromatic Neutrino Signals from Dark Matter Annihilation*, *Phys. Lett.* **B664** (2008) 190, [arXiv:0709.3301].

[185] C. Delaunay, P. J. Fox, and G. Perez, *Probing Dark Matter Dynamics via Earthborn Neutrinos at IceCube*, arXiv:0812.3331.

[186] M. Ahmed *et. al.*, *Search for the lepton-family-number nonconserving decay $\mu \to e + \gamma$*, *Phys. Rev.* **D65** (2002) 112002, [hep-ex/0111030].

[187] L. Lavoura, *General formulae for $f_1 \to f_2\gamma$*, *Eur. Phys. J.* **C29** (2003) 191–195, [hep-ph/0302221].

[188] M. Raidal *et. al.*, *Flavour physics of leptons and dipole moments*, *Eur. Phys. J.* **C57** (2008) 13–182, [arXiv:0801.1826].

[189] B. Aubert *et. al.*, *Search for lepton flavor violation in the decay $\tau^{\pm} \to e^{\pm}\gamma$*, *Phys. Rev. Lett.* **96** (2006) 041801, [hep-ex/0508012].

[190] D. Hooper, F. Petriello, K. M. Zurek, and M. Kamionkowski, *The New DAMA Dark-Matter Window and Energetic-Neutrino Searches*, *Phys. Rev.* **D79** (2009) 015010, [arXiv:0808.2464].

[191] J. L. Feng, J. Kumar, J. Learned, and L. E. Strigari, *Testing the Dark Matter Interpretation of the DAMA/LIBRA Result with Super-Kamiokande*, arXiv:0808.4151.

[192] J. Kumar, J. G. Learned, and S. Smith, *Light Dark Matter Detection Prospects at Neutrino Experiments*, arXiv:0908.1768.

[193] R. Bernabei *et. al.*, *Investigating electron interacting dark matter*, *Phys. Rev.* **D77** (2008) 023506, [arXiv:0712.0562].

[194] A. Dedes, I. Giomataris, K. Suxho, and J. D. Vergados, *Searching for Secluded Dark Matter via Direct Detection of Recoiling Nuclei as well as Low Energy Electrons*, arXiv:0907.0758.

[195] Q.-H. Cao, E. Ma, and G. Shaughnessy, *Dark Matter: The Leptonic Connection*, *Phys. Lett.* **B673** (2009) 152–155, [arXiv:0901.1334].

[196] A. Ibarra, A. Ringwald, D. Tran, and C. Weniger, *Cosmic Rays from Leptophilic Dark Matter Decay via Kinetic Mixing*, arXiv:0903.3625.

[197] J. A. Bearden and A. F. Burr, *Reevaluation of x-ray atomic energy levels*, *Rev. Mod. Phys.* **39** (Jan, 1967) 125–142.

[198] S. Ritz and D. Seckel, *Detailed neutrino spectra from Cold Dark Matter annihilations in the Sun*, *Nucl. Phys.* **B304** (1988) 877.

[199] S. Nussinov, *Technocosmology: could a technibaryon excess provide a 'natural' missing mass candidate?*, *Phys. Lett.* **B165** (1985) 55.

[200] S. M. Barr, R. S. Chivukula, and E. Farhi, *Electroweak fermion number violation and the production of stable particles in the Early Universe*, *Phys. Lett.* **B241** (1990) 387–391.

[201] D. B. Kaplan, *A Single explanation for both the baryon and dark matter densities*, *Phys. Rev. Lett.* **68** (1992) 741–743.

[202] Specific supersymmetric models which generate light neutralinos can be envisaged; for a very recent realization of the light neutralino scenario see for instance E. Dudas, S. Lavignac, and J. Parmentier, *A light neutralino in hybrid models of supersymmetry breaking*, *Nucl. Phys.* **B808** (2009) 237–259, [arXiv:0808.0562].

[203] A. Bottino, F. Donato, N. Fornengo, and S. Scopel, *Light neutralinos and WIMP direct searches*, *Phys. Rev.* **D69** (2004) 037302, [hep-ph/0307303].

[204] A. Bottino, F. Donato, N. Fornengo, and S. Scopel, *Indirect signals from light neutralinos in supersymmetric models without gaugino mass unification*, *Phys. Rev.* **D70** (2004) 015005, [hep-ph/0401186].

[205] A. Colaleo (ALEPH Collaboration), talk at SUSY'01, June 11-17, 2001, Dubna, Russia; J. Abdallah et al. (DELPHI Collaboration), DELPHI 2001-085 CONF 513, June 2001; LEP Higgs Working Group for Higgs boson searches, *Search for the standard model Higgs boson at LEP*, hep-ex/0107029; LEP2 Joint SUSY Working Group (http://lepsusy.web.cern.ch/lepsusy/).

[206] A. A. Affolder *et. al.*, *Search for neutral supersymmetric Higgs bosons in $p\bar{p}$ collisions at $\sqrt{s} = 1.8$ TeV*, *Phys. Rev. Lett.* **86** (2001) 4472–4478, [hep-ex/0010052]; V. M. Abazov *et. al.*, *Search for pair production of scalar bottom quarks in $p\bar{p}$ collisions at $\sqrt{s} = 1.96$-TeV*, *Phys. Rev. Lett.* **97** (2006) 171806, [hep-ex/0608013].

[207] A. Bottino, F. Donato, N. Fornengo, and S. Scopel, *Implications for relic neutralinos of the theoretical uncertainties in the neutralino nucleon cross-section*, *Astropart. Phys.* **13** (2000) 215–225, [hep-ph/9909228]; A. Bottino, F. Donato, N. Fornengo, and S. Scopel, *Size of the neutralino nucleon cross-section in the light of a new determination of the pion nucleon sigma term*, *Astropart. Phys.* **18** (2002) 205–211, [hep-ph/0111229].

[208] Other papers where the influence of the hadronic uncertainties on the neutralino-nuclei cross sections are discussed include: J. R. Ellis, A. Ferstl, and K. A. Olive, *Re-evaluation of the elastic scattering of supersymmetric dark matter*, *Phys. Lett.* **B481** (2000) 304–314, [hep-ph/0001005]; E. Accomando, R. L. Arnowitt, B. Dutta, and Y. Santoso, *Neutralino proton cross sections in supergravity models*, *Nucl. Phys.* **B585** (2000) 124–142, [hep-ph/0001019]; A. Corsetti and P. Nath, *Gaugino Mass Nonuniversality and Dark Matter in SUGRA, Strings and D Brane Models*, *Phys. Rev.* **D64** (2001) 125010, [hep-ph/0003186]; J. L. Feng, K. T. Matchev, and F. Wilczek, *Neutralino Dark Matter in Focus Point Supersymmetry*, *Phys. Lett.* **B482** (2000) 388–399, [hep-ph/0004043]; J. R. Ellis, K. A. Olive, and C. Savage, *Hadronic Uncertainties in the Elastic Scattering of Supersymmetric Dark Matter*, *Phys. Rev.* **D77** (2008) 065026, [arXiv:0801.3656]; J. Giedt, A. W. Thomas, and R. D. Young, *Dark matter, the CMSSM and lattice QCD*, arXiv:0907.4177.

[209] K. Freese, P. Gondolo, H. J. Newberg, and M. Lewis, *The Effects of the Sagittarius Dwarf Tidal Stream on Dark Matter Detectors*, *Phys. Rev. Lett.* **92** (2004) 111301, [astro-ph/0310334]; R. Bernabei *et. al.*, *Investigating halo substructures with annual modulation signature*, *Eur. Phys. J.* **C47** (2006) 263–271, [astro-ph/0604303]; L. D. Duffy and P. Sikivie, *The Caustic Ring Model of the Milky Way Halo*, *Phys. Rev.* **D78** (2008) 063508, [arXiv:0805.4556].

[210] T. Bruch, A. H. G. Peter, J. Read, L. Baudis, and G. Lake, *Dark Matter Disc Enhanced Neutrino Fluxes from the Sun and Earth*, *Phys. Lett.* **B674** (2009) 250–256, [arXiv:0902.4001].

[211] For a thorough overview of the recent activity in this field, see for instance the talks and contributions presented at the TAUP 2009 Conference (http://taup2009.lngs.infn.it/prog.html).

[212] F. Donato, N. Fornengo, and P. Salati, *Antideuterons as a signature of supersymmetric dark matter*, *Phys. Rev.* **D62** (2000) 043003, [hep-ph/9904481]; H. Baer and S. Profumo, *Low energy antideuterons: Shedding light on dark matter*, *JCAP* **0512** (2005) 008, [astro-ph/0510722]; F. Donato, N. Fornengo, and D. Maurin, *Antideuteron fluxes from dark matter annihilation in diffusion models*, *Phys. Rev.* **D78** (2008) 043506, [arXiv:0803.2640].

[213] A. Bottino, N. Fornengo, G. Polesello, and S. Scopel, *Light neutralinos at CERN LHC in cosmologically-inspired scenarios: New benchmarks in the search for supersymmetry*, *Phys. Rev.* **D77** (2008) 115026, [arXiv:0801.3334].

[214] J. N. Bahcall, M. H. Pinsonneault, and S. Basu, *Solar models: Current epoch and time dependences, neutrinos, and helioseismological properties*, *Astrophys. J.* **555** (2001) 990–1012, [astro-ph/0010346].

[215] J. N. Bahcall, *Neutrino Astrophysics*. Cambridge University Press, July, 1989. See also http://www.sns.ias.edu/~jnb/SNdata/sndata.html.

[216] J.-M. Levy, *Cross-section and polarization of neutrino-produced tau's made simple*, hep-ph/0407371.

[217] H. K. Dreiner, H. E. Haber, and S. P. Martin, *Two-component spinor techniques and Feynman rules for quantum field theory and supersymmetry*, arXiv:0812.1594.

[218] R. Mertig, M. Bohm, and A. Denner, *FEYN CALC: Computer algebraic calculation of Feynman amplitudes*, *Comput. Phys. Commun.* **64** (1991) 345–359.

[219] B. Kayser, *Majorana Neutrinos and their Electromagnetic Properties*, *Phys. Rev.* **D26** (1982) 1662.